ESD-TR-67-630

SECOND QUARTERLY TECHNICAL REPORT - LARGE APERTURE SEISMIC ARRAYS (LASA)

December 1967

DIRECTORATE OF PLANNING AND TECHNOLOGY
ELECTRONIC SYSTEMS DIVISION
AIR FORCE SYSTEMS COMMAND
UNITED STATES AIR FORCE
L. G. Hanscom Field, Bedford, Massachusetts

Sponsored by:

Advanced Research Projects Agency, Washington, D.C.
ARPA Order No. 800

(Prepared under Contract No. AF19628-67-C-0370 by General Atronics Corp., 1200 East Mermaid Lane, Philadelphia, Pennsylvania 19118.)

LEGAL NOTICE

When U. S. Government drawings, specifications or other data are used for any purpose other than a definitely related government procurement operation, the government thereby incurs no responsibility nor any obligation whatsoever; and the fact that the government may have formulated, furnished, or in any way supplied the said drawings, specifications, or other data is not to be regarded by implication or otherwise as in any manner licensing the holder or any other person or conveying any rights or permission to manufacture, use, or sell any patented invention that may in any way be related thereto.

OTHER NOTICES

Do not return this copy. Retain or destroy.

ESD-TR-67-630

SECOND QUARTERLY TECHNICAL REPORT - LARGE APERTURE SEISMIC ARRAYS (LASA)

December 1967

DIRECTORATE OF PLANNING AND TECHNOLOGY
ELECTRONIC SYSTEMS DIVISION
AIR FORCE SYSTEMS COMMAND
UNITED STATES AIR FORCE
L. G. Hanscom Field, Bedford, Massachusetts

Sponsored by:

Advanced Research Projects Agency, Washington, D.C.
ARPA Order No. 800

(Prepared under Contract No. AF19628-67-C-0370 by General Atronics Corp., 1200 East Mermaid Lane, Philadelphia, Pennsylvania 19118.)

FOREWORD

This research was supported by the Advanced Research Projects Agency. The Electronic Systems Division technical project officer for Contract F19628-67-C-0370 is Major Cleve P. Malone (ESLE).

We wish to acknowledge the very considerable support and assistance that have been provided during the course of this program by the Advanced Research Projects Agency, the Earth Sciences Division of Teledyne, Inc., the Electronic Systems Division Seismic Array Program Office, the Institute for Defense Analyses, the Lincoln Laboratory, and the Vela Seismological Center.

This technical report has been reviewed and is approved.

PAUL W. RIDENOUR, Lt. Col., USAF
Chief, Development Engineering Division
Directorate of Planning and Technology
Electronic Systems Division

ABSTRACT

Four topics are discussed in this progress report. The first topic is related to the masking of underground nuclear tests with large earthquakes. Computer simulations, using signals from actual seismic events, suggest that test detonations one magnitude unit smaller than the earthquake can be detected, providing the shot time is some two minutes after the time of occurrence of the earthquake. The second topics deals with the effects of signal-to-noise ratio and local travel time-anomalies on the accuracy of epicenter location using large seismic arrays. Both theoretical analyses and computer simulations indicate standard deviations of angular errors on the order of 0.3° for either a 10 dB signal-to-noise ratio or a peak anomaly on the order of 1/20th of a second. The third topic deals with the application of a previously developed coda-correlation discriminant to DIMUS (hardlimited) seismograms. This discriminant makes use of the average paired correlation coefficient of the 10-second portion of seismic arrivals commencing 3 seconds after P-wave onset for an array of widely separated stations. Results to date indicate a moderate degradation of the discriminant for the DIMUS seismograms compared to the unclipped seismograms. The fourth topic deals with the automatic identification of the pP phase of earthquakes, for events in the 40 to 150 km depth region. Excellent results have been obtained with this automatic scheme, and not only is the pP phase properly identified, but also the sP phase. This combination allows depths to be estimated with considerable confidence.

TABLE OF CONTENTS

TABLE OF CONTENTS - Continued

APPENDICES

LIST OF FIGURES

SECTION I

INTRODUCTION

This is the Second Quarterly Technical Report on Contract F19628-67-C-0370. The report summarizes progress on four topics: masking of underground tests with large earthquakes, beamforming and other techniques for epicenter location, a DIMUS (hardlimited) version of the coda-correlation discriminant, and an extension of the automatic pP test to depths greater than 40 km.

Section II is a continuation of a discussion in our First Quarterly Technical Report on the problem of detecting covert nuclear tests in the vicinity of large earthquakes. In this discussion, a detection system consisting of a network of single stations surrounding the earthquake epicenter plus a continental-size array was proposed. Under the assumption that the single-station network would detect a covert test if the signal from the test preceded that from the earthquake at any of the stations, minimum earthquake-test delay times necessary for the test to avoid detection were derived as a function of test site position. The continental-size array imposes maximum earthquake-test delay times for the test to avoid detection. Some calculations were presented indicating the general properties of the earthquake contribution to the array output.

In order to obtain a measure of the sensitivity of the continental-size array, we have performed several additional calculations that are summarized in this report. The most important of these are based on a simulated detection problem with an assumed nuclear test near a larger earthquake. This simulation is based on actual seismic data, and involves several values of the following parameters: earthquake-test delay time, test site location, relative magnitudes of the two events. Results are summarized in terms of plots that give the maximum delay time imposed by the array as a function of test site location for

each of two test magnitudes. These plots suggest that if the enormous number of computations necessary to implement this detection system could be managed, it would very significantly reduce the probability that a covert nuclear test would go undetected.

Section III presents several theoretical derivations related to the problem of epicenter location by beamforming or by plane-wave fitting following individual arrival time measurements at each station. A highly idealized model of the problem is analyzed with the objective of gaining insight into the actual seismic problem. More specifically, the plane-wave fit based on arrival-time measurements is stated, and three methods of arrival-time measurement are analyzed. In general, the best of the arrival-time measurements is the correlation time pick, which requires perfect knowledge of the signal waveshape. The beamforming calculation is also analyzed, and it is shown that it yields the same results as the correlation time pick followed by a plane-wave fit. This indicates one important advantage of the beamforming, since this calculation does not require prior knowledge of the exact signal waveshapes. The results of this section are summarized in terms of a few examples. In one of these, a uniform 21-element array of total aperture 200 km, with a phase velocity of 20 km/sec and a signal-to-noise ratio of 10 dB, leads to a standard deviation in angular measurement of 0.3°.

The principal limitation of the theoretical analysis is that closed form solutions are available only with rather idealized assumptions. In order to study more realistic assumptions under controlled conditions, we have also performed several simulations. These simulations, which are summarized in Section IV, are based on actual seismic records from a large surface-focus event recorded at LASA-Montana. In these simulations controlled amounts of additive noise or travel-time errors are added to each seismic record and four different methods of

epicenter estimation are tested. Two of these methods are based on conventional beamforming: in one case the pattern is defined by an energy calculation, in the other by a peak value. Two calculations based on DIMUS (hardlimited) seismograms are also presented. In all cases an automatic event detector is used to define the interval of interest so that the calculations will be as realistic as possible.

The results of these simulations are summarized in tables and figures, which show that the additive noise leads to errors comparable to those predicted by the simplified theory of Section III, whereas the simulated time errors lead to more serious errors than expected. The reason for the latter discrepancy is not well understood, but is probably a consequence of modeling sampled data with continuous waveforms. There is considerable spread in the simulated data now available, but it appears that both of the DIMUS-based calculations yield performance levels quite comparable to those obtained from analog waveforms.

Section V is a brief report on calculations of the DIMUS (hardlimited) version of the coda-correlation discriminant, which worked well with analog waveforms. The calculations summarized in Section V indicate that the discriminant based on DIMUS waveforms leads to a less complete (but possibly useful) separation of moderate depth earthquakes from other events.

Section VI reports experimental results of applying an extended automatic pP test to deep earthquakes, using data from continental-size arrays. The result of processing eight events are very encouraging. In many cases the test has identified both pP and sP. In some cases the test has yielded depth estimates that conflict with C&GS depths. As is illustrated in Section VI, it appears in some cases that the C&GS depths result from mistaking sP for pP. The test results are summarized in tables and figures, and several seismograms are presented to confirm and explain the test results.

SECTION II

DETECTION OF UNDERGROUND NUCLEAR EXPLOSIONS IN THE PRESENCE OF LARGE NATURAL EVENTS

The problem of detecting an underground nuclear explosion that occurs shortly after an earthquake and in the same geographical vicinity was discussed in an earlier report [1]. A hypothetical detection system consisting of a continental-size array plus a set of single stations encircling the earthquake epicenter at close ranges (perhaps 40°) was considered. It was concluded that, from the point of view of trying to hide a nuclear test in the earthquake's signal, the continental-size array imposes a maximum allowable delay between the earthquake and the test, which is a function of both the relative locations and magnitudes of the test and the earthquake. Roughly speaking, the maximum delay is the time after which the earthquake's signals have decayed sufficiently that an underground nuclear test could be detected. The single-station network, on the other hand, imposes a limit on how soon after the earthquake a nuclear test can be concealed without being detected by one of these single-seismometer stations. This minimum delay is imposed by the assumption that if the signal from the test precedes that of the earthquake at any single station, the test will be detected.

Plots of the energy received in nonoverlapping one-second time windows as a function of time-after-onset were presented for several stations that recorded two large natural events. It was observed that the energy-decay rate varied from station to station and that the energy decay curve for a single station was far from smooth. The arrival of additional phases after the P-phase, with varying relative strengths, produces several irregular (and often large) peaks in the energy vs. time curve, both for single stations and for the array output. The apparently irregular behavior of these curves makes it unlikely

that any simple model would suffice to predict detection performance of a continental-size array in this context. For this reason we have resorted to a simulation, using actual seismic records from a large earthquake, to study the sensitivity of a continental-size array as a function of the relative magnitudes and locations of the two events and the time between them.

Two methods of detection, which were motivated by the time-varying nature of the coda energy levels, have been studied by means of simulation. These two methods are very similar to calculations used in an automatic pP enhancement method which was discussed in an earlier report [2]. All of the results presented in this section are based on a magnitude-5.5 earthquake as recorded at fifteen stations located in the continental United States. The earthquake occurred in the Fox Islands on 1 Sept. 1964.

The contents of this section may be summarized as follows. The energy-ratio detection statistic, ε, which is defined as the average power in a one-second window divided by that of the preceding five seconds, is first discussed. Then another detection statistic, which is obtained by multiplying ε by the average paired correlation coefficient obtained for the same one-second interval, is considered. Following the presentations of these two detection statistics, the expected performance of both is studied, and conclusions are drawn indicating how the minimum detectable magnitude of an event may be related to the average power in the output of the continental-size array. Following this discussion, curves of minimum detectable nuclear-test magnitude as a function of the earthquake-shot delay time, for selected points in the vicinity of the earthquake's epicenter are presented and discussed. Finally, the results of this simulation are summarized in terms of allowable intervals for escaping detection with the methods discussed, as a function of the nuclear test's magnitude and the relative position of the test site and the earthquake's epicenter.

2.1 THE ε DETECTION STATISTIC

If a simple energy detector were used with the array output to detect a possible test, a time-varying threshold would be necessary to take advantage of the general decay in the energy level of the interfering earthquake signal. As a simpler approach, we have considered an energy ratio statistic and a constant threshold. This detection statistic is defined as the ratio of the average power in a one-second interval to that of the previous five-second interval. The five-second integration interval was chosen as adequate to smooth out the short term fluctuations that are apparent in the energy decay curves.

The ε statistic is calculated, as a function of time, from the array output. The array output is calculated for each of several possible test epicenters by aligning the seismograms so that signals from the test epicenter would arrive in phase, normalizing the seismograms, and adding them. Two normalizations of the seismograms have been used. For the first, all seismograms are normalized to have the same P-phase energy (defined by a one-second time window). In the case where some stations have poor signal-to-noise ratios, this normalization can lead to excessive noise in the array output. For times well after the earthquake, when the coda energy is of the same order as the noise, this noise is a significant limitation on detection performance. This problem can be alleviated by using maximal-ratio combining, in which each record is weighted by the ratio of the square root of the P-phase energy to the average power in the noise preceding the P-phase. One potential problem in using the maximal-ratio combining is that the directional properties of the array may be degraded. As will be illustrated in the data presented below, it appears that the maximal-ratio combining is to be preferred, despite this potential disadvantage.

Figure 2.1 illustrates the behavior of ε as a function of time when the array is steered at the earthquake's epicenter; this figure is based on maximal-ratio combining. The maximum excursion

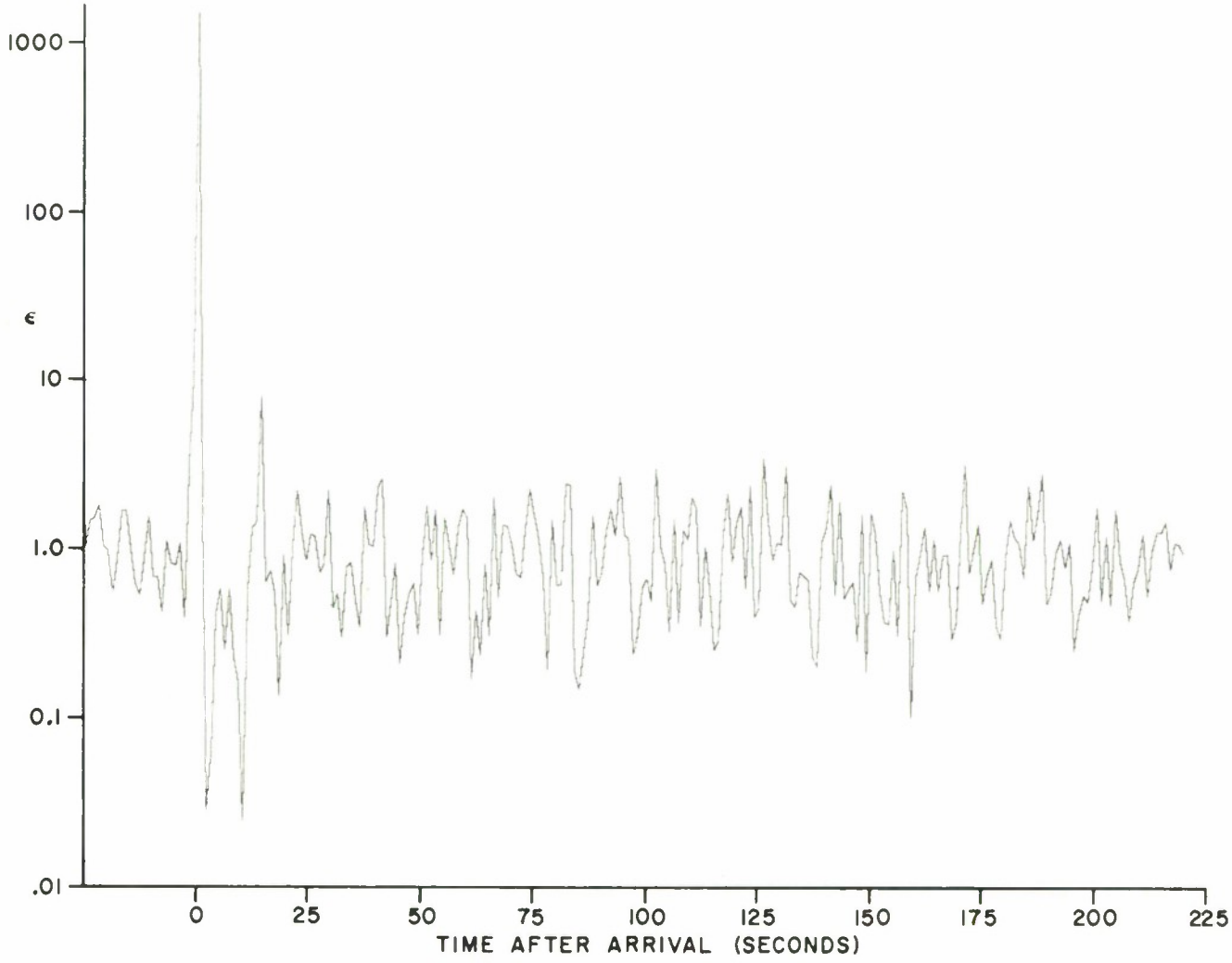

FIGURE 2.1
THE ϵ DETECTION STATISTIC
ARRAY STEERED AT THE EPICENTER

is 1700, and the only other large excursion occurs roughly 15 seconds after the arrival of the event.

The same curve has been calculated with the array steered to each of thirty grid points surrounding the earthquake's epicenter. These grid points were defined by six bearings and distances of 1, 3, 5, 7 and 9 degrees from the earthquake's epicenter. The results of these calculations indicate average levels of ε very close to 1.0, except in time intervals corresponding to arrivals of some phases from the earthquake. The rms value of this statistic is also close to unity.

In order to set a threshold that excludes all but a few false alarms it is necessary to tabulate the maximum excursions of ε as a function of the test epicenter to which the array is steered. Figure 2.2A gives these maximum values at each grid point surrounding the earthquake's epicenter for the case of equal P-phase energy normalization. Figure 2.2B is the same presentation based on maximal-ratio combining. Maximum excursions as high as 50 in Figure 2.2A and 150 in Figure 2.2B occur.

These maximum excursions, and hence the allowable detection thresholds, may be reduced significantly by excluding the times corresponding to P-phase arrivals from these calculations. As discussed in more detail in a previous report [3] this region of time can be more effectively monitored by a network of single stations surrounding the region of interest. For this reason, we shall exclude these times from our calculations of array characteristics. Excluding those times that could be monitored by a single station network that is well distributed in azimuth and has an average range of 40° from the earthquake's epicenter, leads to the maximum ε values given in Figure 2.3.

In Figures 2.2 and 2.3, the maximal-ratio combining leads to larger maximum excursions of ε than the equal P-phase

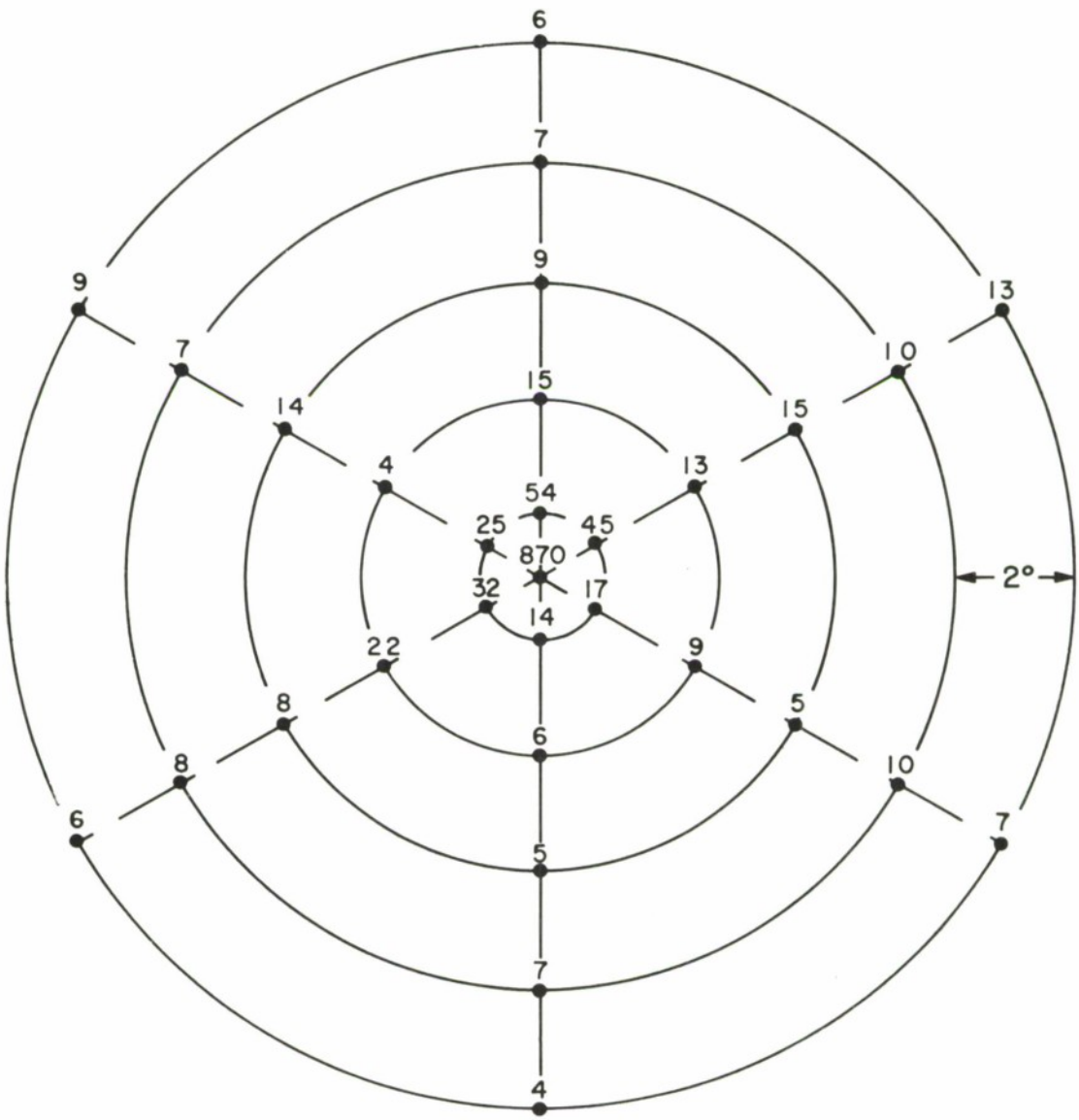

RECORDS NORMALIZED TO
SAME P-PHASE ENERGY

FIGURE 2.2A
MAXIMUM EXCURSIONS OF ϵ STATISTIC
INCLUDING P-PHASE ARRIVALS

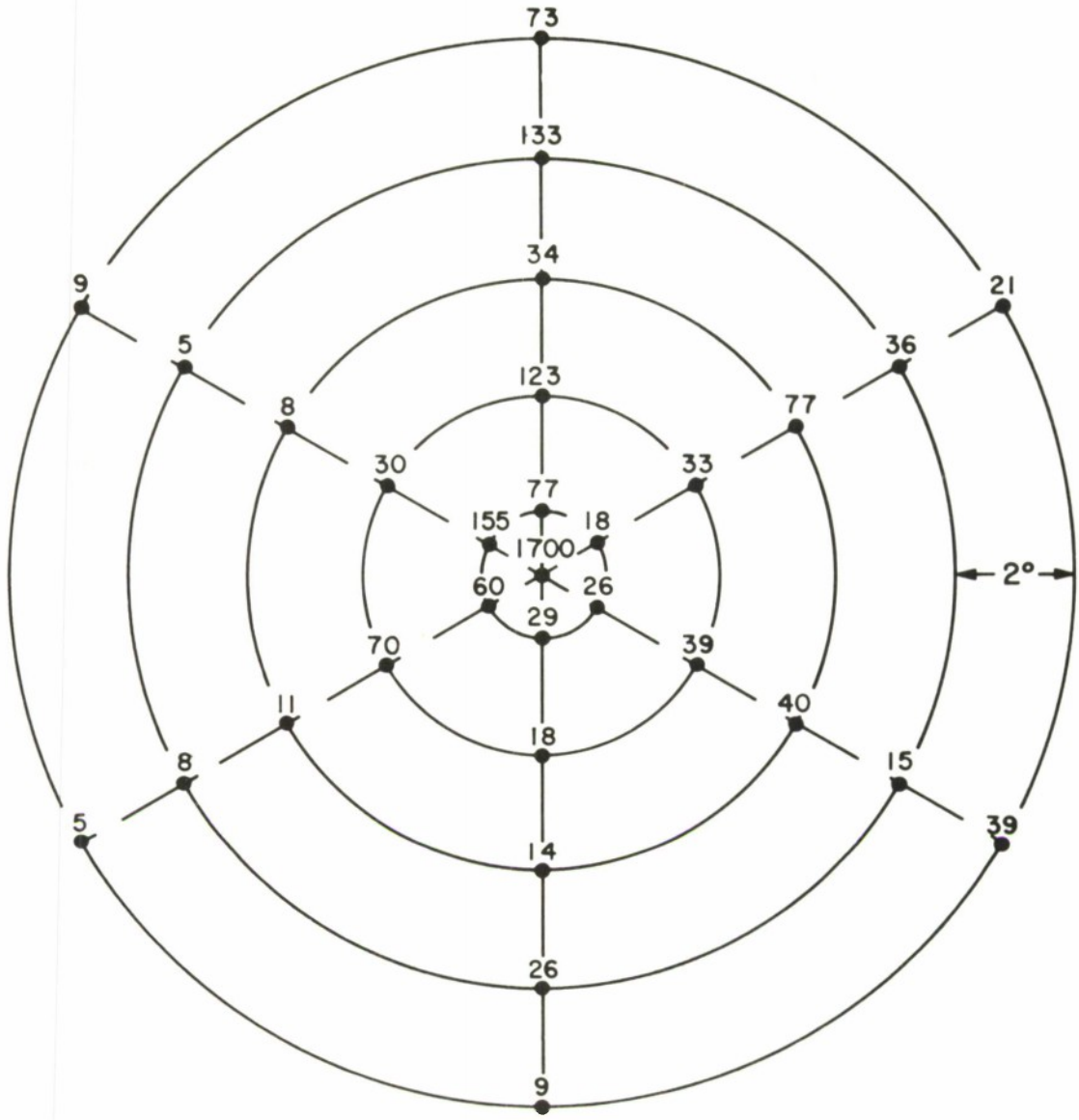

FIGURE 2.2 B
MAXIMUM EXCURSIONS OF ϵ STATISTIC
INCLUDING P-PHASE ARRIVALS

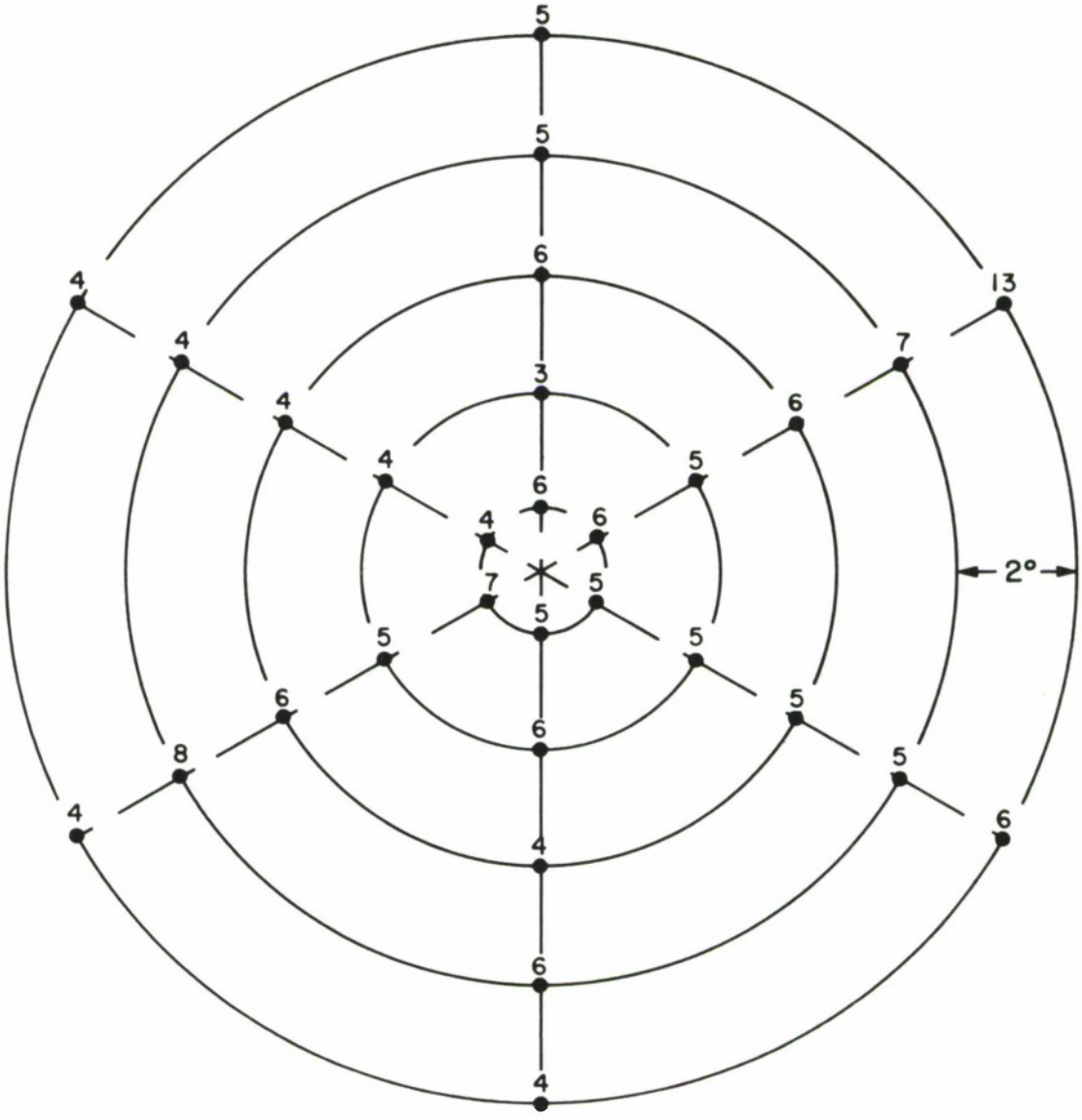

RECORDS NORMALIZED TO
SAME P-PHASE ENERGY

FIGURE 2.3 A
MAXIMUM EXCURSIONS OF ϵ STATISTIC
EXCLUDING P-PHASE ARRIVALS

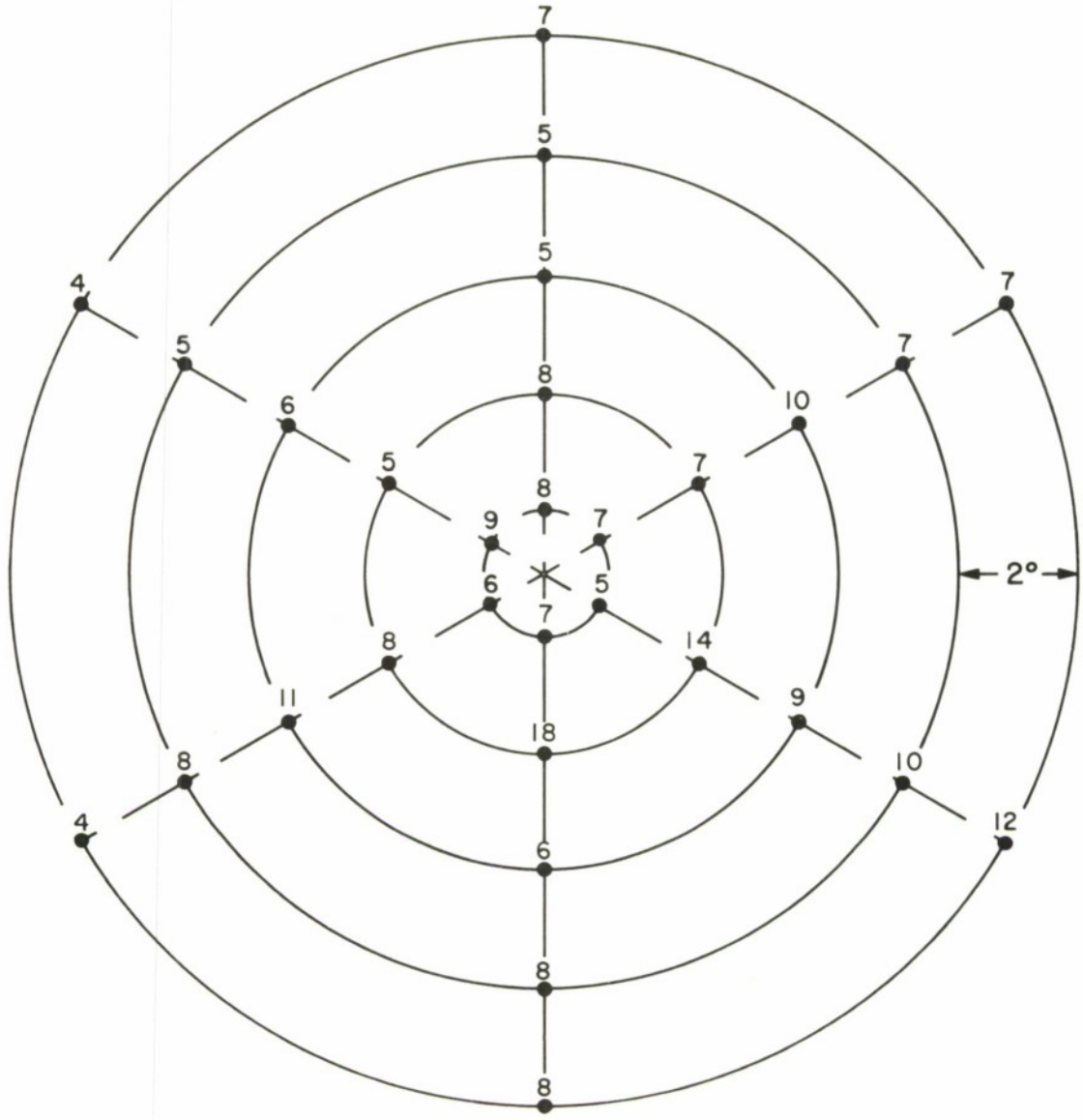

RECORDS NORMALIZED USING
MAXIMAL-RATIO COMBINING

FIGURE 2.3B
MAXIMUM EXCURSIONS OF ϵ STATISTIC
ENCLUDING P-PHASE ARRIVALS

energy normalizations. If we wanted to allow a margin of safety of a factor of two, we would have to choose a detection threshold of at least 26 for the equal P-phase energy case and 36 for the maximal-ratio case. Since these numbers seem rather large, we have also considered an alternate detection statistic, η, in the hope that it would turn out to be a more sensitive statistic.

2.2 THE η DETECTION STATISTIC

A second detection statistic, η, is defined as the product of ε and the average paired correlation coefficient calculated from the corresponding one-second interval of all of the seismograms. The objective in using this statistic is the reduction of "spurious" peaks in the array output compared to "legitimate" peaks that result from correlated arrivals at each station.

Some properties of the η statistic may be observed from Figure 2.4, which is a plot of the logarithm of the magnitude of η vs. time. Since maximal-ratio combining is used in both cases, each value of η in Figure 2.4 is just the product of the corresponding value of ε in Figure 2.1 and the average paired correlation coefficient for that time. Figure 2.4 indicates that the η statistic is generally quite low compared to the ε statistic except at the correlated P-phase arrival (recall that the beam is steered to the earthquake epicenter) and at the secondary peak 15 seconds later. (Based on earlier studies[4] of this event, we do not think that this secondary peak is pP since pP has been found within five seconds of P.)

Figure 2.5 shows the maximum of the η detection statistic when the total records are considered (including the P-phase arrivals). It is apparent that these values are significantly smaller than the ε's shown in Figure 2.2. There is still a large excursion of η in Figure 2.5B at the grid point Az=0 and R=7. At this same grid point the corresponding maximum

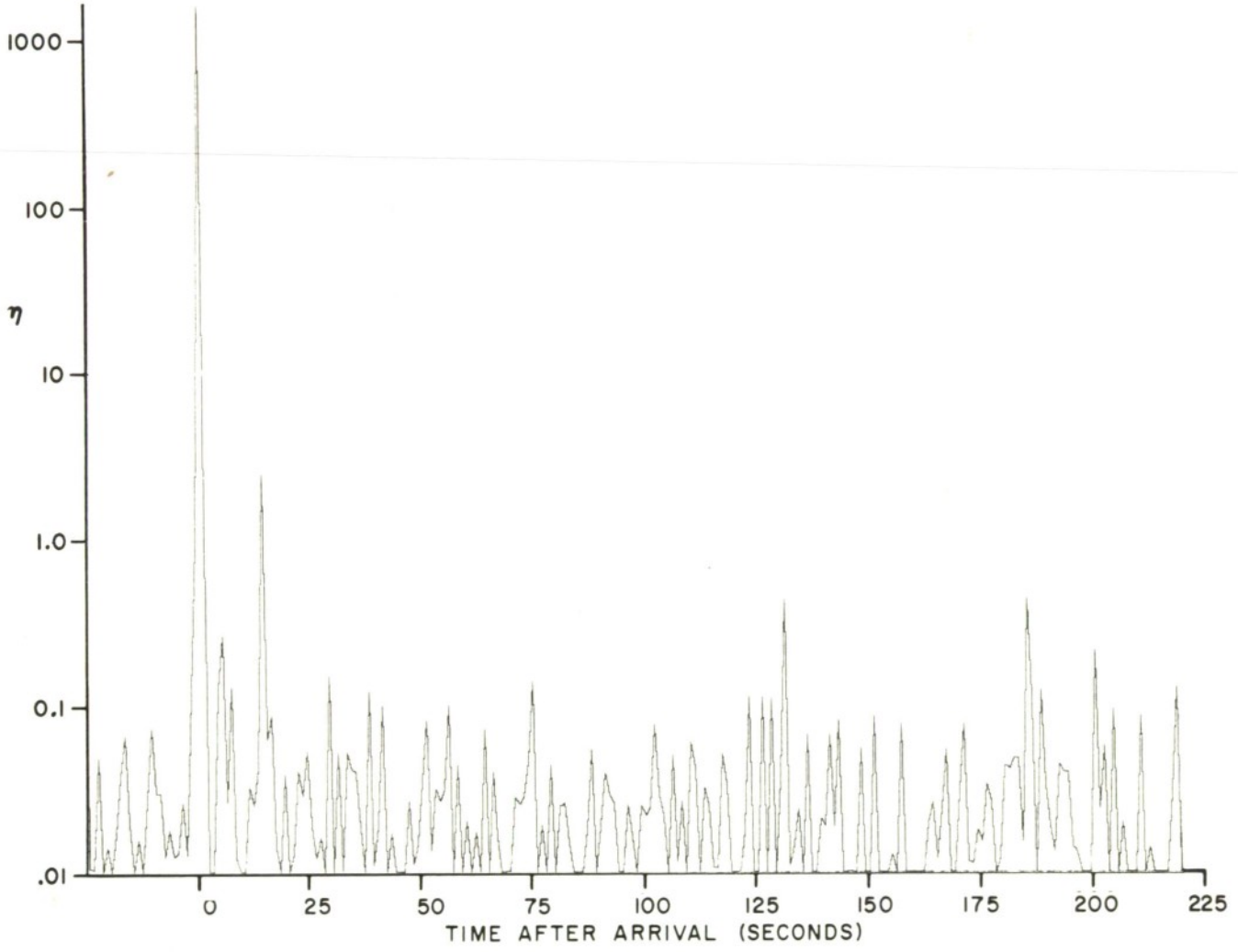

FIGURE 2.4
THE η DETECTION STATISTIC
ARRAY STEERED AT THE EPICENTER

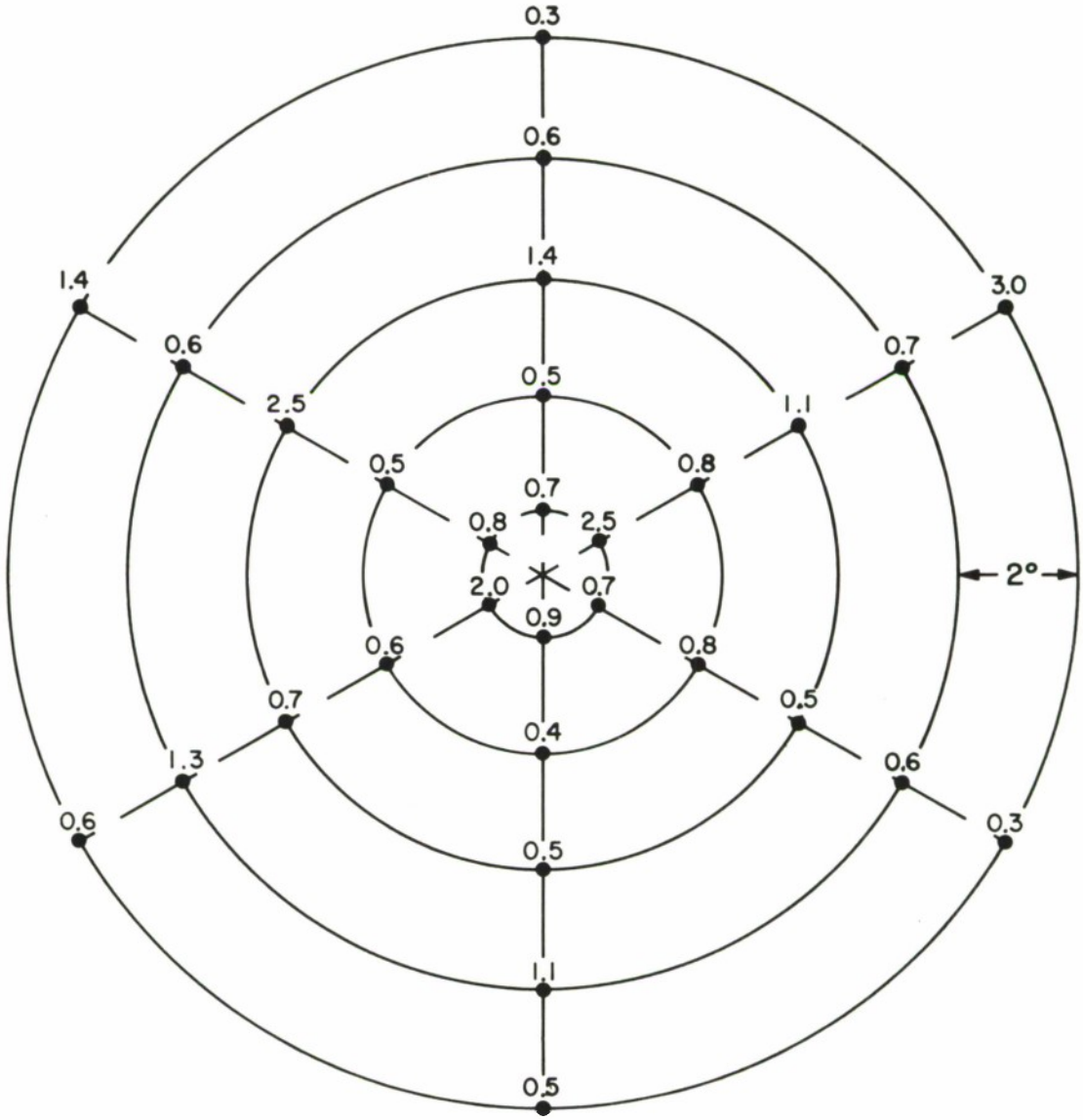

RECORDS NORMALIZED TO
SAME P-PHASE ENERGY

FIGURE 2.5A
MAXIMUM EXCURSIONS OF η STATISTIC
INCLUDING P-PHASE ARRIVALS

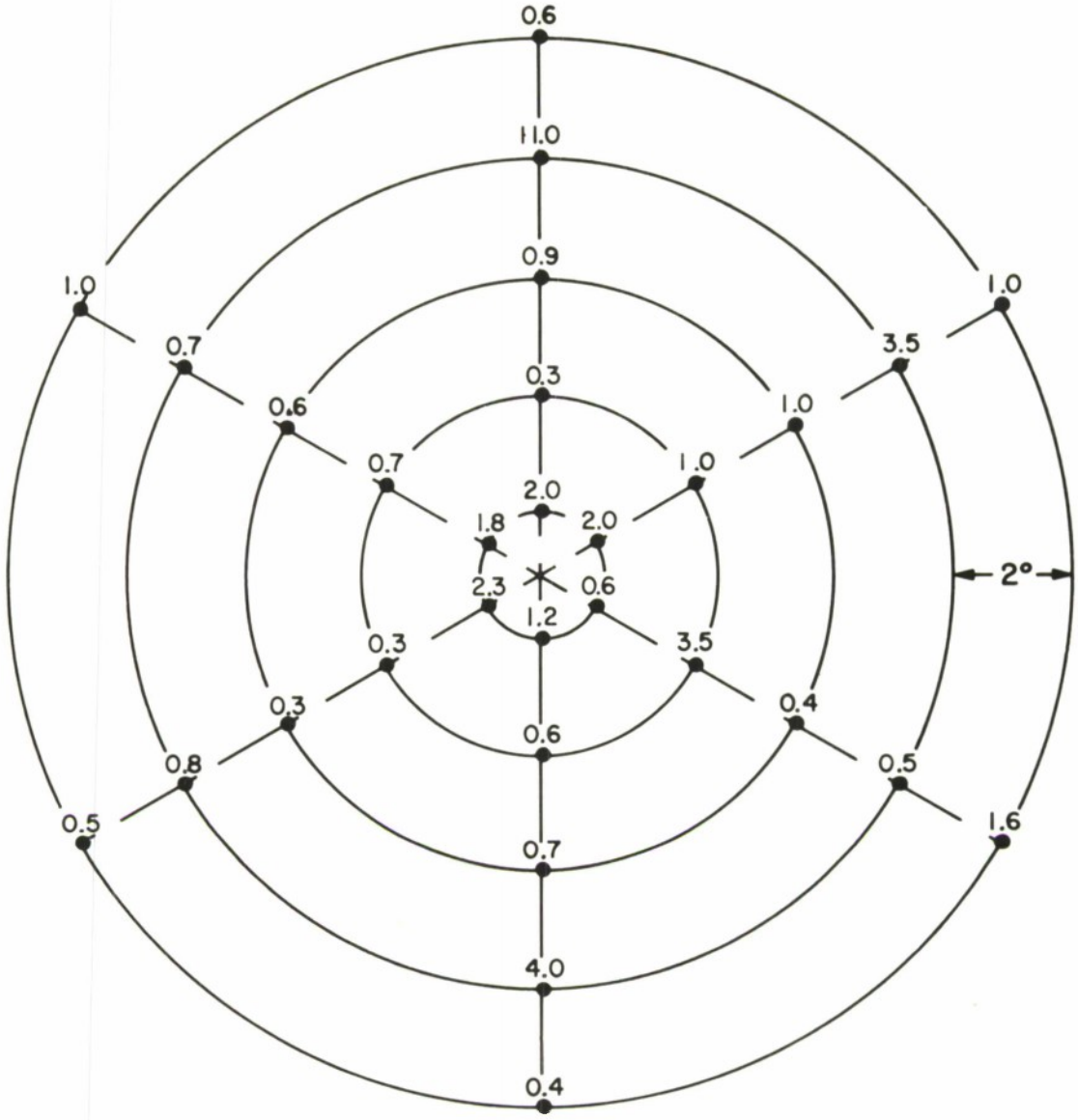

RECORDS NORMALIZED USING
MAXIMAL-RATIO COMBINING

FIGURE 2.5B
MAXIMUM EXCURSIONS OF η STATISTIC
INCLUDING P-PHASE ARRIVALS

value of ε was found to be 133. Figure 2.6 shows the maximum excursions of this statistic when the time interval that would be covered by the single-station network is excluded. The maximum excursions obtained indicate that in the case of maximal-ratio combining, an η of 2.0 (3 dB greater than the maximum) is a conservative detection threshold. Using the equal P-phase energy normalization, the corresponding threshold would be 6.0.

2.3 COMPARISON OF THE PERFORMANCE OF THE ε AND η DETECTION STATISTICS

The preceding figures give some indication of what thresholds could be used with ε and with η in order to avoid false alarms. This is, of course, only part of the story. We now wish to examine the sensitivity of these two statistics to the actual presence of a second seismic event in the coda of the first. To study this question several simulations have been performed. In these simulations a scaled replica of the P-phase of each seismogram is added to the same seismogram at a time corresponding to the arrival of a hypothetical test that is set off 60 seconds after the earthquake and is located at a designated grid point.

The results of these calculations are summarized in Figures 2.7 and 2.8. Each graph contains six curves, one for each grid point at a fixed range. Each curve represents the locus of pairs of values of ε and η as the scale factor for the added P-phase is varied. Thus these plots allow us to examine the relative values of ε and η as the magnitude of the (simulated) second event is increased. It may be observed from these figures that the general form of the ε-η relation does not vary a great deal from grid point to grid point. Also indicated on these plots are the thresholds suggested by the earlier figures as sufficient to avoid false alarms. It is clear from these plots that the η statistic will cross its "false-alarm proof" threshold before the ε statistic crosses its correspondingly conservative threshold.

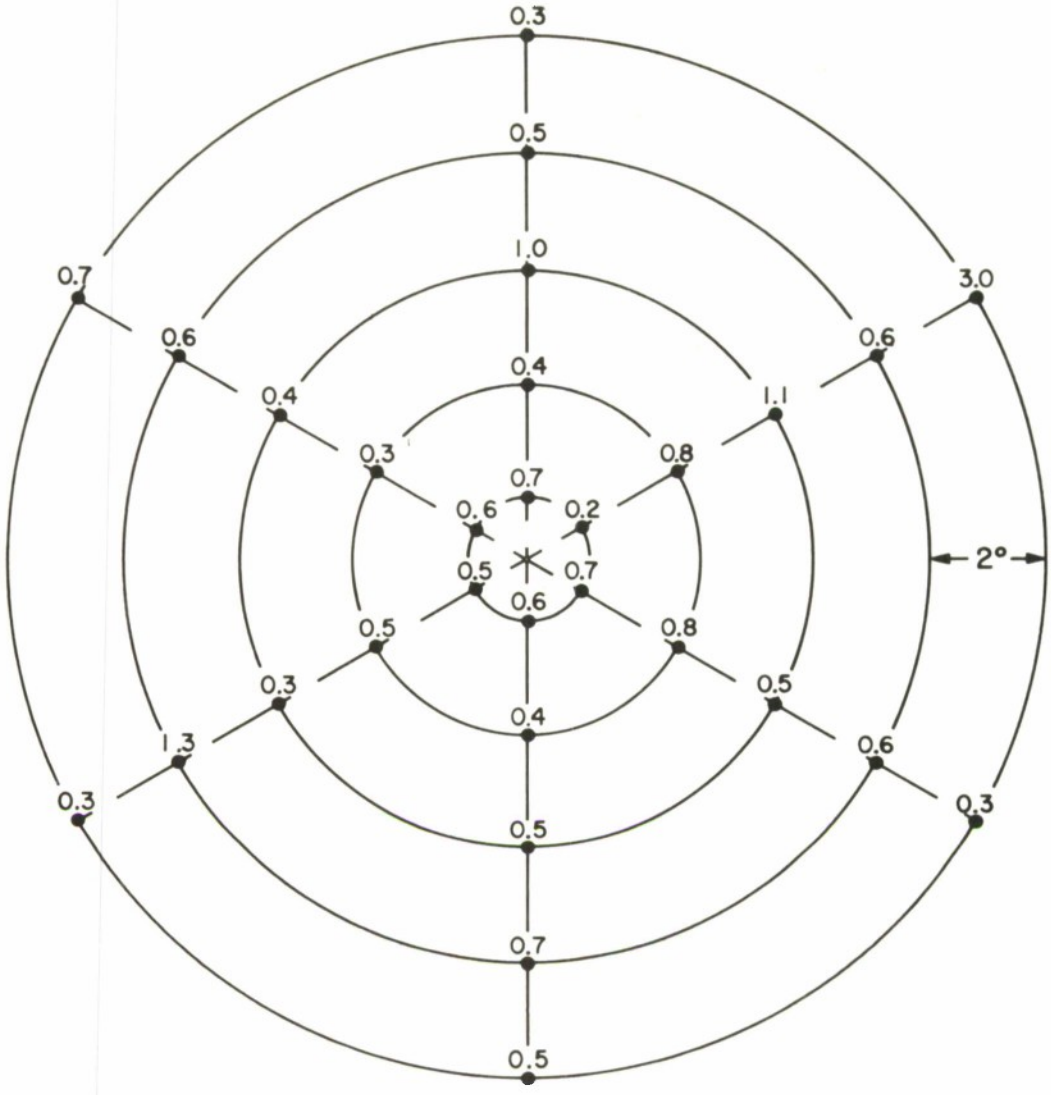

RECORDS NORMALIZED TO
SAME P-PHASE ENERGY

FIGURE 2.6A
MAXIMUM EXCURSIONS OF η STATISTIC
EXCLUDING P-PHASE ARRIVALS

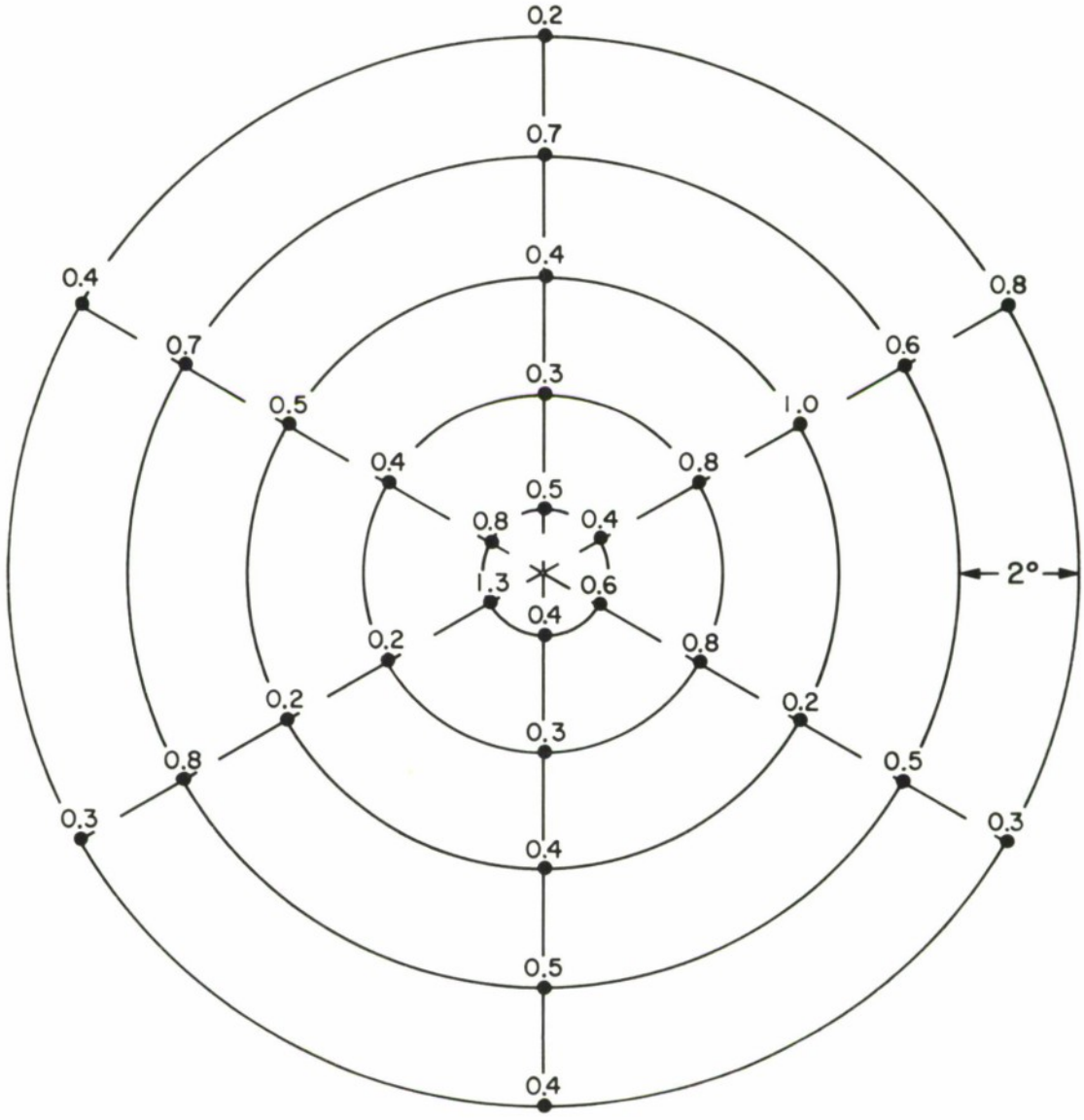

RECORDS NORMALIZED USING
MAXIMAL-RATIO COMBINING

FIGURE 2.6 B
MAXIMUM EXCURSIONS OF η STATISTIC
EXCLUDING P-PHASE ARRIVALS

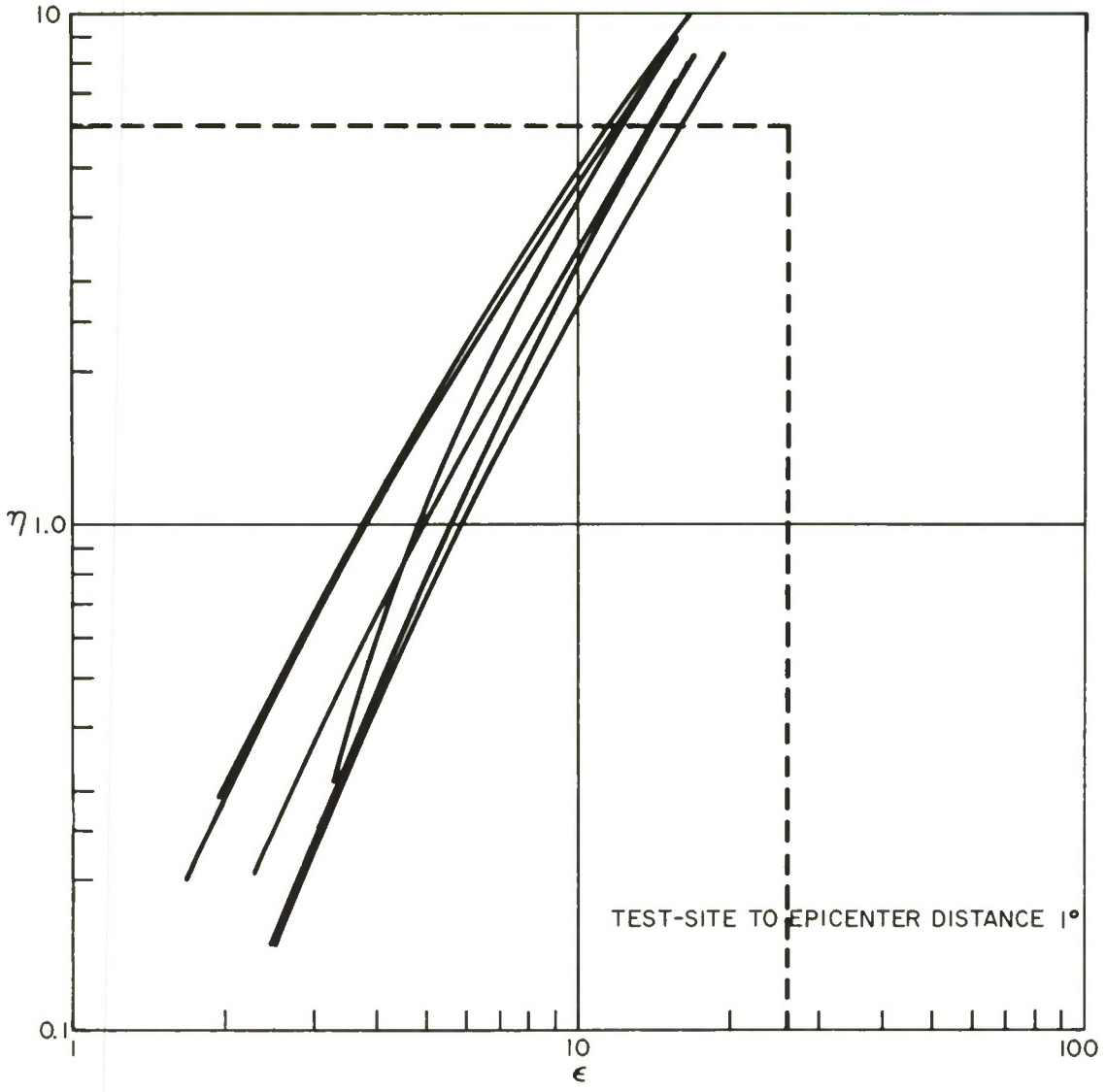

FIGURE 2.7 A
RELATION BETWEEN ϵ AND η
(RECORDS NORMALIZED TO SAME P-PHASE ENERGY)

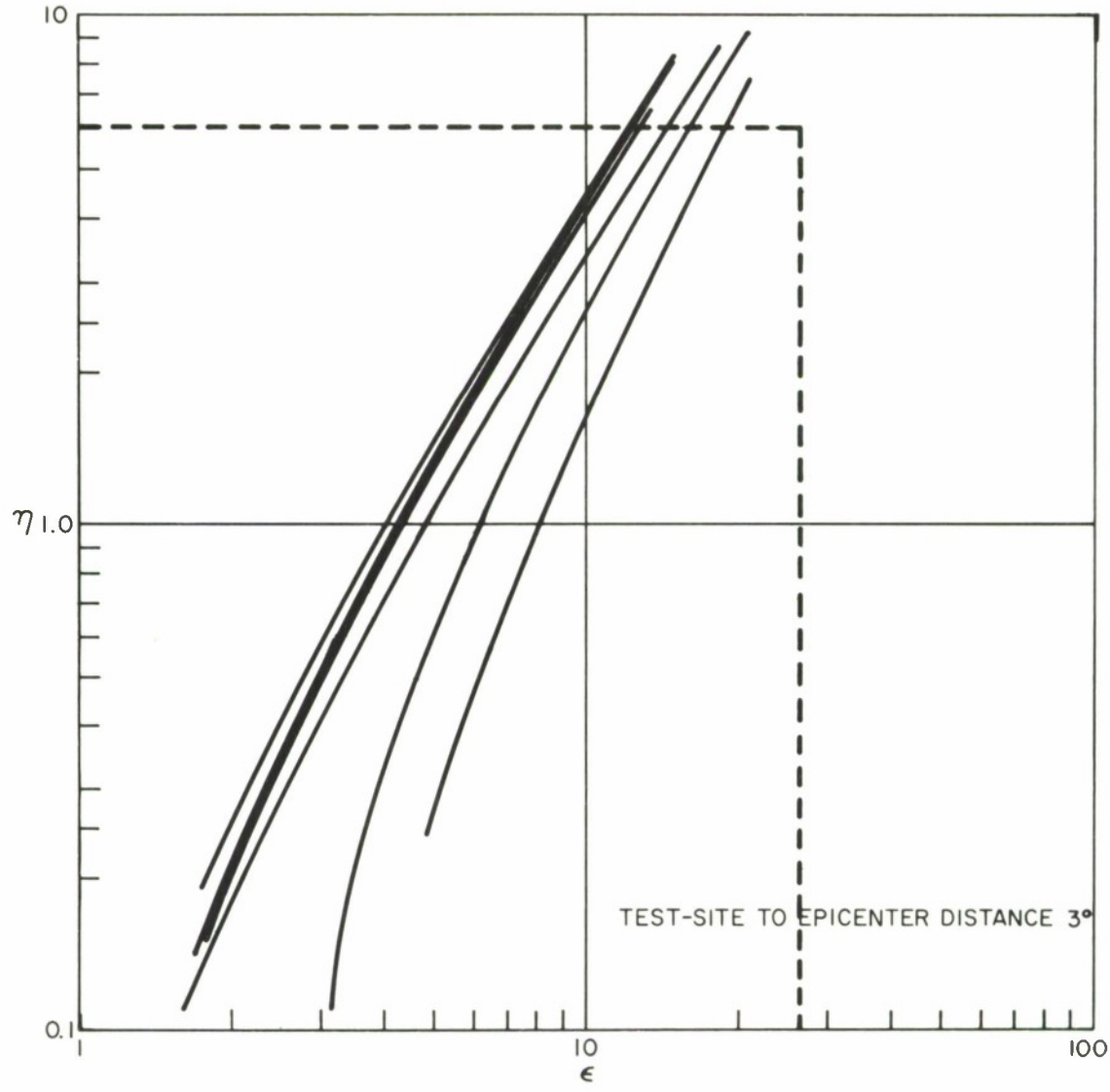

FIGURE 2.7B
RELATION BETWEEN ϵ AND η
(RECORDS NORMALIZED TO SAME P-PHASE ENERGY)

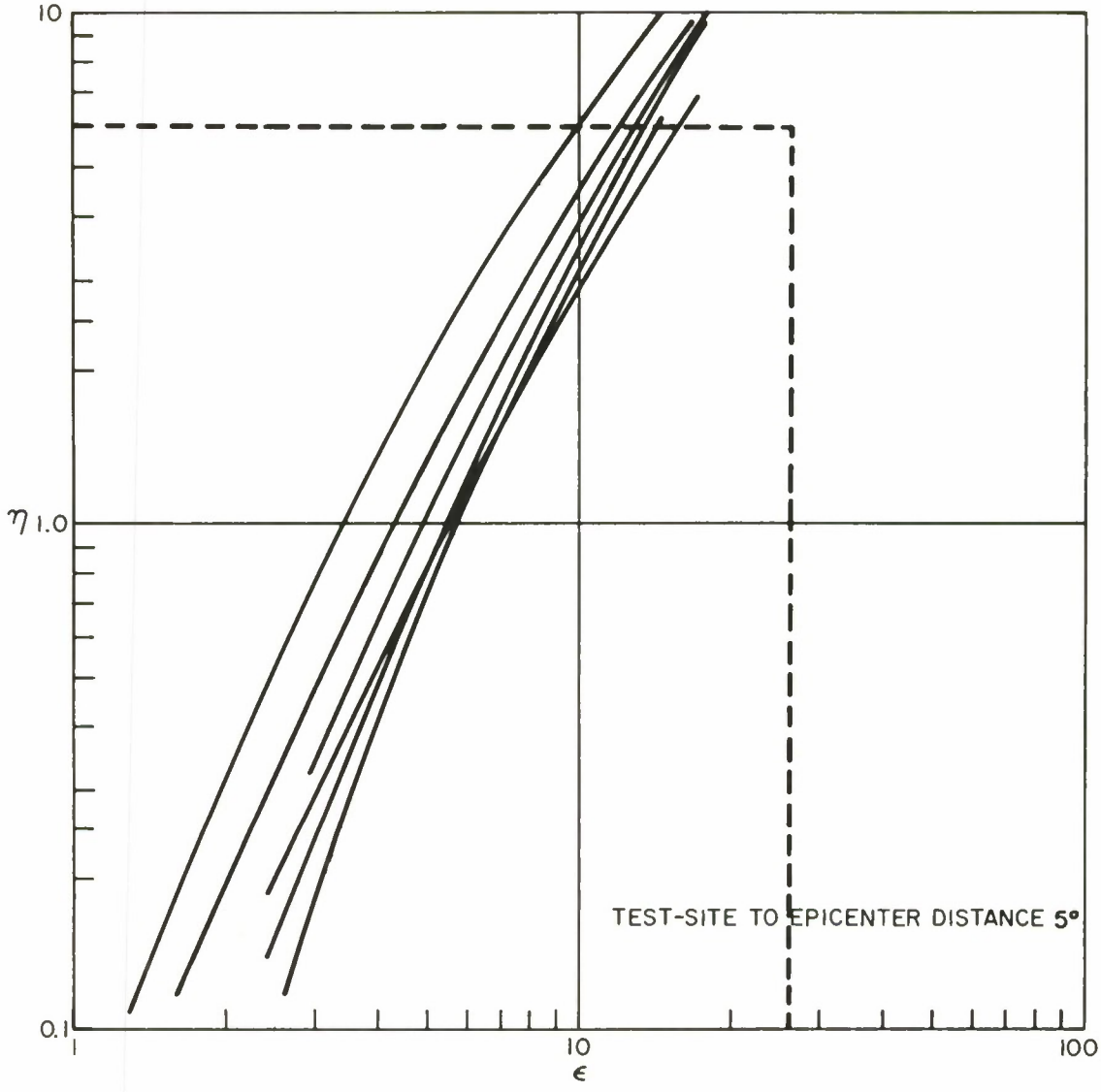

FIGURE 2.7C
RELATION BETWEEN ϵ AND η
(RECORDS NORMALIZED TO SAME P-PHASE ENERGY)

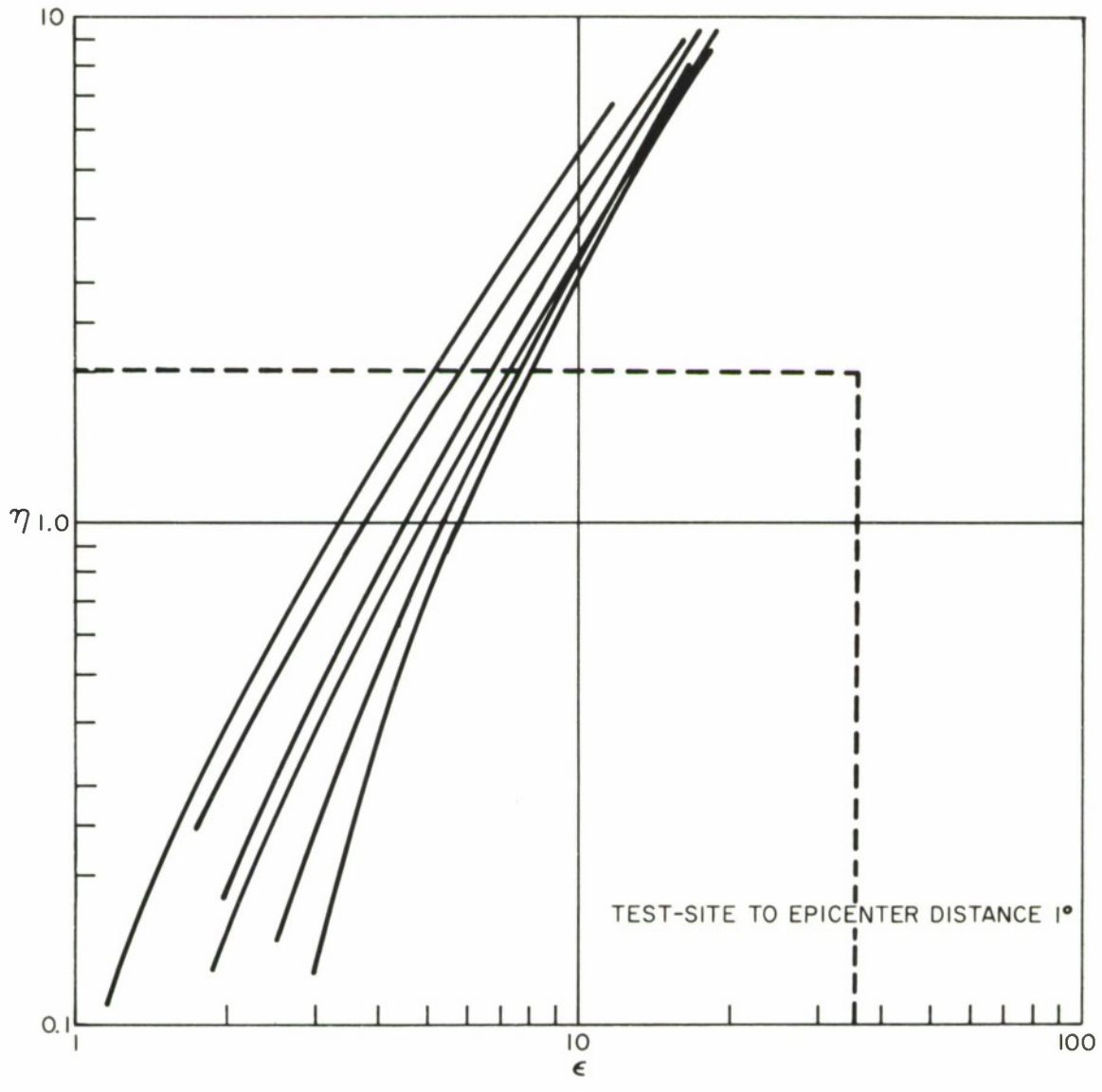

FIGURE 2.8A
RELATION BETWEEN ϵ AND η
(RECORDS NORMALIZED USING MAXIMAL-RATIO COMBINING)

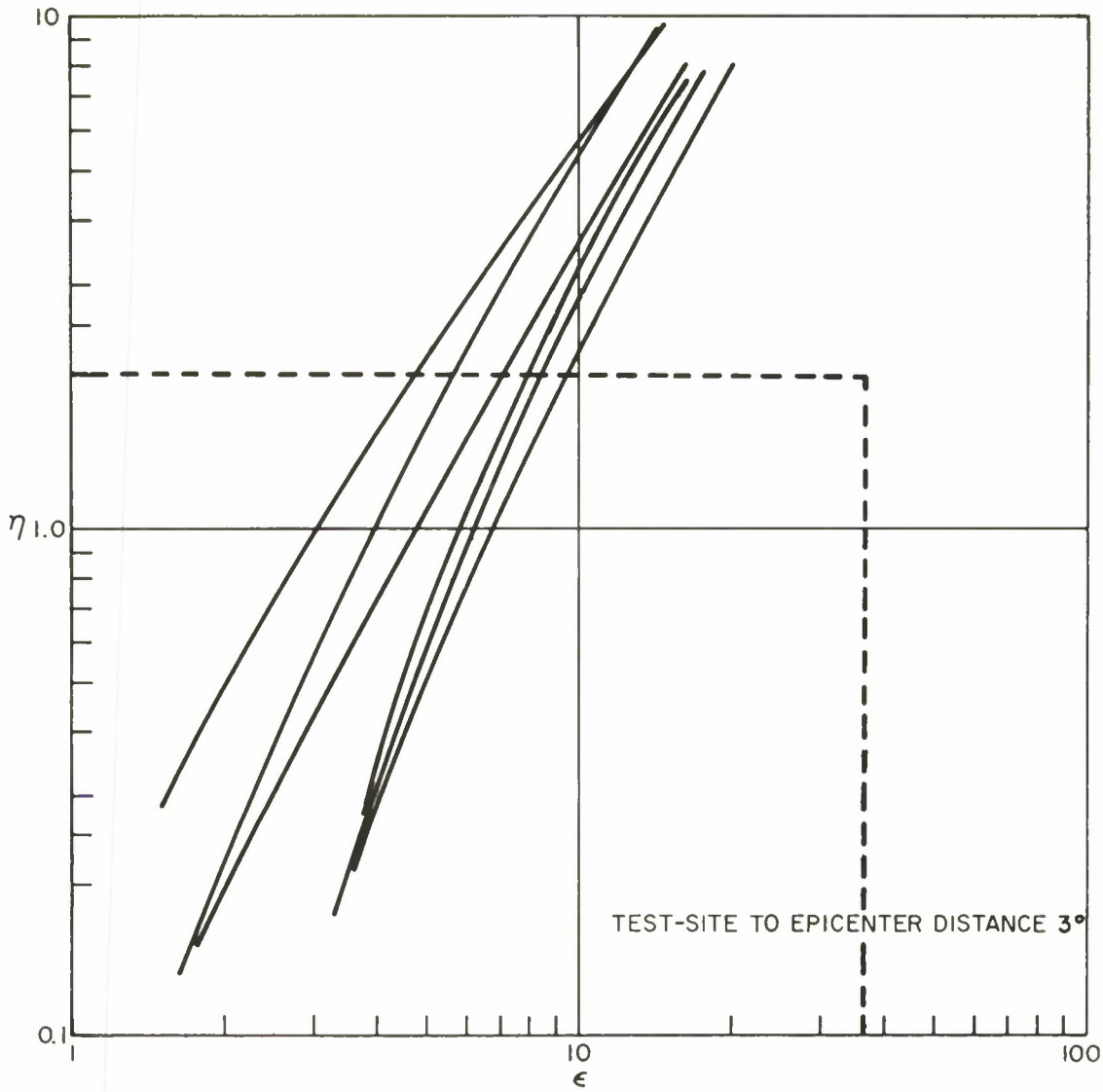

FIGURE 2.8B
RELATION BETWEEN ϵ AND η
(RECORDS NORMALIZED USING MAXIMAL-RATIO-COMBINING)

The difference is only minor in the case of the equal P-phase energy normalization, but it is quite large in the case of the maximal-ratio combining. For example, in Figures 2.8A and B, at the point where the η threshold is exceeded, ε is at only about one-fifth of its threshold. Therefore, comparing both statistics on the basis of a conservative (no false alarms) threshold, it appears that the η statistic is more sensitive by about a factor of five in power (roughly 7 dB). Furthermore, at the level at which detection occurs, ε is less than 10. This implies that detection is assured if a one-second interval of the array output has a power level that is 10 dB above that of the preceding five seconds, provided that the maximal-ratio array output is used, and the η statistic is used for detection. With this observation we can approximately describe the sensitivity of the array, as a function of grid point and delay, by examining the average energy in a five-second time window as a function of time after the earthquake for each grid point. For a given time and grid point it is assumed that the minimum detectable shot energy is 10 dB larger than the corresponding five-second average energy.

2.4 MINIMUM DETECTABLE MAGNITUDE AS A FUNCTION OF DELAY TIME AND GRID POINT

As suggested by the preceding paragraph the array's detection sensitivity for each grid point as a function of time can be calculated by computing average power curves for the array output that are smoothed over five seconds, and adding the 10 dB required for detection to these curves. Some results of this calculation are presented in Figures 2.9 through 2.11. Figure 2.9 shows the detectable magnitude of a nuclear test when the test site coincides with the earthquake's epicenter. From this figure it can be observed that a nuclear explosion of the same magnitude as the earthquake would not be detectable if the test site and the earthquake epicenter coincided and the explosion

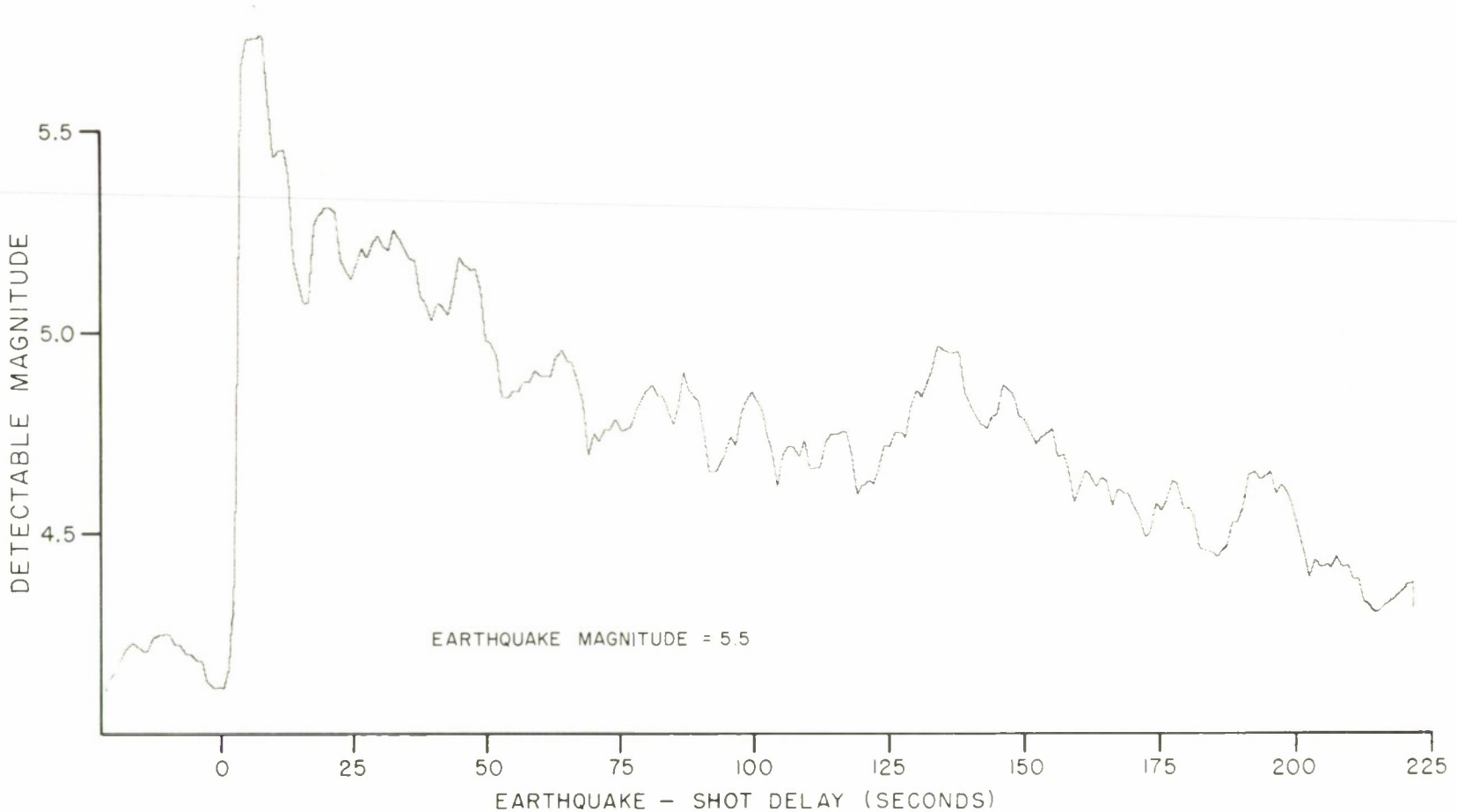

FIGURE 2.9
DETECTABLE MAGNITUDE VS. DELAY
(TEST-SITE LOCATED AT EPICENTER)

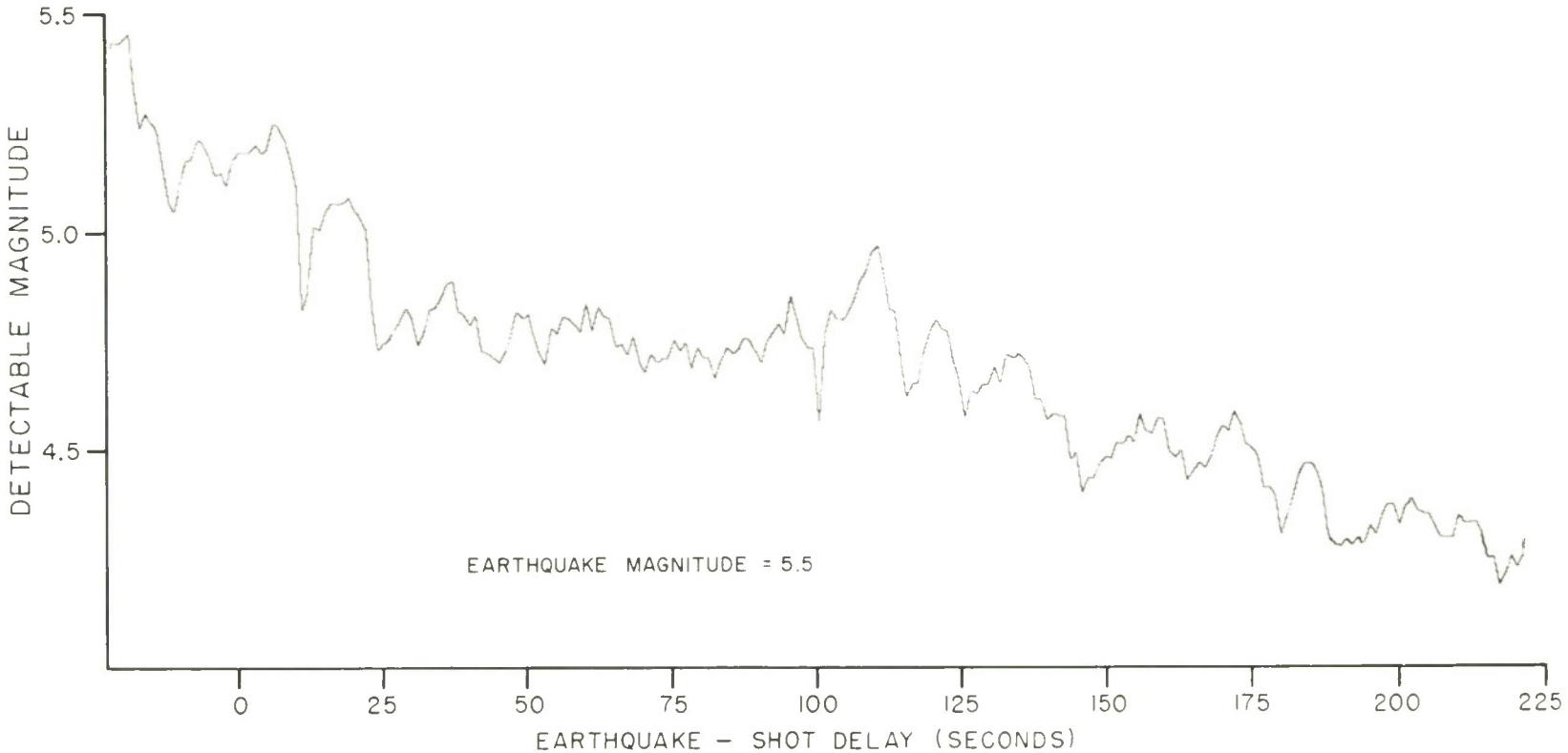

FIGURE 2.10
DETECTABLE MAGNITUDE VS. DELAY
(TEST-SITE LOCATED AT AZ = 240°, R = 3°)

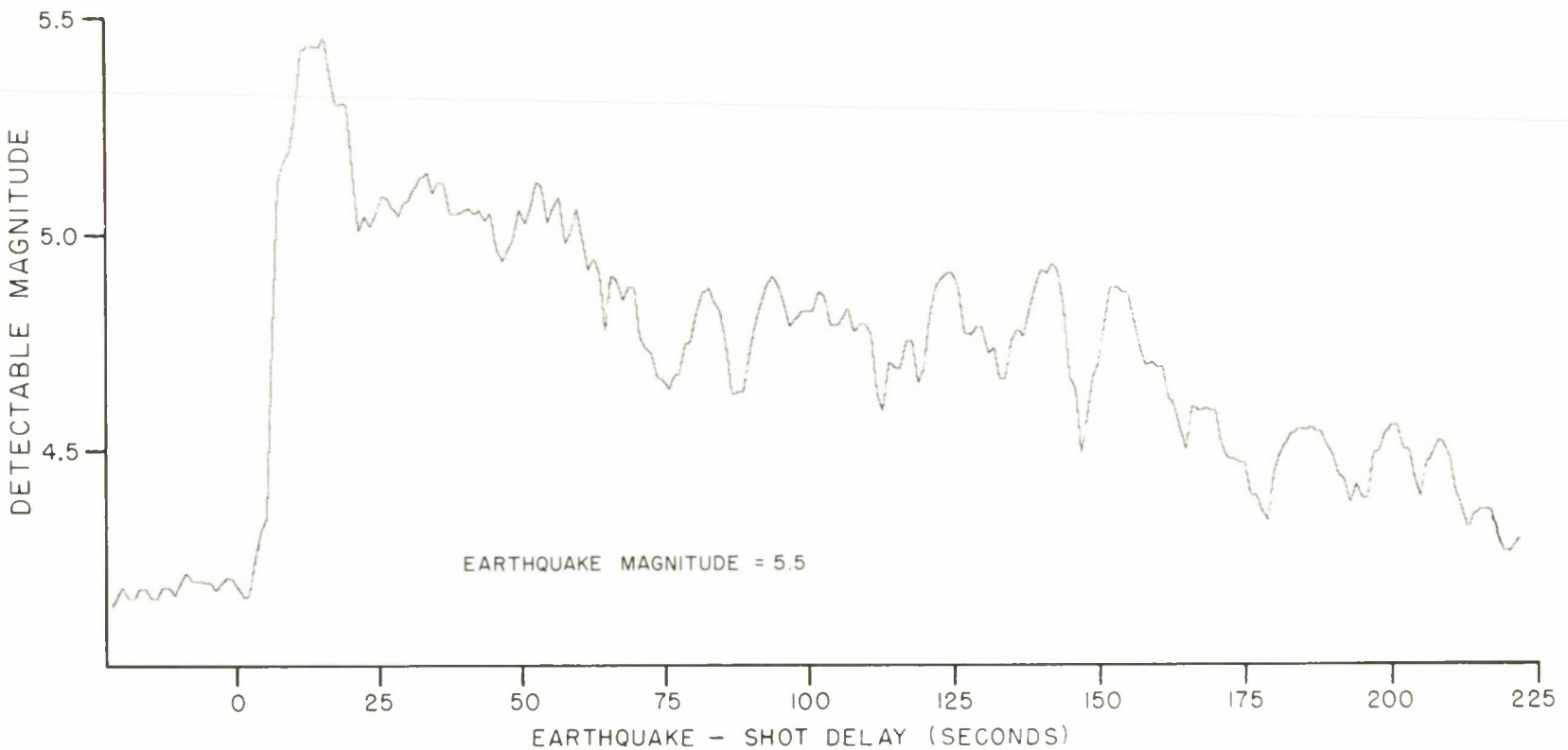

FIGURE 2.11
DETECTABLE MAGNITUDE VS. DELAY
(TEST-SITE LOCATED AT AZ = 0°, R=5°)

occured within 5-10 seconds after the earthquake. Similarly, it can be observed that a nuclear test which is 0.5 magnitude units smaller than the natural event will be detected if it occurs later than 50 seconds after the natural event and the epicenters coincide.

This same calculation performed for all of the grid points considered above indicates that a nuclear test with the same magnitude as the natural event considered, could be detected at all of the other grid points, independent of the earthquake-shot delay. Figures 2.10 and 2.11 show the detectable magnitude as a function of delay for two representative grid-points, Az = 0°, R = 5° and Az = 240°, R = 3°.

2.5 TIME INTERVALS AVAILABLE FOR CONCEALING NUCLEAR TESTS

The monitoring capabilities of the continental-size array will now be summarized in terms of the time intervals over which a nuclear test can be detonated without risk of detection for various points in the epicenter region. Figure 2.12 shows the time-intervals outside of which the detection system formed by a continental-size array and a single station network will detect an explosion of magnitude 5.0 for different test site locations. As in earlier figures, the earthquake's epicenter is in the center of the figure. The two numbers shown at each grid point correspond to the minimum delay imposed by the single-station network and the maximum delay imposed by the continental-size array. The minimum waiting time indicated in Figure 2.12 is a consequence of the assumed monitoring by a single station network, that is, well distributed in azimuth and located at an average range of 40° from the epicenter. Grid points marked with an X identify the test site locations for which the minimum waiting time is greater than the maximum imposed by the array. Observe that the system considered will detect a 5.0 magnitude explosion occurring with a delay greater than 50 seconds. When the test site does not coincide with the epicenter of the natural

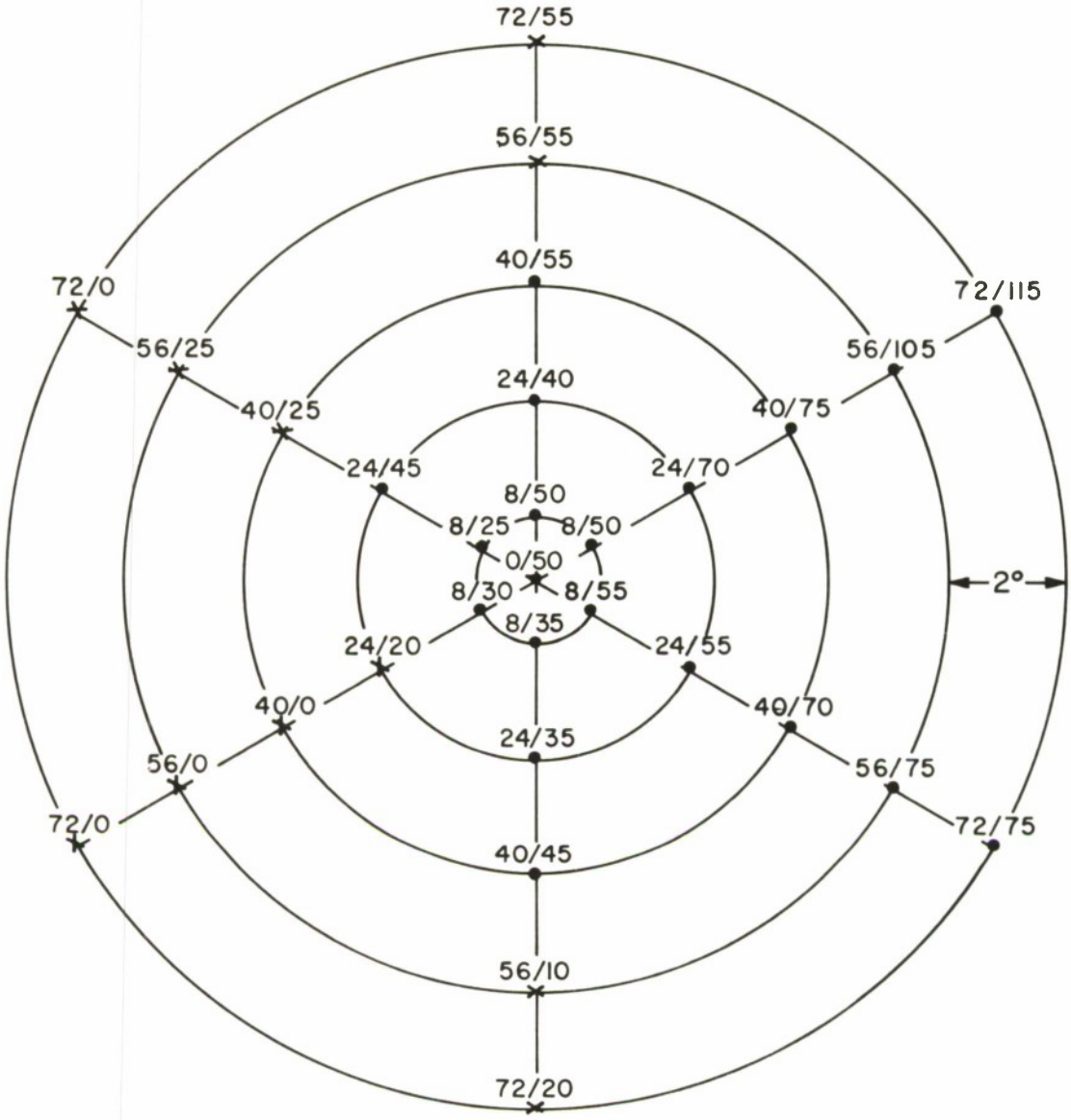

FIGURE 2.12
TIME INTERVALS AVAILABLE FOR CONCEALING
(TEST MAGNITUDE 5.0)

event, the time intervals in which explosions of 5.0 magnitude would not be detected are shorter than 50 seconds.

The continental-size array that is assumed in these calculations is located to the east of the earthquake's epicenter. Therefore, grid points shown on the right-hand side of Figure 2.12 are closer to the array than the earthquake epicenter. It can be observed that it is easier to detect an explosion when the array and the test site are located on opposite sides of the epicenter of the earthquake, than otherwise.

The presentation of Figure 2.12 is repeated in Figure 2.13 for the case of a mangitude 4.5 explosion, i.e., one magnitude unit less than the natural event. The minimum delay imposed by the single station network is, of course, the same as in Figure 2.12. However, the maximum allowable delay times are considerably larger. It can be seen that, for coincident epicenter and test site, a nuclear explosion would be detected with the system described only if it occurred with a delay greater than about three minutes.

An additional constraint on the maximum earthquake-nuclear explosion delay could be derived by considering the single-seismometer stations that are located on the opposite side of the epicenter from the continental array. Signals arriving at these stations from grid points situated between the epicenter and the array might arrive with a considerable delay. As an example, a nuclear explosion of magnitude 4.5 and which occurs at a site located on the grid point Az = 60° and R = 9° with a delay of 260 seconds, will arrive at some of the single stations (those for which the azimuth from the epicenter is approximately 240°) with a delay of approximately 330 seconds. Delays of this size might lead to detection of the signal arriving from the nuclear test on the record obtained from the single seismometer.

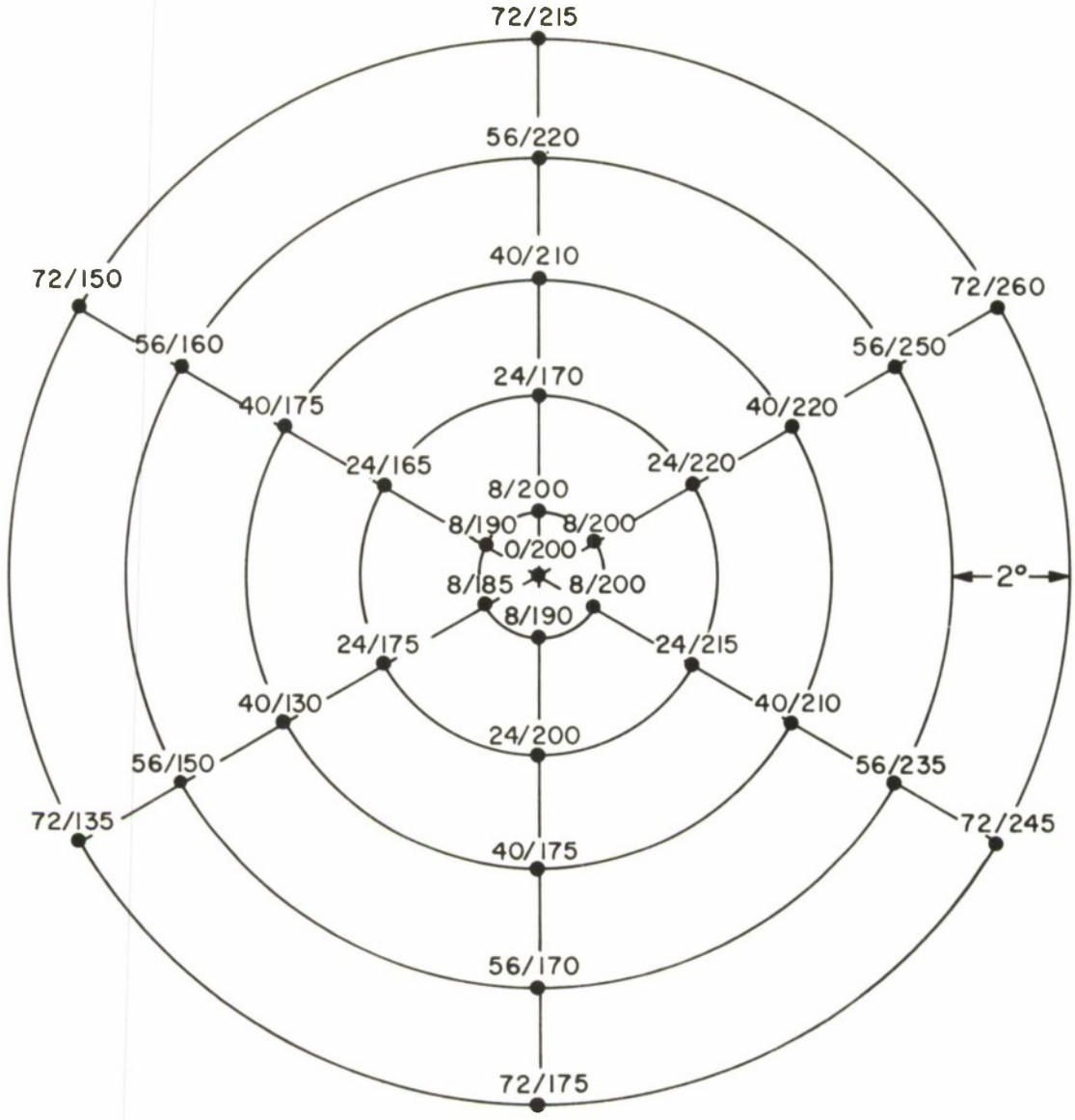

FIGURE 2.13
TIME INTERVALS AVAILABLE FOR CONCEALING
(TEST MAGNITUDE 4.5)

2.6 SUMMARY AND CONCLUSIONS

The capabilities of a hypothetical detection network, consisting of a continental-size array and a network of single stations, have been summarized in terms of the allowable time intervals during which a nuclear test could be detonated in the vicinity of an earthquake without risking detection, as a function of the magnitude of the test and the position of the test site relative to the array and the earthquake epicenter. These intervals are presented in Figures 2.12 and 2.13, for shots that are 1/2 and 1 magnitude unit smaller than the earthquake. The limitations imposed by these intervals suggest that the practical problems of concealing a nuclear test from a detection network of the sort described here would be quite formidable.

Unfortunately, an enormous number of computations would be necessary to implement the detection network. If it were only necessary to monitor a small number of potential test sites, the computation problem would, of course, be more manageable. One possibility for reducing the number of computations would be to increase the beamwidth of the array by reducing its aperture, but this would presumably degrade the sensitivity of the system.

The calculations presented in this section are all based on data from a single earthquake. As far as we know, there is nothing unusual about this earthquake and these results are representative of what could be obtained with other earthquakes. It would probably be useful, however, to process data from another event in order to confirm this conjecture and to see how much detailed variation there is between events. We do not anticipate that the detailed fluctuations between events would, in themselves, be of interest, except that knowledge of their extent would allow conservative detection levels to be estimated with some confidence that they would be generally applicable.

SECTION III

BEAMFORMING FOR EPICENTER LOCATION - THEORETICAL BACKGROUND

The problem of estimating epicenters of seismic events using only data from LASA-Montana has been studied by several groups. In an earlier report [5], we presented experimental results based on a beamsplitting technique and some tentative conclusions concerning the dependence of the precision of the epicenter estimates on certain parameters. As discussed in that report, the original motive for the beamsplitting technique was that the coherent nature of the processing would yield better results (perhaps at the expense of additional complexity) than could be obtained with conventional plane wave fits that were based upon independent time picks on the separate (noisy) seismograms. In many cases, at least, it now appears that travel-time anomalies, not additive noise, are the major contributor to errors in epicenter location. In these cases the original motive for using the beamsplit technique is no longer obviously valid. With this in mind, as well as our earlier experience reported previously, we have been re-examining the beamsplitting technique for locating epicenters with a view toward learning the irreducible limits on location precision and simplifying the complexity of the calculations used to make these estimates. In this section, we shall present theoretical analyses of some rather idealized problems that are related to the epicenter location problem. Results of simulation studies are discussed in Section IV.

The contents of this section are organized as follows. Section 3.1 states the assumptions that are common to all of the derivations. The most important of these are that an identical signal waveform is present at each seismometer, the noise waveforms are independent but share a common statistical description, and the signal-to-noise ratio is large enough that all errors are small. Section 3.2 summarizes the form of a least squares

(regression) fit to a set of time picks, and gives the variance in the estimate of a parameter, m, that is proportional to the cosine of the angle of incidence, in terms of the variance of the estimates of the individual time picks. Section 3.3 summarizes the performance of three methods of estimating individual arrival times: a zero crossing pick, a maximum value pick, and a cross-correlation with a perfect replica of the signal. Section 3.4 discusses the beamforming calculation and demonstrates its equivalence to the plane wave fit following a correlation time pick. The important point here is that the beamforming technique does not require prior knowledge of the detailed waveshape of the signal, whereas the correlation time pick does require this knowledge. Finally, Section 3.5 summarizes the results in terms of a few examples. In one of these, a 21-element, 200-km array with a 20 km/sec phase velocity, and a 10 dB signal-to-noise ratio, leads to a standard deviation in angular measurement of 0.3°. The details of the more involved derivations presented in this section are presented in Appendices A and B.

3.1 STATEMENT OF ASSUMPTIONS

We assume a uniform linear array with N elements indexed by i. The waveform at the i^{th} element is assumed to be given by

$$x_i(t) = s(t-im+\tau_i)+n_i(t) \qquad (3\text{-}1)$$

where the $n_i(t)$ are independent stationary noise processes with a common power density spectrum, $S_n(f)$, the τ_i are independent, identically distributed random variables that correspond to perturbations on the arriving wavefront, and s(t) is given by

$$s(t) = \sin 2\pi f_0 t \qquad -T/2 < t < T/2 \qquad (3\text{-}2)$$

$$= 0 \qquad \text{elsewhere}$$

where T is the period of the sinewave. The parameter m in Equation (3-1) is related to the velocity, c, the element spacing, Δ, and the angle of incidence, θ, by

$$\frac{\Delta}{c} \sin\theta = m \qquad (3\text{-}3)$$

where θ and c are both measured in the plane of the array.

For the application of interest here, $f_0 \approx 1$ Hz, but the parameter will be retained in the formulation in order to show parameter dependence and allow scaling of results.

We shall consider two general schemes for estimating the parameter m in Equation (3-1). The first will consist of estimating the "arrival time," y_i, from each of the $x_i(t)$; in the absence of noise this estimate would be

$$y_i = im - \tau_i \tag{3-4}$$

The y_i are then combined, e.g., by a least squares regression, to estimate m. (It is for this reason that we shall find it convenient to refer to m as the slope. It is the slope of the correct regression line; it is not the slope of the wavefront.) The second general scheme consists of forming a delayed sum for the array, $g(t,\hat{m})$.

$$g(t,\hat{m}) = \sum_{i=1}^{N} x_i(t+\hat{m}i) \tag{3-5}$$

and then choosing $\hat{m}$ to maximize the integral of $g^2(t,\hat{m})$ over some time interval.

3.2 SLOPE ESTIMATE FROM UNRELIABLE TIME PICKS

It is assumed that the observed arrival times are given by

$$y_i = im + b + z_i \tag{3-6}$$

where the z_i are zero-mean random variables with

$$\overline{z_i z_j} = \delta_{ij} \tag{3-7}$$

and m and b are unknown constants.

One way to estimate m is to choose $\hat{m}$ and $\hat{b}$ in such a way as to minimize the mean square error, $\varepsilon(\hat{m},\hat{b})$:

$$\varepsilon(\hat{m},\hat{b}) = \frac{1}{N} \sum_{i=1}^{N} (y_i - i\hat{m} - \hat{b})^2 \tag{3-8}$$

This defines the standard regression fit to the data points, and it is easy to show that $\hat{m}$ is given by the following expression.

$$\hat{m} = \frac{\sum_{i=1}^{N} (i - \frac{N+1}{2}) y_i}{\frac{1}{12} N(N^2-1)} \tag{3-9}$$

which may be rewritten using Equation (3-6) to yield

$$\hat{m} = m + \frac{\sum_{i=1}^{N} (i - \frac{N+1}{2}) z_i}{\frac{1}{12} N(N^2-1)} \tag{3-10}$$

The variance of $\hat{m}$ may be calculated from Equation (3-10) and the result is

$$\text{var}[\hat{m}] = \frac{12}{N(N^2-1)} \tag{3-11}$$

It should be recalled that this is based on the z_i having unity variance; Equation (3-11) may be generalized by multiplying the right side by the variance of the z's.

Several observations about the estimate given by Equation (3-10) may be made. The estimate was derived by minimizing the mean square error given by Equation (3-8). It turns out that the estimate weights the time measurements linearly with distance from the center of the array, as would seem intuitively reasonable. In the case that the z_i are Gaussian, the estimate given by Equation (3-9) may be shown to be maximum likelihood and minimum variance. In the case where the z_i are not Gaussian, it is not obvious that the least squares criterion results in a minimum variance estimate of m. One generalized class of estimates can be obtained by changing the weights applied to the y_i in Equation (3-9) (and appropriately correcting the denominator to maintain an unbiased estimator). It turns out that this is equivalent to minimizing a weighted error function:

$$\varepsilon_w(\hat{m},\hat{b}) = \frac{1}{N} \sum_{i=1}^{N} (y_i - i\hat{m} - \hat{b})^2 a_i \tag{3-12}$$

It may be shown that of all possible choices of the weights, a_i, the uniform weights ($a_i = 1$) lead to the minimum variance estimate of m [6]. Thus the estimate of Equation (3-9) appears reasonable for more than just Gauss errors.

3.3 ACCURACY OF TIME PICKS ON INDIVIDUAL RECORDS

There are several ways in which the arrival time for a given record might be estimated. In this section we shall discuss the statistical properties of three methods. Our objective in considering these methods is to indicate how the variance of the time picks (and hence that of $\hat{m}$) might depend on the level and shape of the noise spectrum. As before (see Equations 3-1 and 3-2) we assume that each record consists of one period of a sine wave plus stationary noise, and it is desired to estimate the "arrival time" of the signal. The three cases derived in Appendix A are: 1) the zero crossing near the center of the transient is selected, 2) the point of maximum value near the end of the transient is selected, and 3) the record is correlated with a perfect replica of s(t) and the time of maximum correlation is selected. The variances of the time picks due to the noise are given as σ_1^2, σ_2^2, and σ_3^2 for the three methods. (See Equations A-8, A-9 and A-17 of Appendix A.) In all three derivations, large signal-to-noise ratios and small errors are assumed.

$$\sigma_1^2 = \frac{1}{\omega_0^2} \int S_n(f)df \tag{3-13}$$

$$\sigma_2^2 = \frac{1}{\omega_0^2} \int \left(\frac{f}{f_0}\right)^2 S_n(f)df \tag{3-14}$$

$$\sigma_3^2 = \frac{1}{\omega_0^2} \int \left[\frac{2}{\pi}\left(\sin\pi \frac{f}{f_0}\right)\left(\frac{ff_0}{f_0^2-f^2}\right)\right]^2 S_n(f)df \tag{3-15}$$

where $\omega = 2\pi f$ is used for convenience in some of the expressions.

A quick check on the consistency of Equations (3-13)-(3-15) is the case of extremely narrowband noise, for which $S_n(f)$ consists only of impulses at $\pm f_0$. In this case all three variances are equal, as would be expected. It does appear to be possible to choose a power density spectrum for the noise such that the third case is worse than the first case, but for most reasonable assumptions about the power density spectrum of the noise, one would guess that the correlation technique would lead to a better estimate than the zero crossing estimate. This seems like a reasonable intuitive guess simply because the correlation estimate involves an integration over time that should help to reduce the effects of the noise.

It is difficult to make general conclusions about the relative size of the three variances without making specific assumptions about $S_n(f)$, since the multipliers of $S_n(f)$ in each of the integrands of Equations (3-13)-(3-15) do not satisfy the same rank ordering for all f. Comparing σ_1^2 and σ_2^2, it is clear that the shape of $S_n(f)$ is important. The time pick based on the maximum is less (more) sensitive to noise below (above) f_0 than the time pick based on the zero crossing. The reasonableness of this result can be understood by considering the effects of the extremes of a dc offset or a low level high frequency noise on the two picks. Comparing σ_1^2 and σ_3^2 is a little more difficult. The multiplier in the integrand of Equation (3-15) is less than unity for most, but not all, f. (It equals unity at $f=f_0$ and reaches a maximum at a slightly higher frequency.) Therefore, it would be expected in general that $\sigma_3^2 < \sigma_1^2$ but there do exist (rather artificial) cases where the reverse is true.

If in the third case, white noise of spectral level N_0, is assumed,

$$S_n(f) = N_0 \tag{3-16}$$

The variance of the time estimate turns out to be

$$\sigma_3^2 = N_0/\pi\omega_0 \tag{3-17}$$

In order to compare this result to the variance that would obtain in the case of a zero crossing time pick, assume that the power density spectrum of the noise is given by

$$S_n(f) = N_0 \qquad |f| < B \tag{3-18}$$
$$= 0 \qquad |f| > B$$

Then it follows that

$$\sigma_1^2 = \frac{N_0}{\pi\omega_0}\frac{2\pi B}{\omega_0} \tag{3-19}$$

The motive for the different assumptions about the power density spectrum is that the correlation technique implies a filtering of its own, whereas the zero crossing time pick does not. Clearly, if there were a good deal of noise energy in a different region of the spectrum than the signal energy, it would be sensible to filter it out before choosing the time of the zero crossing. The parameter B in Equation (3-18) would presumably be somewhat larger than f_0, but not very much larger. This being the case, it may be seen that the variance for the zero crossing pick is not very much larger than that of the correlation pick. Furthermore, in writing Equation (3-18) we have excluded the possibility of filtering out the very low frequency region of the noise, which presumably could be done without serious distortion of the signal. The principal conclusion intended from Equations (3-17) and (3-19) is that while the correlation time pick is usually superior to that of the zero crossing time pick, it appears that the principal reason for this is that a narrowband filtering is involved, and if an equivalent narrowband filtering is inserted before the zero crossing time pick, relatively little difference would exist between these two estimates. It should be stressed that all of these comments are based on the assumption of identical signals at each element. If this is not the case, the correlation pick would presumably be degraded. Furthermore, in the case of the zero crossing pick with nonidentical signals, the effect of prefiltering would have to be carefully considered.

3.4 BEAMFORMING

The beamforming technique of estimating epicenters for seismic events is fundamentally different from the plane-wave-fit technique discussed above. In the beamforming technique the array is "steered" to several trial epicenters and the epicenter yielding the largest energy in the array output is chosen as the estimate of the true epicenter. The steering of the array is accomplished by aligning each seismogram before addition in such a way that if the test epicenter were the true epicenter, the signal portion of each waveform would add coherently in the array output. In general, it would be expected that the beamforming technique involves more computations than the conceptually simpler plane-wave fit based on separate time picks from each channel. More calculations are involved because, unless some simplification is developed, the array output must be calculated for several steerings of the beam and each array output is based on a delay-and-sum computation. The question naturally arises as to why beamforming should be used for the location of seismic events. The principal reason is that it may be a useful technique for reducing the noise contribution to epicenter location errors. This would be expected because the beamforming technique is coherent in the sense that all of the signals are added prior to any estimation procedures and, in general, predecision processing is preferable to other alternatives. A secondary reason for using beamforming rather than the plane-wave fit is that the best of the time pick procedures discussed above depends upon perfect knowledge of the waveshape of the signal component in each record. The beamforming technique does not require perfect knowledge of the signal, although, in its simplest form, it does assume that the same signal is present at each seismometer. It will be shown below that in the case of small errors the beamforming technique is essentially equivalent in performance to the correlation time pick followed by a plane-wave fit. This derivation will be presented to indicate the potential value of the beamforming

technique: results comparable to those obtainable from the best of the other techniques may be achieved without prior knowledge of the signal waveform.

In the two-element case the beamforming estimate of the slope, m, is obtained by maximizing the following expression:

$$\int[x_1(t)+x_2(t+\hat{m})]^2dt = \int[s(t)+n_1(t)+s(t+\hat{m}-m)+n_2(t+\hat{m})]^2dt \quad (3\text{-}20)$$

In this derivation it is assumed that the limits of the integral loosely bound the duration of the signal term. In this derivation, as well as all others in this section, a large signal-to-noise ratio will be assumed so that there is little difficulty in approximately locating the signal and thereby setting the appropriate limits on the integral. The choice of $\hat{m}$ in Equation (3-20) influences the value of the integral only through the cross-terms obtained by expanding the square. Therefore, Equation (3-20) will be maximized when the expression below is maximized.

$$\int[s(t)s(t+\hat{m}-m)+s(t)n_2(t+\hat{m})+s(t+\hat{m})n_1(t)+n_1(t)n_2(t+\hat{m})]dt \quad (3\text{-}21)$$

If we neglect the second order noise term, what remains is an expression very similar to the expression that would appear in the case of a time pick via correlation with a perfect replica of the signal. In the case of the correlation time pick (see Appendix A) there is only a single signal-noise term instead of the two cross-terms that appear in expression (3-21). Otherwise the expression given in (3-21) is identical to the one that appears in the case of a correlation time pick. From this observation it follows that the variance of the estimate $\hat{m}$ in this problem will be twice the variance calculated for the correlation time pick and given by Equation (3-15). If the slope $\hat{m}$ were estimated by using the correlation time pick on each of the two elements and then drawing a straight line between the resulting estimates, the variance in the resulting estimate would also be twice that of the estimate of the individual time picks. Therefore, it may be concluded in the two-element case that, correct to first order

effects of the noise, the beamforming technique yields an estimate of the slope that has the same variance as that obtained by making independent correlation time picks in each waveform and drawing a straight line between the resulting times. This observation indicates the superiority of the beamforming technique in the two-element case since no prior assumption about the signal is necessary to carry out this technique, whereas a perfect replica of the signal is used in the correlation time picks involved in the other technique.

The two-element case has been presented here because the equation is sufficiently simple that it is easy to relate this problem to that of the correlation time pick. The N-element case is somewhat more complicated (and hence less transparent) and is considered in Appendix B. It turns out that just as in the two-element case, assuming large signal-to-noise ratios, the beamforming technique and the plane-wave fit based on correlation time picks are completely equivalent. Thus, as noted above, the beamforming technique appears especially valuable in the case of consistent, but unknown, signal waveshapes.

The derivation in Appendix B that is cited in the preceding paragraph assumes a perfectly planar wavefront corrupted by additive noise. The complementary derivation also appears in Appendix B: no noise, but random small perturbations on the plane wavefront. In both cases the beamforming calculation yields the same result as the plane-wave fit. It appears that the same result would apply (still considering only first order effects) in the combined case of noise and travel-time errors, but we have not bothered to demonstrate this.

3.5 EXAMPLES

In order to summarize the preceding theoretical results, we shall consider some specific parameter values. If we assume a uniform N-element array of total aperture 200 km, and a phase velocity of 20 km/sec, we have (see Equation 3-3):

$$m = \frac{\Delta}{c} \sin\theta = \frac{\frac{200}{N-1}}{20} \sin\theta = \frac{10}{N-1} \sin\theta \qquad (3\text{-}22)$$

With a timing error variance of σ_τ^2 we would have (see Equation 3-11)

$$\text{var } \hat{m} = \left(\frac{10}{N-1}\right)^2 \text{var } \sin\hat{\theta} = \frac{12}{N(N^2-1)} \sigma_\tau^2 \qquad (3\text{-}23)$$

If we assume that θ is close to 0,

$$\text{var } \sin\hat{\theta} \simeq \text{var } \hat{\theta} \qquad (3\text{-}24)$$

and, therefore,

$$\text{var } \hat{\theta} = \left(\frac{N-1}{10}\right)^2 \frac{12}{N(N^2-1)} \sigma_\tau^2$$

$$= \frac{12}{100} \frac{N-1}{N(N+1)} \sigma_\tau^2$$

$$\sigma_\theta = 0.35\sqrt{N-1/N(N+1)}\ \sigma_\tau \qquad (3\text{-}25)$$

To be more specific, the radical in Equation (3-25) is approximately 0.28 (0.21) for N = 11 (N = 21). Assuming an 11-element array, we have

$$\sigma_{\hat{\theta}} \simeq 0.1\sigma_\tau \qquad (3\text{-}26)$$

where it should be recalled that τ is measured in seconds and θ in radians.

If the τ's were uniform over the interval $0 \pm 1/40$ sec, as could occur as a result of unsynchronized 20/sec sampling, we would have

$$\sigma_\tau = \sqrt{3}/3 \cdot 1/40 = 0.0144$$

$$\sigma_{\hat{\theta}} = 0.00144 \text{ radians} \qquad (3\text{-}27)$$

$$\simeq 0.08°$$

[With the 21-element array this number would be 0.06°.]

Using Equation (3-3) we can calculate what noise level would contribute the same amount of uncertainty in the time pick for a zero crossing time pick. Assuming f_0=1, and defining (S/N) as the ratio of the signal energy to the average noise power, we have

$$\sigma_\tau^2 = \frac{1}{\omega_0^2} \int S_n(f)df$$

$$= \frac{1}{(2\pi)^2} \frac{1}{\frac{1}{2}(S/N)} = \frac{1}{2\pi^2(S/N)} \qquad (3\text{-}28)$$

The σ_τ given by Equation (3-27) implies a (S/N) given by

$$(S/N) = \frac{3\cdot(40)^2}{2\pi^2} = 270 \simeq 24 \text{ dB} \qquad (3\text{-}29)$$

As another example, with the 11-element array, Equations (3-28) and (3-26) imply that a 10 dB signal-to-noise ratio leads to

$$\sigma_\tau^2 \simeq 0.005$$

$$\sigma_{\hat{\theta}} \simeq 0.4^\circ \qquad (3\text{-}30)$$

A 21-element array of the same dimensions would imply

$$\sigma_{\hat{\theta}} \simeq 0.3^\circ \qquad (3\text{-}31)$$

SECTION IV

BEAMFORMING AND OTHER METHODS FOR EPICENTER LOCATION SIMULATION RESULTS

The results of a number of simulated angular measurements using the center elements of the LASA subarrays are described in this section. As described in Section III, the analytical approach toward specifying uncertainties in angular measurements resulting from additive noise or travel-time anomalies requires a number of assumptions that may not be realistic. For this reason, it was decided that a better understanding of the effects of these kinds of interference might be obtained from a number of computer-simulated measurements. To perform these simulations, the seismograms from a magnitude-5.8 Kazakh event (as recorded at the center elements of the twenty-one LASA subarrays) were used as input signals. These signals were chosen for two reasons. First, the signal-to-noise ratio of the individual seismograms was high (20 dB or greater); by adding different amounts of noise, it was therefore possible to simulate a wide range of signal-to-noise ratios. Moreover, with this high signal-to-noise ratio, it was possible to remove travel-time anomalies from the original records prior to the simulation so that controlled anomalies could be inserted and their effects studied. Second, this collection of seismograms is typical of those received from teleseismic ranges. Since the records differed from sensor to sensor, calculations with these signals are expected to be far more realistic than those which could be made assuming identical seismic signals.

To simplify calculations these seismograms were aligned, in time, so that they appeared to have come from an epicenter due north of the array at a range corresponding to a phase velocity of 20 km/sec ($\approx 80°$). No attempt was made to compute epicenter locations, but rather the effects of additive noise and local travel-time anomalies on arrival angle were studied. Further, computations were limited to the case of a constant phase velocity

(azimuth scan), since the results obtained in this manner are directly translatable to errors in range, and hence to errors in epicenter determination.

This discussion begins with a description of the four methods of angular measurement that have been studied: plane-wave fit, analog peak-signal and energy beams, and a DIMUS beam. Following this, a method of automatic time-of-arrival measurement that has been employed as an input for all of the angle measurement system mentioned above will be discussed. The ground rules of the actual computations will then be discussed, and the results of the computations presented. Finally, comparisons, where possible, will be made with the theoretical discussion of Section III.

4.1 PLANE-WAVE FIT

The following procedure was used to determine the least-squares, plane-wave fit to the arriving signals. First, it is assumed that the general angle of arrival of the plane wave is known to within a small error. In the simulations, the correct arrival azimuth, due north, was taken. Next, a line is drawn through the center element of the array (A0) perpendicular to the assumed direction of the arrival of the plane wave. Projections of the various center elements of the LASA clusters on this line permit the determination of the incremental time shifts that must be applied to the various seismograms in "steering" the array in the vicinity of due north. Next, arrival times of a particular feature (in this case a zero crossing of the signal that is chosen in a manner that will be described below) of the signals for each seismogram are compared with the corresponding arrival time for the A0 seismogram. Arrival time differences for these various records are then converted to distances, using the assumed phase velocity of 20 km/sec and the geometry of the projection of the array. A least-squares fit of these distances to a line passing through A0 gives a measure of the difference

between the assumed angle of arrival and that which is estimated from the data. Since the assumed angle of arrival is the correct one, the computation gives a direct measure of the error in angular measurement that would be obtained using this method.

4.2 ANALOG BEAM - PEAK SIGNAL

This method of angular measurement, and all others discussed in this report, assumes that the incoming signal can be characterized as a plane wave. With this assumption, the array is steered to successive angles, and the maximum value of the array output for each angle is taken to be the value of the array pattern for that angle. The angle of arrival of the signal is defined as the angle for which this pattern assumes its maximum value.

A more detailed description of this calculation follows. First, the seismograms from each element of the array are normalized so that the peak of the absolute value of the signals is identical for all sensors. The various signals are then advanced or delayed in time. These delays are computed from the projection of the location of the sensors on a line through the center of the array, the steering angle, and the assumed phase velocity of 20 km/sec. The seismograms are then summed, and the sum is examined in a time window of two seconds centered on the arrival time of the signal at the center element of the array. The peak of the absolute value of the sum seismogram in this time window is taken to be the array output. The choice of time window was made to include the coherent portions of the seismograms, and to allow for some advance and retardation of signals from sensors other than the one at the center of the array.

For all pattern calculations described in this section, the patterns were developed in 0.1° steps for the region of $\pm 3°$ about the assumed angle of arrival. In an attempt to minimize fine structure in the main lobe of the array patterns obtained, local averaging of the pattern was performed. Each point of the

patterns presented represents the average of the five adjacent points of which it is the center. No analytical optimization of this smoothing was attempted, and in fact, the experimental results suggest that further smoothing might produce better results.

4.3 ANALOG BEAM - ENERGY

This computation of the angle of arrival of signals corresponds exactly to that just described, except that the beam output is taken to be the energy contained in the time window rather than the peak signal in this interval. This is essentially the beamforming calculation that is considered in Section III. This method was expected to perform somewhat better than the peak or plane-wave fit in the presence of low signal-to-noise ratios.

4.4 DIMUS BEAM

With a DIMUS processor, the outputs of the sensors of the array are hardlimited before any array processing takes place. Thus the array output consists of the summation (properly delayed in time) of the hardlimited outputs of the various sensors of the array. The peak value definition of a pattern would not be satisfactory in this case, since the peak value of this summed seismogram in the time window described above, is constant over the range of angles which fall between the 3 dB points of the analog (peak) beam pattern. This is because the relative time delays that are required across the array to cause the conventional array pattern to fall to the 3 dB level correspond roughly to a relative time offset of one-half period between sensors located at the extremes of the aperture of the array. With hardlimited signals, this is precisely the minimum time shift which can cause any change in the array output, since the hardlimited signals remain constant over each half cycle of the signals.

Because of this property we have devised an alternate calculation for the DIMUS array measurements of angle, in which the conventional hardlimited outputs of the sensors are replaced

with synthetic seismograms which are zero except in the vicinity of the zero crossings of the original seismograms. At those sample points at which the original seismogram possesses a zero crossing, that sample point, and the one immediately succeeding, are set to unity with a sign which corresponds to the direction of the zero crossing of the original seismogram. These synthetic seismograms are then delayed, as in the case of steering an analog beam, and summed. This summed seismogram is then squared, and the integral, with respect to time, is taken over the two-second interval centered around the onset of the arrival time of the seismic signal.

Since the total information of the hardlimited inputs to the DIMUS must be contained in the zero crossings of the signals, this form of processing gives large outputs when zero crossings of the same sign are coincident in the synthetic seismograms (n^2 vs. n, where n is the number of (coincident) zero crossings), and also gives a premium for alignment of several zero crossings in sequence (a factor of m, where m is the number of successive zero crossings within the time window).

4.5 AUTOMATIC DETECTION OF ARRIVAL TIME

The various methods of angular determination described in the preceding sections all require a knowledge of the onset time of the signal at the array. Although this arrival time is known *a priori* from the construction of the simulation tests, it was believed that the simulations would be more realistic if they included, as an integral part of the calculations, the automatic detection of arrival time as measured from the seismograms themselves. The implementation of this automatic detector was carried out with the output of the unphased sum of a DIMUS beam as discussed in a previous report [7]. It has earlier been shown that with DIMUS processing, it is very likely that the first motion of seismic signals will be emphasized, and in fact nearly always will result in DIMUS outputs that saturate during the first few half cycles of the seismic record [8]. Thus, in the case of

the simulation tests, it is expected that the portion of the DIMUS output corresponding to first motion will be nearly equal to 21 (the number of seismometers in the array). Hence, if the magnitude of the DIMUS output exceeds a threshold set at 18, the following zero crossing should correspond to that which we have used as a definition of arrival time. This zero crossing on the sum seismogram is then used as a reference point, and the individual seismograms are searched in the vicinity of this time for zero crossings of the same polarity as that for the array output. These zero crossings are then identified as the arrival times of the signals at the various sensors.

Of course, the output of the DIMUS will be a function of the direction in which the array is steered; however, as previously stated, the peak signal output from the array is expected to be only a weak function of angle in the vicinity of the actual arrival angle of the wavefront. To test the validity of this assumption, a linear array (11 elements) with a 200 km aperture was synthesized using eleven of the seismograms used for the rest of the simulation tests, and the array was scanned in three-degree steps with a signal-to-noise ratio of 3 dB. Results of this simulation are shown in Figure 4.1. From the figure, it can be seen that, provided the DIMUS beam is steered within a small region (several degrees) of the true arrival angle, the detector should respond properly. Hence, the unphased DIMUS detector appears to work well, and, since the automatic detection of arrival times makes for a more realistic simulation, it was employed in all of the calculations presented here.

Before proceeding, it should be noted that the DIMUS detector did not always identify the proper zero crossing in the simulations. On occasion it picked either the actual onset of first motion of the signals or the second zero crossing after this time. Examination of results obtained using only the proper zero crossing, as opposed to using all results,

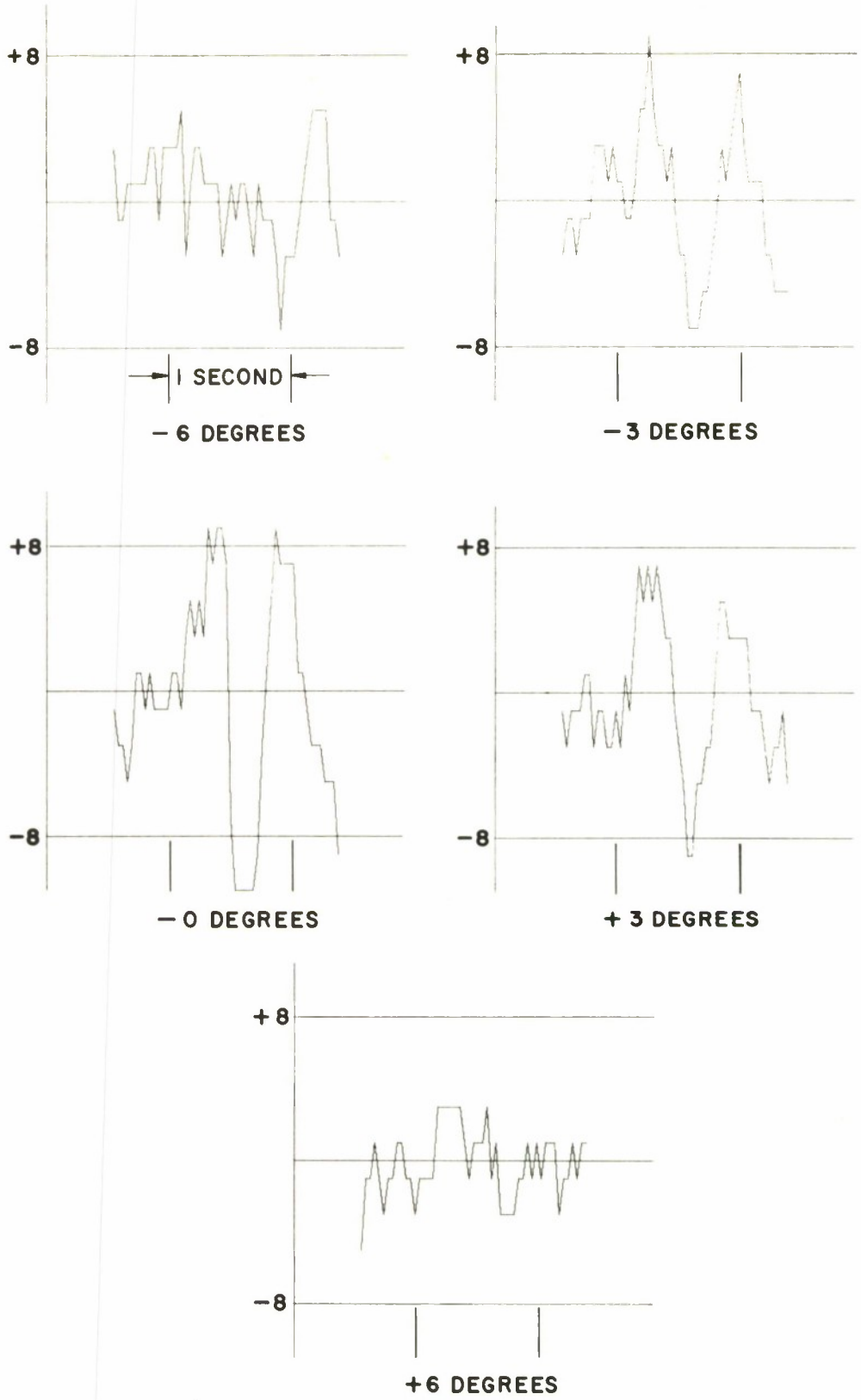

FIGURE 4.1
DIMUS ARRAY OUTPUTS FOR SELECTED AZIMUTHS
SIGNAL TO NOISE =3dB

showed no significant difference in the angular measurements to be discussed in later sections. As a result, no further attention was paid to this phenomenon.

4.6 METHOD OF ADDING NOISE AND ANOMALIES

The noise samples added to the various seismograms to test the effects of signal-to-noise ratio on angular accuracy were developed in the following manner. A random number generator was used to develop twenty-one uncorrelated series of numbers for each simulation trial. These series of numbers were taken to be samples of noise taken 0.05 seconds apart. To tailor the spectrum to these noise signals to represent an approximation of seismic noise, each series was passed through a recursive filter, derived from a three-pole Butterworth filter, with 3 dB points at 0.5 and 1.5 Hz. The twenty-one independent noise records thus obtained were scaled by an appropriate constant and added to the twenty-one input seismograms. As stated earlier, these seismograms are normalized so that the peak value of each, in the time window from first motion to one second later, is equal to unity. The noise scale factor was obtained for each signal-to-noise ratio by assuming that each of the original seismograms had the same signal energy as one period of a 1 Hz sinewave of unity peak value for two trials -- one at 10 dB, and one at 3 dB signal-to-noise ratio. Successive trials were then made with different sets of noise samples. Twelve such pairs of trials were included in the simulations reported here.

For the simulations used to study the effects of local travel-time anomalies, the following procedure was used. For each trial, a set of twenty independent random numbers was generated from a uniform distribution defined between $\pm n/20$ sec, where n is the maximum error in sample points. The resulting numbers were rounded off to the nearest number of sample points (between $\pm n$) and applied as delays to each of the seismograms, except A0. Nine simulations each were made for n=1 and n=2. It should be

noted that the resulting (discrete) anomaly distributions are not quite uniform. (The probabilities associated with $\pm n$ are too small by a factor of 1/2.) The standard deviations of the anomalies generated as described were 0.035 and 0.07 seconds, respectively.

4.7 RESULTS WITH NOISE ALONE

Results of the simulations with noise alone can be illustrated by Figures 4.2, 4.3 and 4.4. Figure 4.2 gives representative seismograms at element B1. Figure 4.3 shows the outputs of the analog and DIMUS beamformers for one trial with a signal-to-noise ratio equal to 10 dB. Also illustrated in this figure are the analog array peak and energy patterns, as well as the DIMUS array pattern. On these patterns, a + indicates the peak of the pattern and a Δ, the angular location of the plane-wave fit. Figure 4.4 is the same presentation for a signal-to-noise ratio of 3 dB. Figure 4.5 presents histograms of the number of trials with a given error in angular measurement for each of the four computation schemes employed: plane-wave fit, analog peak and energy patterns, and the DIMUS pattern. Both the 3 and 10 dB cases are included. From the figure it can be stated that the distribution of errors appears nearly uniform for the lower signal-to-noise ratio, and approaches a more peaked shape for the higher signal-to-noise ratio.

Table I summarizes these results in terms of the means and standard deviations of the angle estimates without regard to *a priori* knowledge of the actual arrival angle. Examination of the table permits several observations. First, there appears to be a bias in the estimate of the arrival angle, which shows a general decrease with increasing signal-to-noise ratio. Second, the standard deviation of the error in measurement of arrival angle (from the mean of the data) generally decreases with increasing signal-to-noise ratio. Finally, the errors in measurement obtained with a signal-to-noise ratio of 10 dB are within acceptable limits for azimuth determination in an operational system.

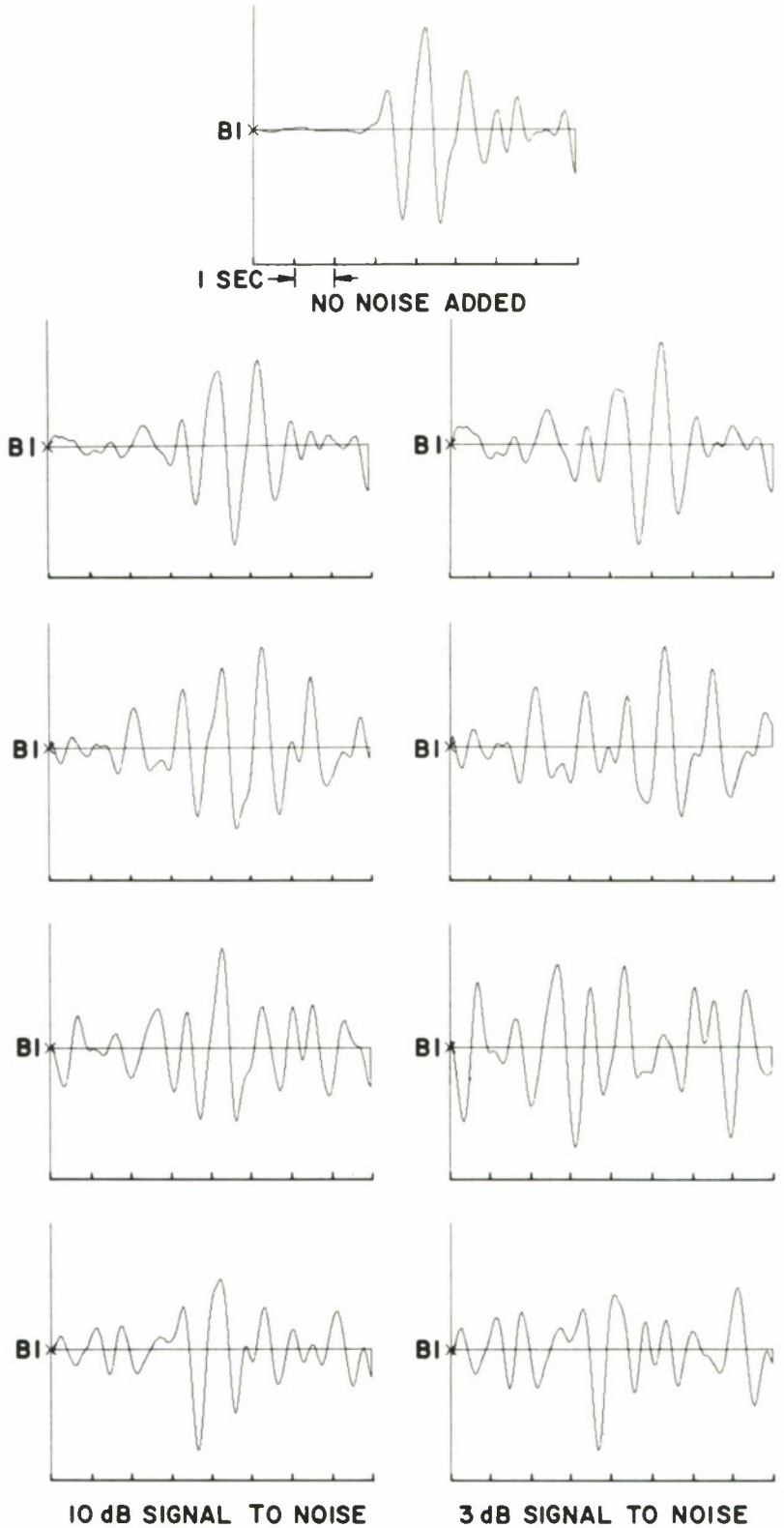

FIGURE 4.2
SIGNAL SEISMOMETER OUTPUTS FOR NINE SIMULATION TRIALS

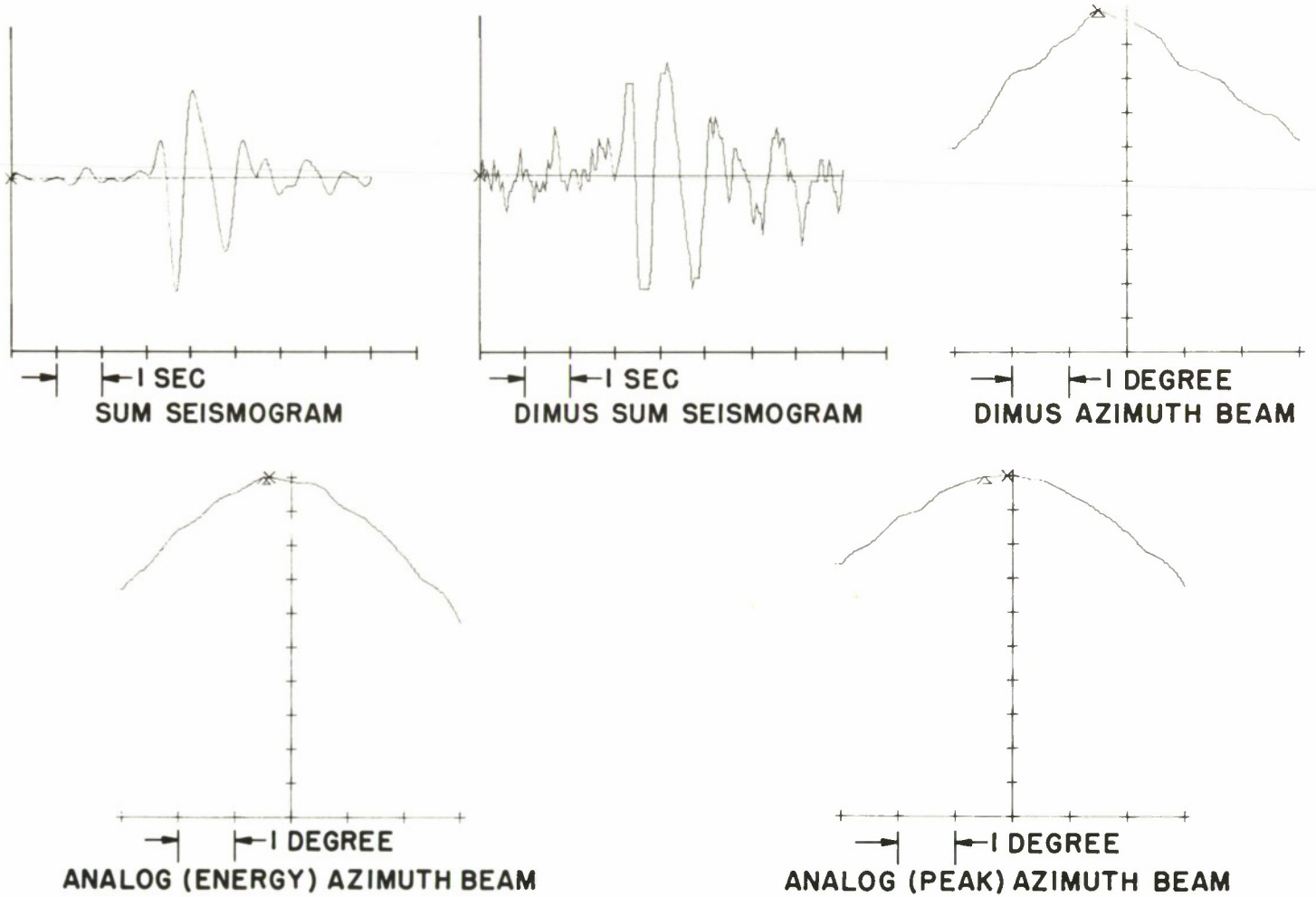

FIGURE 4.3
REPRESENTATIVE RESULTS FOR ONE TRIAL WITH NOISE ADDED
SIGNAL TO NOISE = 10 dB

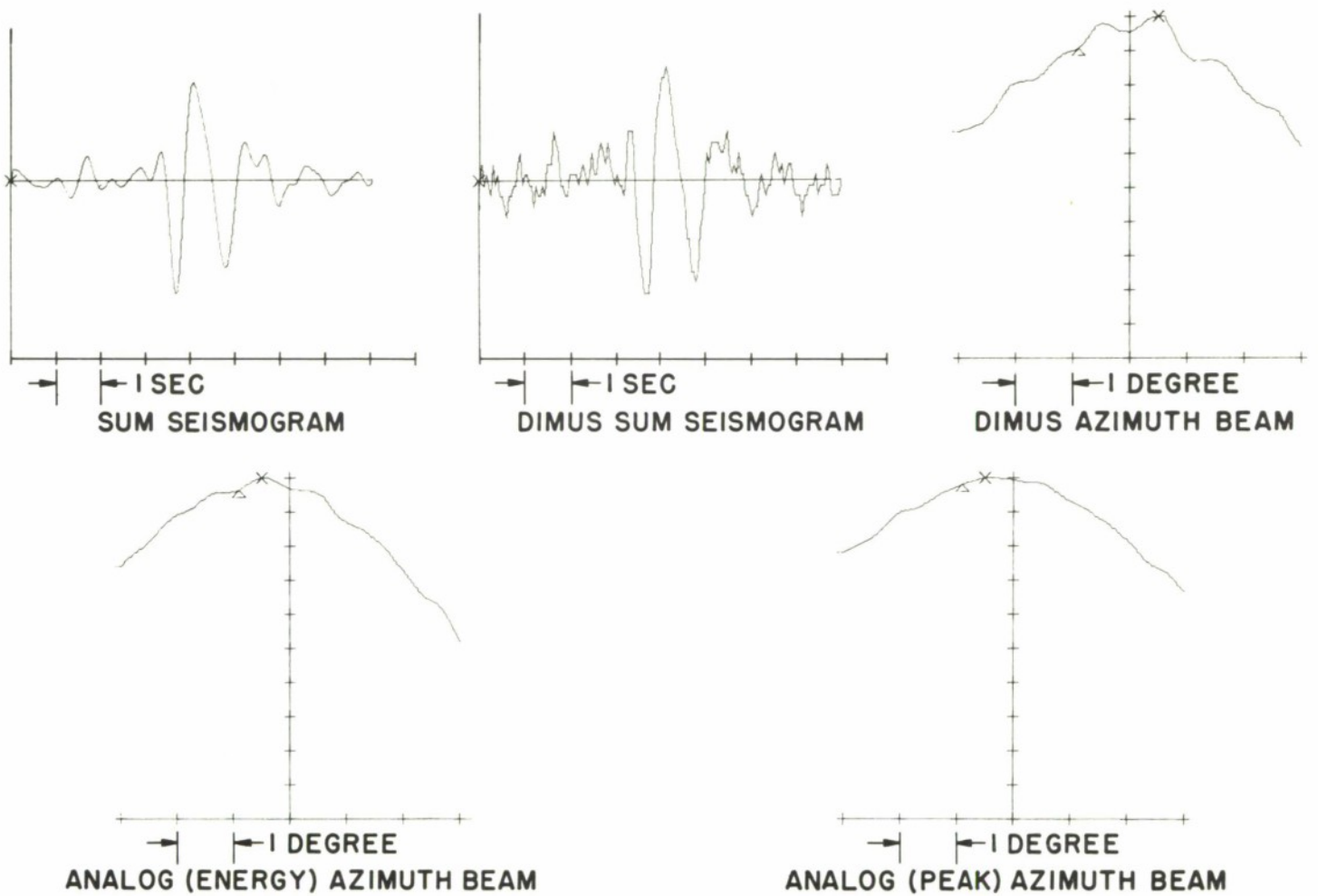

FIGURE 4.4
REPRESENTATIVE RESULTS FOR ONE TRIAL WITH NOISE ADDED
SIGNAL TO NOISE = 3 dB

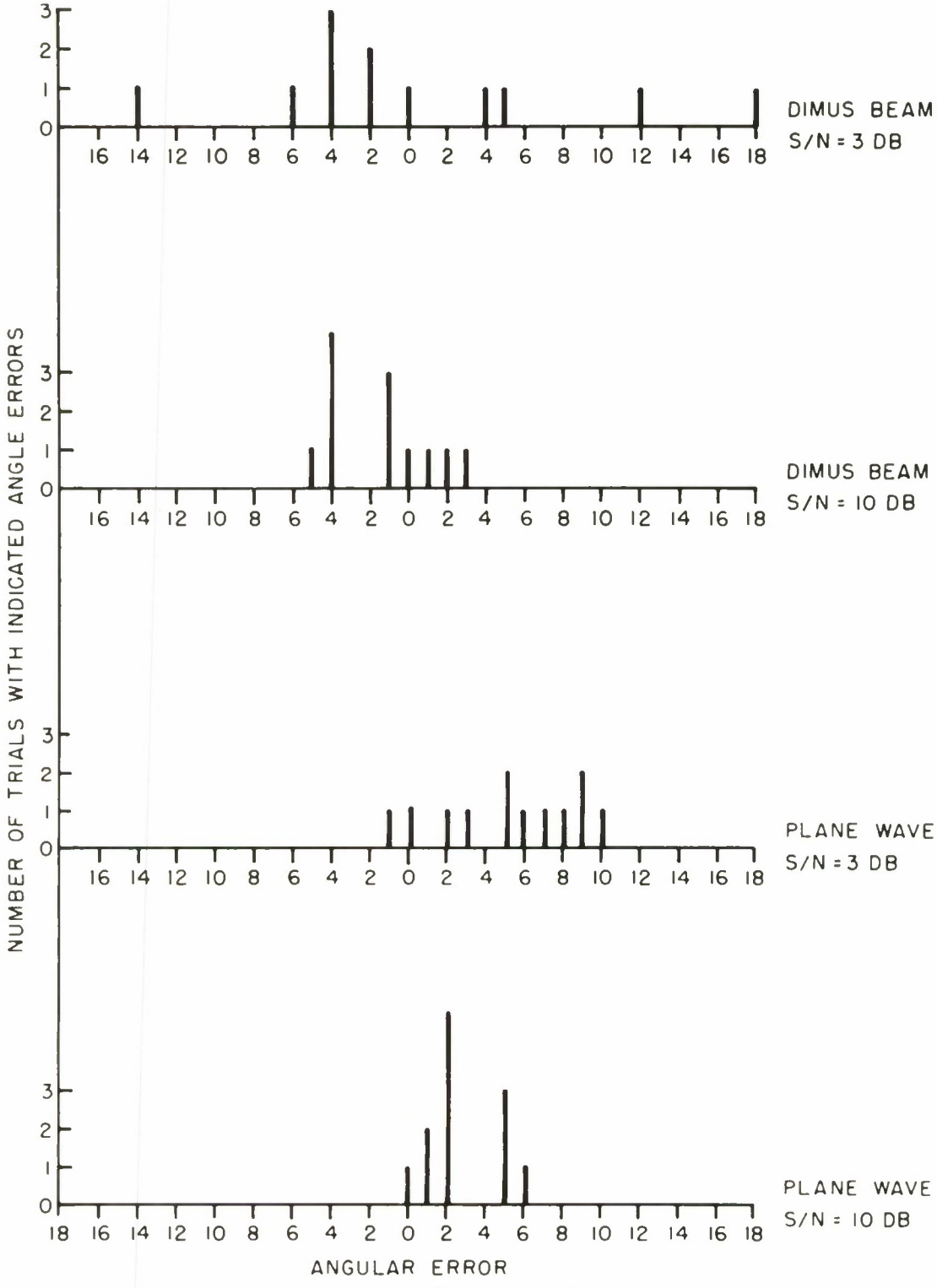

FIGURE 4.5
ERROR DISTRIBUTION
NOISE ALONE

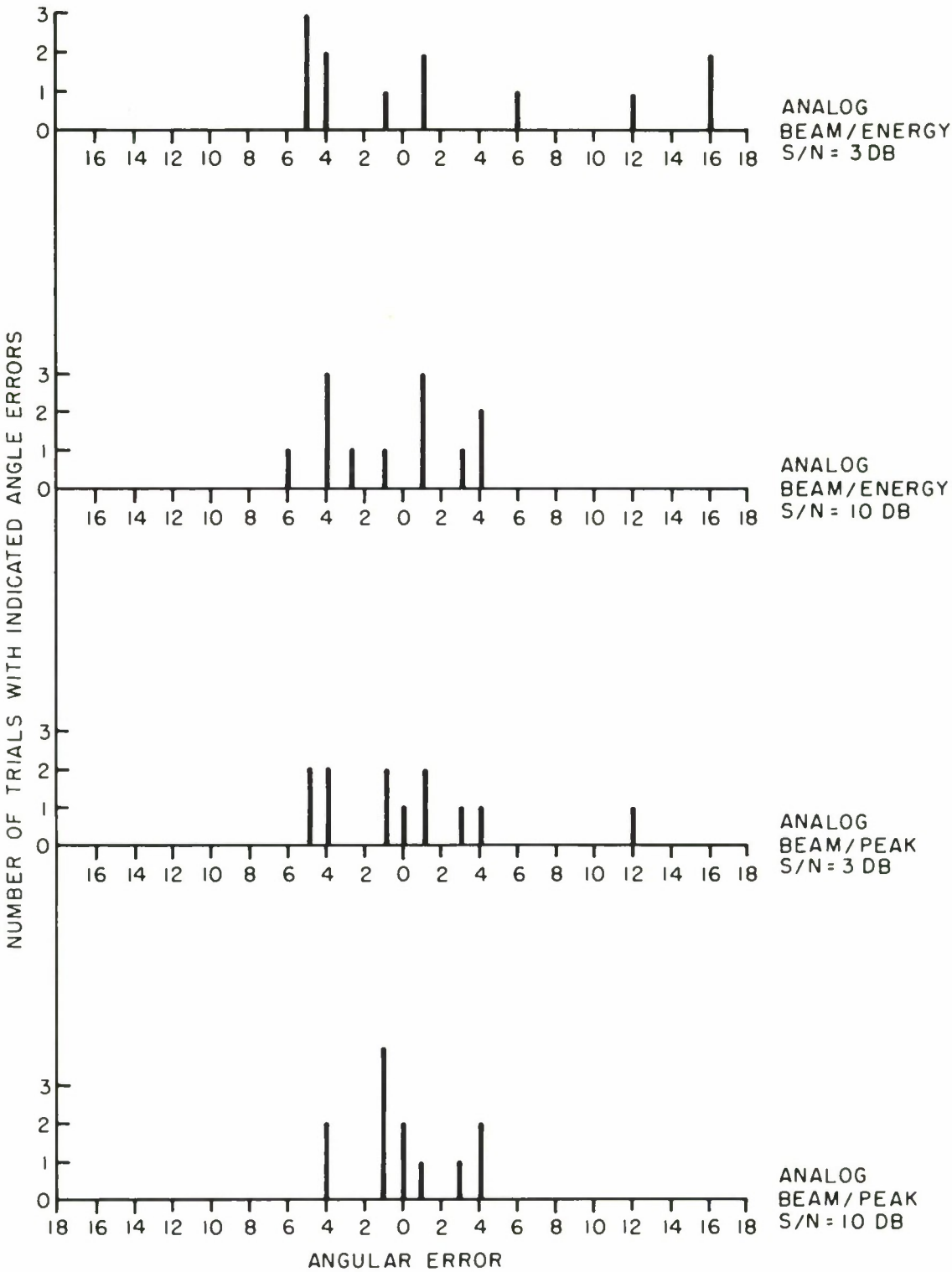

FIGURE 4.5 CONT.
ERROR DISTRIBUTION
NOISE ALONE

TABLE I - SAMPLE MEANS AND STANDARD DEVIATIONS VS. NOISE

	S/N = 10 dB		S/N = 3 dB	
	μ	σ	μ	σ
Plane-Wave Fit	0.28°	0.18°	0.53°	0.35°
Analog Pattern/Peak	0.00	0.20	0.01	0.45
Analog Pattern/Energy	-0.06	0.33	0.23	0.81
DIMUS Pattern	-0.12	0.22	-0.05	0.77

TABLE II - SAMPLE MEANS AND STANDARD DEVIATIONS VS. TIME ANOMALIES

	$\pm$1 Sample Point		$\pm$2 Sample Points	
	μ	σ	μ	σ
Plane-Wave Fit	-0.14°	0.26°	-0.06°	0.39°
Analog Pattern/Peak	-0.21	0.26	-0.32	0.42
Analog Pattern/Energy	-0.20	0.25	-0.25	0.23
DIMUS Pattern	-0.24	0.34	-0.64	0.49

4.8 RESULTS WITH TIME ANOMALIES ALONE

Results obtained from simulations with travel-time anomalies are illustrated by Figures 4.6 and 4.7. For the case of a one-sample point maximum anomaly Figure 4.6 gives the summed seismogram and the DIMUS sum (both were obtained with the array steered at the known arrival angle), the analog pattern-peak, the analog pattern-energy, and the DIMUS pattern. Shown on the plots of the array patterns are the maximum value of the pattern, indicated by a +, and the angle of the plane wave fit, indicated by a Δ. Figure 4.7 gives the same information for the case of a two-sample point maximum anomaly.

Figure 4.8 presents histograms of the number of trials with given angular errors for each of the four methods and for both the cases of one- and two-sample point maximum anomaly. These results are summarized in Table II. Examination of Table II shows that in general the mean error and the standard deviation of this error increase with the size of the anomalies. As in the noise-alone case, angular errors that would be adequate for systems applications appear feasible in the less severe of the two cases considered.

4.9 CONCLUSIONS

Examination of the histograms of errors for all simulation trials made (Figures 4.5 and 4.8) indicates insufficient information to make more than the grossest of estimates of the distribution of these errors. Taken together with the fact that the theoretical treatment of Section III dealt with continuous, rather than discrete times, it is possible only to make qualitative comparisons of predicted and simulated results. With this in mind, compare the standard deviations in angle obtained for a 10 dB signal-to-noise ratio with the value of 0.3° predicted by theory. The spread in simulation results lies between 0.18° and 0.33°,with the smallest standard deviation belonging to a population with a substantial mean error. The agreement is

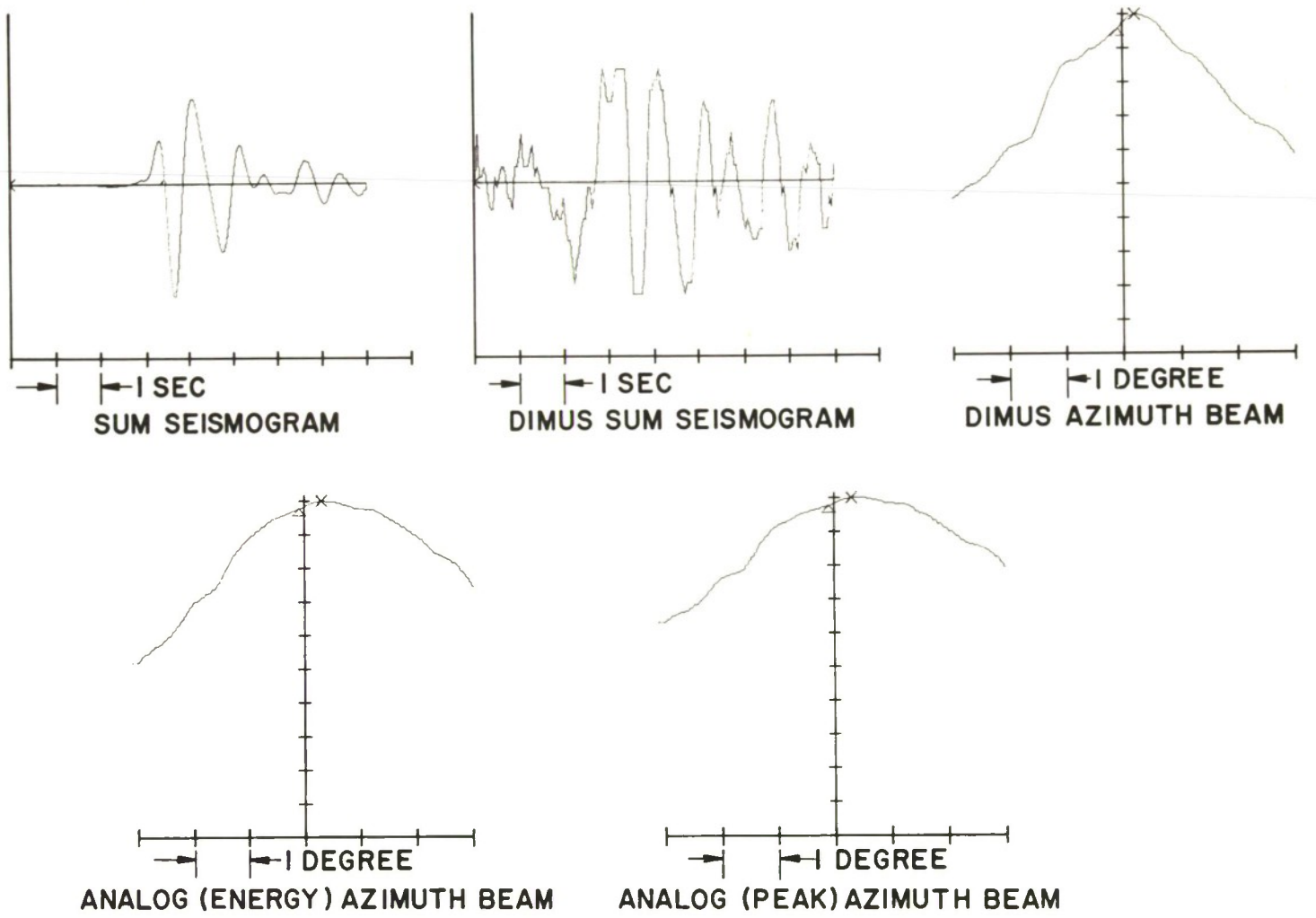

FIGURE 4.6
REPRESENTATIVE RESULTS FOR ONE TRIAL WITH ANOMALIES ADDED
PEAK ANOMALY = 1 SAMPLE POINT

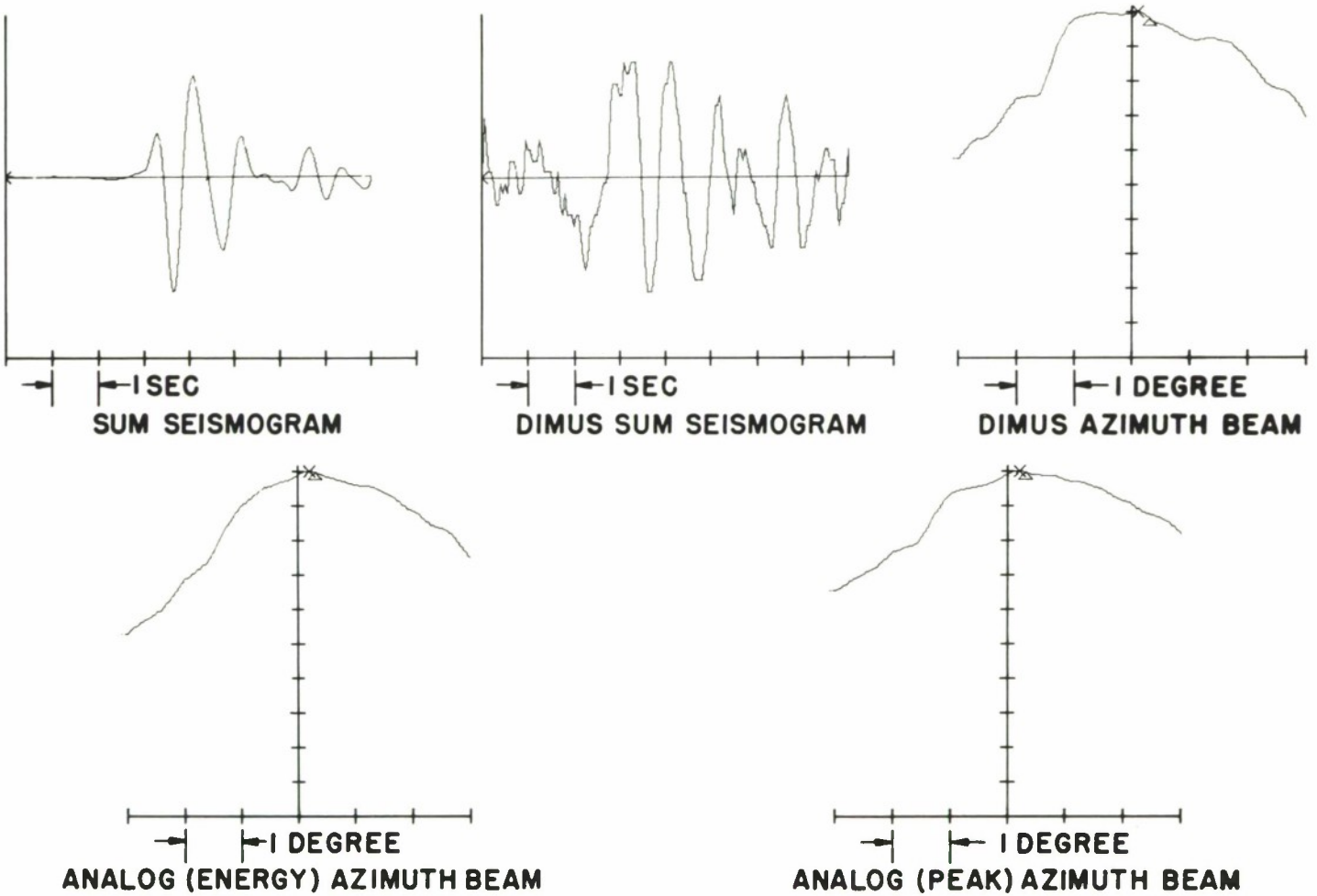

FIGURE 4.7
REPRESENTATIVE RESULTS FOR ONE TRIAL WITH ANOMALIES ADDED
PEAK ANOMALY = 2 SAMPLE POINTS

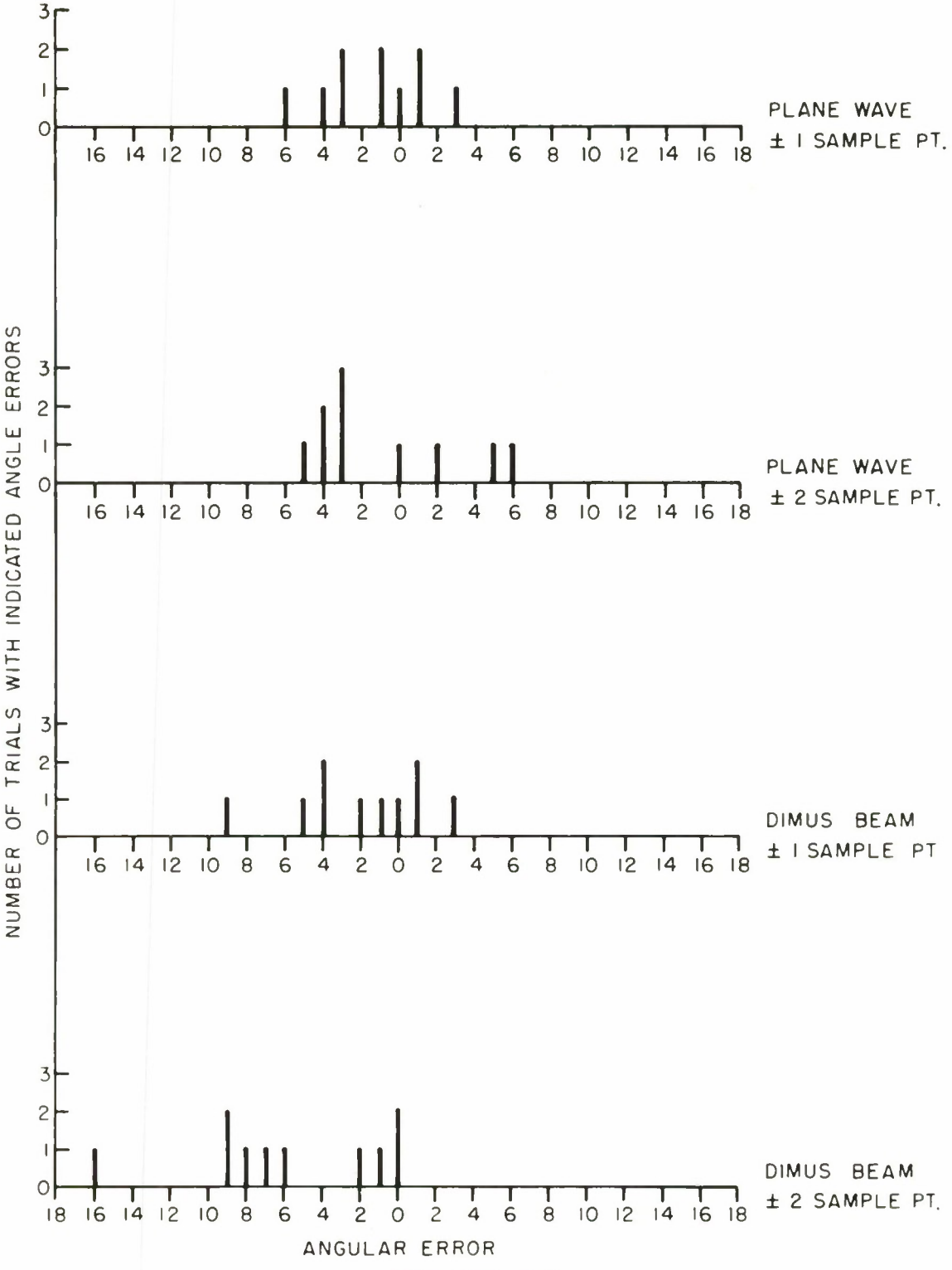

FIGURE 4.8
ERROR DISTRIBUTION
ANOMALIES ALONE

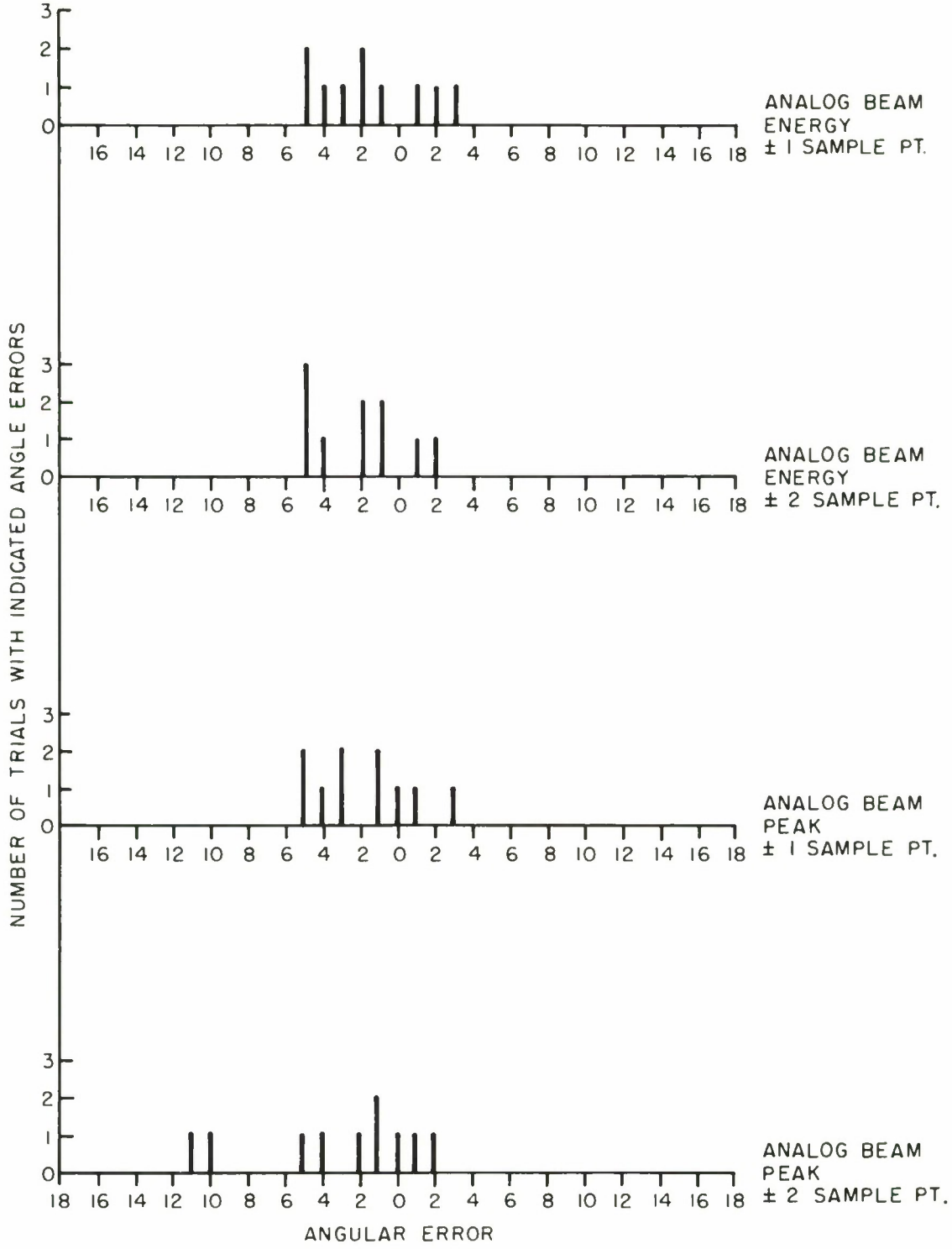

FIGURE 4.8 CONT.
ERROR DISTRIBUTION
ANOMALIES ALONE

as good as could be expected. Examination of Table I shows that the standard deviations of error increase with decreasing signal-to-noise ratio. The mean of the ratios of the 3 dB to 10 dB standard deviations is 2.5, which compares quite well with the theoretically predicted ratio of 2.2. If the DIMUS beam result is removed from the set (there is no reason to expect the peculiar calculations of this beam to agree with the theoretical treatment of Section III), the mean ratio is exactly 2.2 -- better than should be expected.

Results of the anomaly simulations give standard deviations of errors which are, in general, higher than theoretical predictions by a factor of nearly two for both the one and two sample point peak errors (see Table II). What is more important, there are biases in the data samples producing substantial (0.2°) mean errors in angular determination. It is hypothesized that both of the above effects are due to the poor estimates of the error distributions available from the simulation trials. What is perhaps most important, is that it is unlikely that travel-time anomalies can be reduced below the one sample point level. Thus, while the results obtained suggest that for large enough events, noise will not substantially limit the accuracy of event location, we may always be left with a standard deviation of angular error on the order of 0.25°. Since this result is in such large disagreement with the theoretically predicted one, further study is indicated. Before resolution of this problem, however, the simulation results may be translated into geographical terms. This would imply a standard deviation of some 25 kilometers in one component of the determination of an epicenter from a single large array.

SECTION V

CODA-CORRELATION STATISTIC WITH DIMUS (HARDLIMITED) WAVEFORMS

In a previous report [9], data were presented that indicated the average paired correlation coefficient could be a useful discriminant for identifying earthquakes with depths between 10 and 40 km. These calculations, which were based on the outputs of seismometers distributed over thousands of kilometers, indicated significantly more coda correlation for earthquakes in the 10-40 km region than for other earthquakes or for surface-focus events.

We have been studying the possibility of using DIMUS (hardlimited) seismograms for two other discriminants, complexity and spectral ratio [10], and for location [11]. Along with these studies, it is of interest to examine how much the coda-correlation discriminant would be degraded by the use of DIMUS waveforms. Results of repeating these calculations with DIMUS waveforms, obtained from all but one of the same set of 42 events, are summarized in this section. It turns out that the discriminant still appears useful for separating "moderate depth" earthquakes from other events, but the separation is not as clear as it was in the case of analog waveforms.

The calculation of the average paired correlation coefficient has been described in detail elsewhere [12]. For the DIMUS calculations, since all waveforms have a unity rms value in all time intervals, an alternate (but equivalent) implementation of the calculation turns out to be much simpler. This implementation is based on a simple relation between the average paired correlation coefficient and the energy in the sum of the normalized waveforms.

Figure 5.1 is a scatter plot of the coda correlation coefficients calculated from the analog waveform, ρ_C, and those calculated from the DIMUS waveform, ρ_D. Different symbols are

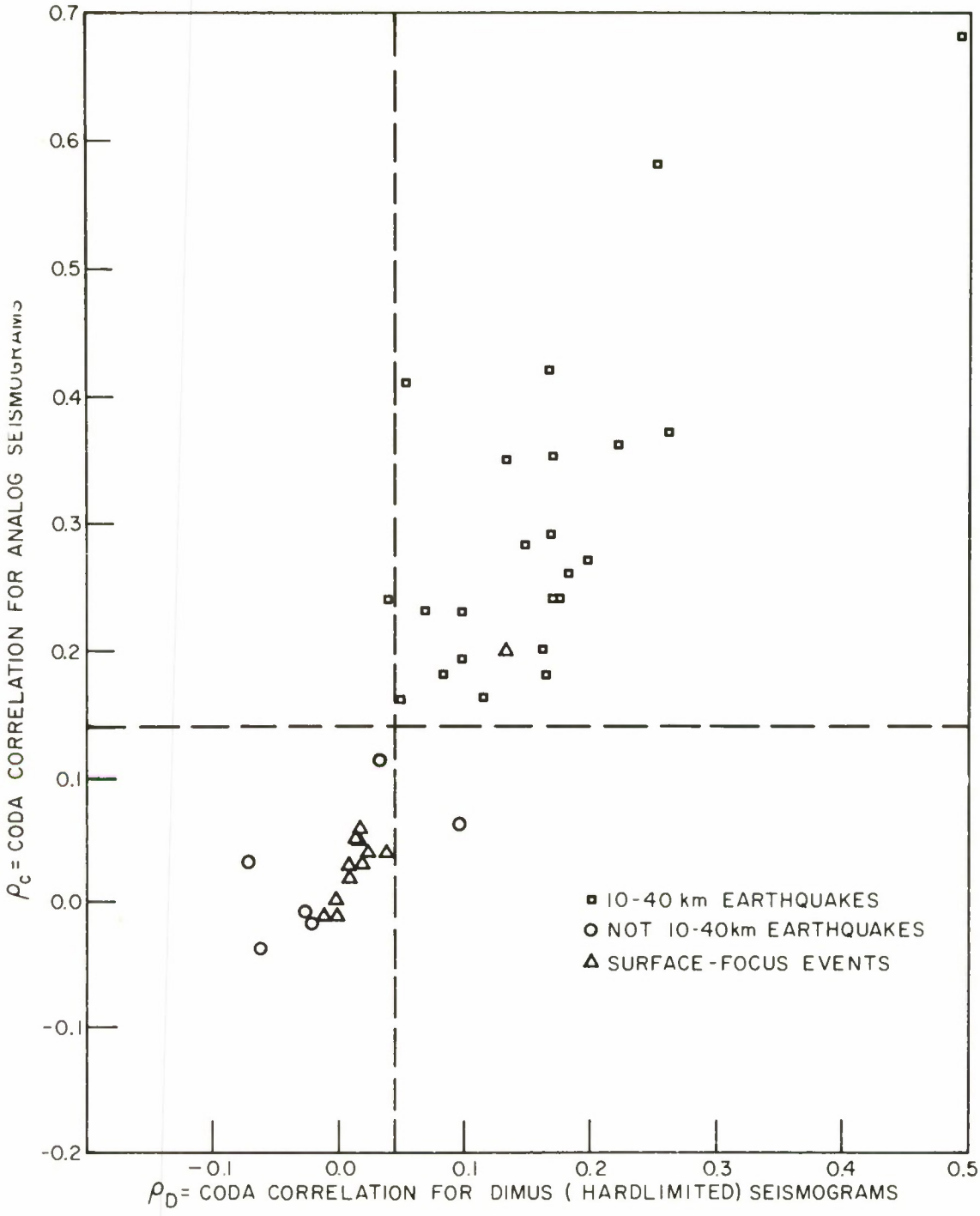

FIGURE 5.1
SCATTER PLOT OF CODA CORRELATION
FOR DIMUS & ANALOG SEISMOGRAM

used for the three different classes of events: earthquakes with depths between 10 and 40 km (23 events), other earthquakes (6 events), and surface-focus events (12 events). Two lines are drawn to illustrate the separation of the points obtained for the moderate depth earthquakes from the others. With the exception of one surface-focus event (with $\rho_c = 0.2$), it is clearly easy to separate the moderate depth earthquakes from the other events with the horizontal line at $\rho_c = 0.14$. In the case of the DIMUS discriminant, a vertical line at $\rho_D = 0.05$ separates most, but not all of the events, and there are several points very close to the line.

It is clear that the DIMUS coda-correlation statistic is inferior to the statistic calculated from the analog waveforms. However, it still provides a fairly good separation of moderate depth earthquakes from other events. We expect, in the near future, to be processing additional events with the analog coda-correlation statistic. For this reason we shall postpone any further comments or conclusions on the performance of the DIMUS coda-correlation statistic until these additional calculations have been performed.

SECTION VI

EXTENDED AUTOMATIC pP TEST

The previously reported work [13] on an extended automatic pP test has been continued using arrays of continental dimensions. It was anticipated that use of continental-size arrays would yield good signal-to-coda enhancement in the phased sum seismogram due to coda decorrelation over the large spatial separations of the seismometers, and due to the increased moveout of the pP phase across the array. The key to the success or failure of the test was the pP alignment procedure, which is based on an assumed depth of the Moho and assumed average velocities above and below the Moho. The P-pP delay times for alignment were calculated using a simple geometric model of surface reflection described below. It was previously indicated and should be emphasized that errors of 10 to 20 km in depth determination of deep-focus events are not important for discrimination purposes.

To date, the extended test has been applied to eight events using arrays of continental dimensions with quite good results. Information concerning these events is summarized in Table III. In several of these events, the test detected sP as well as pP, which proved to be a valuable aid in depth determination.

6.1 DESCRIPTION OF TEST

As described earlier, the automatic pP test proceeds by calculating for each of several "test depths" a delayed sum, in which each seismogram is aligned in such a way that the pP-phases would add coherently if the test depth were correct. Then the energy in the one-second time window that would enclose the summed pP-phase is calculated and divided by a measure of the surrounding energy. Finally, this energy ratio statistic is multiplied by an average paired correlation coefficient and the test depth yielding the largest value is selected.

TABLE III - EVENTS USED FOR AUTOMATIC pP TEST

DATE	REGION	LAT	LON	ORIGIN	DEPTH	MAG
21 MAR 62	S. ALASKA	62.1N	152.7W	1/53/13.3	122	-
19 JULY 62	BOLIVIA	20.6S	68.7W	12/ 2/31.3	160	-
12 SEPT 62	N. CHILE	23.1S	68.8W	12/28/16.3	150	-
6 OCT 62	EQUADOR	1.5S	77.4W	14/ 5/24.0	149	-
10 JAN 63	KAMCHATKA	52.6N	157.2E	17/14/07.3	125	-
15 JULY 63	KAMCHATKA	55.6N	162.0E	8/41/07.5	60	5.2
25 AUG 63	SEA OF OKHOTSK	48.7N	148.8E	2/20/12.7	134	4.7
6 JAN 64	KAMCHATKA	50.9N	157.3E	23/45/23.4	33	5.6

Three changes have been made in converting the test from the 10-40 km region to deeper values. The first change, which is probably not very important, is that the denominator of the maximal-ratio weights used in combining seismograms is now calculated from a 50-second time window following the P wave, rather than the 10-second window used previously. The second change is in the calculation of the energy ratio. The energy in the one-second test-depth window is now compared to the average energy in a five-second window preceding the test-depth window. The third change relates to the alignment procedure, and is crucial to the success of the extended test.

The P-pP delay times are calculated from the JB travel-time tables using the geometry illustrated in Figure 6.1. Point E is the hypocenter of the event; h is the depth of the event. The pP phase is reflected at point 0 on the surface of the earth, and passes through point R at depth h along its path to the seismometer. The incident angle i_0 is calculated from travel-time tables and is almost invariant with depths down to 200 km. The Moho is indicated in Figure 6.1 at a depth of h_m, and all of the following calculations are made for h greater than h_m.

The alignment times are computed as follows. The P-phase travel time to the seismometer is calculated from the JB tables, interpolating linearly with range and depth. The pP-phase travel time to the seismometer is found in two steps by adding the times of travel from E to O to R, say t_1, and from R to the receiver. Let v_a and v_b denote the average velocities above and below the Moho discontinuity respectively, then

$$t_1 = 2[\frac{h_m}{v_a} + \frac{(h-h_m)}{v_b}]/\cos(i_0) \quad \text{seconds} \qquad (6.1)$$

Possible refraction effects at velocity discontinuities are neglected. The travel time from R to the receiver is from JB tables as above, only the range is now the range of E minus $\overline{ER}$, where

$$\overline{ER} = 2h \tan(i_0) \text{ km} = 2h \tan(i_0)/111.195 \text{ degrees} \qquad (6.2)$$

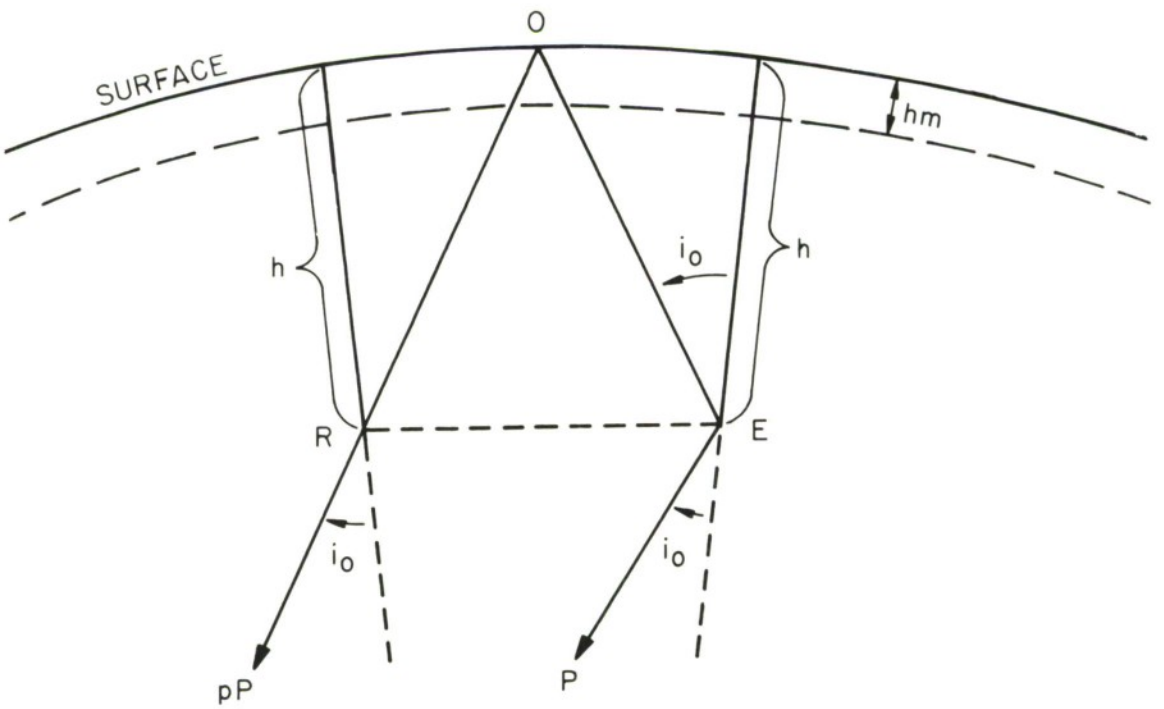

FIGURE 6.1
GEOMETRY OF SURFACE REFLECTION

The parameter values v_a = 6.34 km/sec, v_b = 8.00 km/sec, and h_m = 33.0 km have been used in all calculations to date. Moderate errors in the assumed parameter values will not seriously affect the results of the test. For example, if the Moho is misplaced by 30 km, or if the assumed average velocities are in error by 10%, then the two extreme phasing times will be in error by less than 0.10 sec, for an event with 100 km depth, with epicenter approximately 40° from an array with a 2500 km aperture. This is due to the fact that the P-wave incident angles at the receivers are essentially invariant with depth. Although these parameter variations would not lead to serious phasing errors, they could cause the test statistic to peak at the wrong depth, which, as noted above, would not be critical for discrimination purposes.

An inherent property of the automatic pP test is that it may also detect the sP phase arrival. The sP phase delay relative to the P-phase is a constant factor times the pP phase delay. Since the pP phase delays vary linearly with depth, when the automatic test calculates the test statistic at a depth approximately one-and-one-half times the depth of the event, the sP phase signals will add coherently, and could, if the signals were strong enough, cause the test statistic to peak.

For some events, poor signal-to-noise ratios necessitated filtering of the data. The test results for two events were vastly improved after filtering, which was done with a recursive, bandpass digital filter derived from a low-pass three-pole Butterworth analog filter. The 3 dB points of the passband were 0.6 Hz and 3.25 Hz.

6.2 EXPERIMENTAL RESULTS

A measure of the effectivenss of the automatic depth test might be a comparison with the C&GS reported depths. C&GS depths, though, seem not to be a reliable standard, and whenever possible, we have referred to the original seismograms to resolve discrepancies. Only two of the eight events tested agreed with

the C&GS depth determinations. Two other events suggest that C&GS mistakenly identified sP as pP. The depth results of three other events conflict with the C&GS reported depths rather severely. A presentation of seismograms with phase identifications is made in support of the automatic test for one of these three events, and for the two events where we believe sP was mistaken for pP. The final event was listed by C&GS as 33 km, indicating that they were unable to make a depth estimate; the automatic test, however, did show a peak in the test statistic, which is again supported by illustrative seismograms.

The two events which demonstrated good agreement between the automatic test depths and the C&GS depths both had large signal-to-noise ratios. The 21 March 1962 event had an average single station signal-to-noise ratio of 30, and the 15 July 1963 event had an average single station signal-to-noise ratio of 212. In both cases, the phases were easily identifiable by eye on all seismograms. The test results are shown in Figure 6.2D and Figure 6.2B, respectively.

The two events for which we believe sP was mistaken as pP by C&GS were 12 September 1962 and 19 July 1962. The test statistic of Figure 6.2A shows the pP phase clearly at 101 km and the sP phase following at 153 km for the 12 September 1962 event. This delay corresponds well to relative transverse and longitudinal wave velocities. An illustrative set of seismograms is presented in Figure 6.4, with the pP, sP and PcP phases identified on each at locations corresponding to a depth of approximately 101 km. The 19 July 1962 event produced only one rather strong peak when the automatic test was performed with unfiltered seismograms (see Figure 6.2C). This peak occurred at a depth of 147 km, 13 km from the C&GS listed depth, and would have been accepted as the correct depth except that the test was repeated with filtered seismograms. After filtering, another clear peak emerged at 97 km, as can be seen in Figure 6.3A, indicating that the peak at 147 km was in fact the sP phase.

A review of the seismograms for this event indicates that 97 km is the correct depth for this event. Seismograms for this event are presented in Figure 6.5 with the pP and sP arrival times indicated for a 97 km depth event.

The three events for which the automatic test disagrees with C&GS estimates occurred on 25 August 1963, 10 January 1963, and 6 October 1962. The first of these, the 25 August 1963 event, was studied in an earlier report [14] and seemed to be an event with depth between 10 and 40 km, although C&GS has it listed at 134 km. When the extended test was performed with this event, there were no peaks in the test statistic in the 33 to 200 km depth range. The maximum value of the test statistic was 0.35. An isolated peak of magnitude less than 1.0 in the test statistic is not considered meaningful by itself; hence we believe that this event was not in the 33 to 200 km depth region. No plot is presented for this event.

The 10 January 1963 event was more interesting. The automatic test showed a depth of 55 km (see Figure 6.2E), while the C&GS depth is 125 km. Three illustrative seismograms are presented in Figure 6.6, showing pP, sP and, on one seismogram, PcP phases for an event of 55 km depth. The seismograms are rather noisy and yet the pP phases corresponding to a 55 km depth event stand out quite well.

The 6 October 1962 event was a low magnitude event (the actual magnitude is not listed by C&GS). The pP phase could not be identified by C&GS at any station. The C&GS depth of 149 km comes from an unrestrained epicenter calculation, which, however, was supported by S-phase arrivals at several stations at close proximity to the event location [15]. The seismograms for this event are very poor, and the automatic test yielded no peaks in the test statistic when performed with unfiltered data. When performed with filtered data, the automatic test showed a vast improvement. As shown in Figure 6.3B, a clear peak occurred at 77 km, and a smaller peak occurred at

109 km, suggesting pP and sP, respectively. We have not yet had the opportunity to confirm this result on the filtered seismograms.

The final event, 6 January 1964, is a magnitude 5.6 earthquake, which overloaded several of the stations used in the automatic depth test. In addition, the seismograms (see Figure 6.7) show very strong codas, which make it easy to misidentify a phase arrival. As a result, C&GS made no depth estimate for this event. The automatic test yielded a clear peak at 155 km, which is difficult to verify or refute from the seismograms. Overloading is present on three of the nine stations, and this badly degrades the quality of those signals. If there were a phase arrival at a point of overloading, the signal distortion would cause a low average paired correlation, and would probably cause the automatic test to miss that phase. In support of the automatic depth test peak at 155 km, it is observed that the average paired correlation was 0.35 and the energy in the test depth window compared to the average energy in the coda window was 4.7. An extraneous peak of this nature is highly unlikely in the signal region following the P-phase by more than ten seconds. Since the only phase arrivals which could possibly add coherently in the automatic test are pP and sP, it seems likely that this event occurred at a depth of at least 100 km. The results of the test are shown in Figure 6.2F.

6.3 SUMMARY AND CONCLUSIONS

The extended automatic pP test has been applied to eight events using continental-size arrays. The experimental results were good for all eight events. In three events the test detected the sP phase arrivals as well as the pP phase arrivals. On two of these three events it appears that C&GS also detected the sP phase arrivals and mistook them for pP. Since sP delay times are the same as the pP delay times within a constant factor, both phases can be added coherently by the automatic test. The appearance of the sP phase in addition to the pP phase in the test results has proved useful in depth determinations.

As was anticipated, the use of continental-size arrays with the corresponding increased moveout for the pP phase and the large spatial separation of stations does serve to reduce the coda-correlation among seismometers. This eliminates the presence of confusing, multiple peaks in the test statistic, which were present to some extent when the automatic test was performed with LASA-Montana data.

For two events, pre-filtering of the data was found to be necessary. After filtering, the test results improved vastly. The erroneous result obtained with unfiltered data for the 19 July 1962 event was corrected when the test was applied to filtered data, yielding clear peaks for both pP and sP. Unfiltered data for the 6 October 1962 event yielded no test statistic peaks, but the filtered data yielded two consistent peaks corresponding to the pP and sP phase arrivals.

The alignment time calculations have proved adequate for the events tested. At the time the test was developed, only the JB travel-time tables were available to us. It was therefore necessary to use a simple model to calculate sufficiently precise P-pP differential travel times. More recently, we have obtained the 1966 Herrin tables [16], which include pP travel-time tables that would be adequate for the automatic pP test. Comparison of differential P-pP arrival times obtained from our model and Herrin's tables indicate that the discrepancies are probably not important. We have checked two ranges for each of two depths corresponding to events discussed above. In one case both our model and the Herrin table predicts the same differential arrival time for a depth of 155 km. In the other case the differential arrival time predicted by the model for a depth of 101 km corresponds to a depth of 113 km in the Herrin tables. Since the discrepancies are not large, a conversion of the test to take advantage of these tables does not, at this time, seem to be worth the effort.

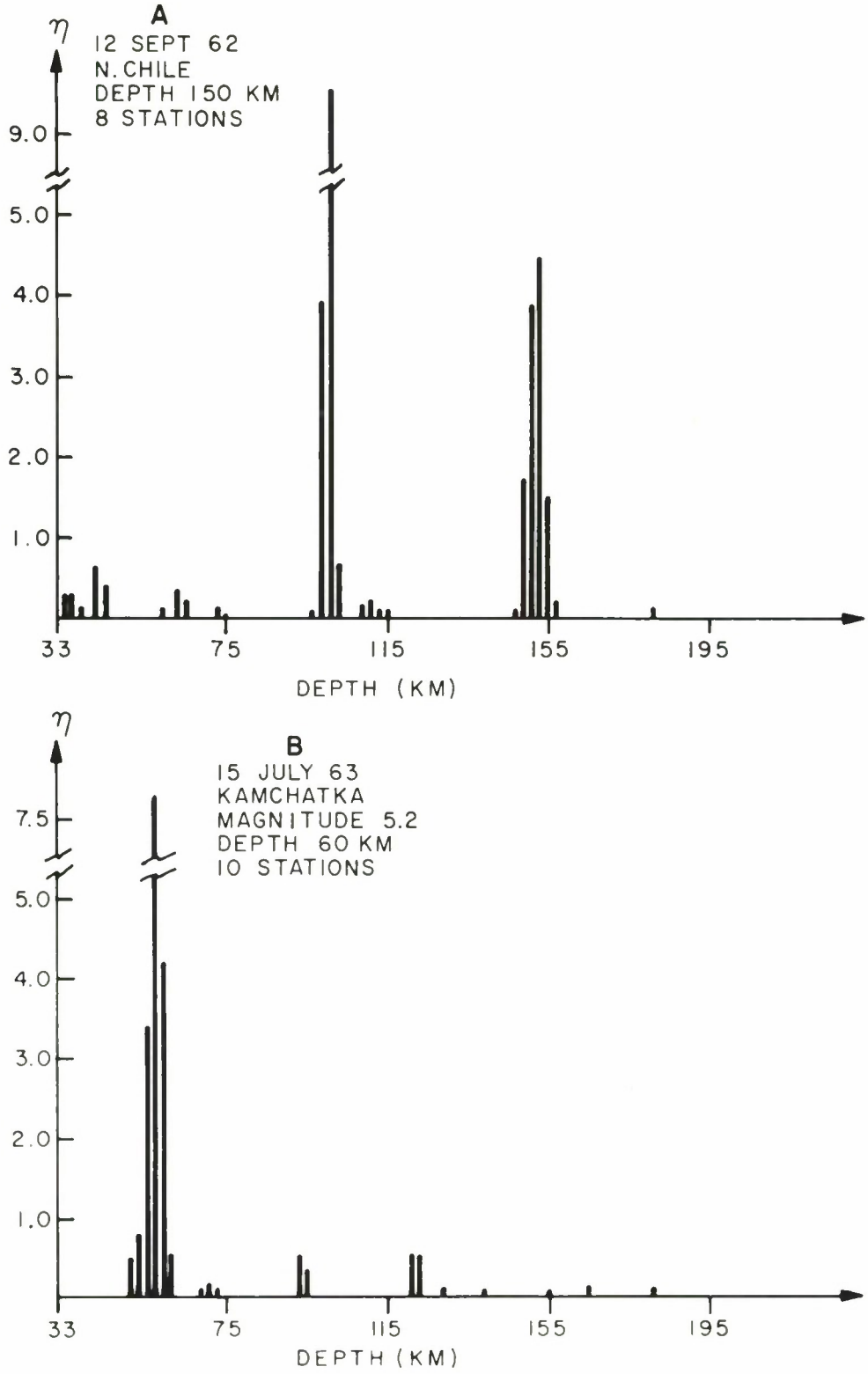

FIGURE 6.2 (A-B)
EXTENDED AUTOMATIC $_{p}$P TEST

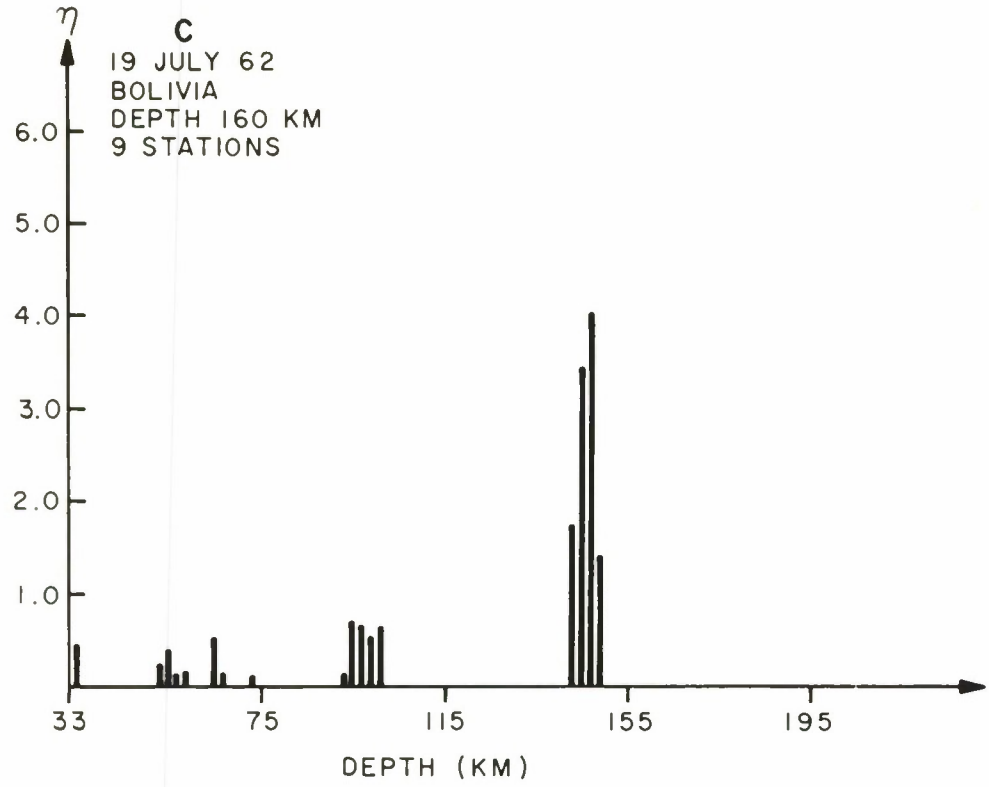

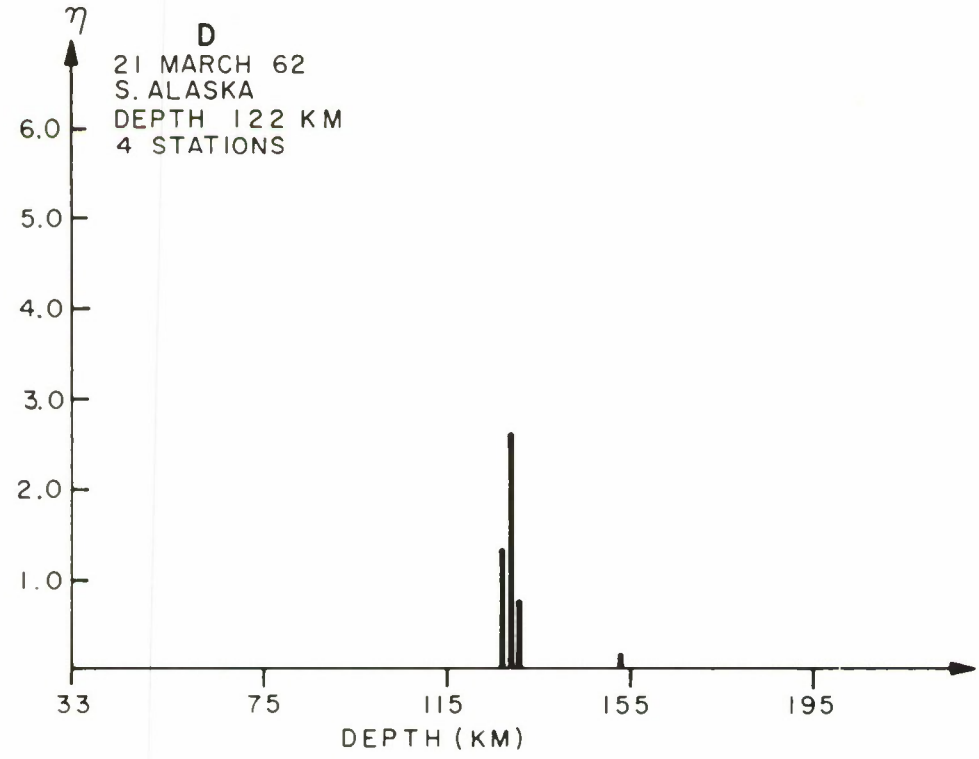

FIGURE 6.2 (C-D)
EXTENDED AUTOMATIC $_p$P TEST

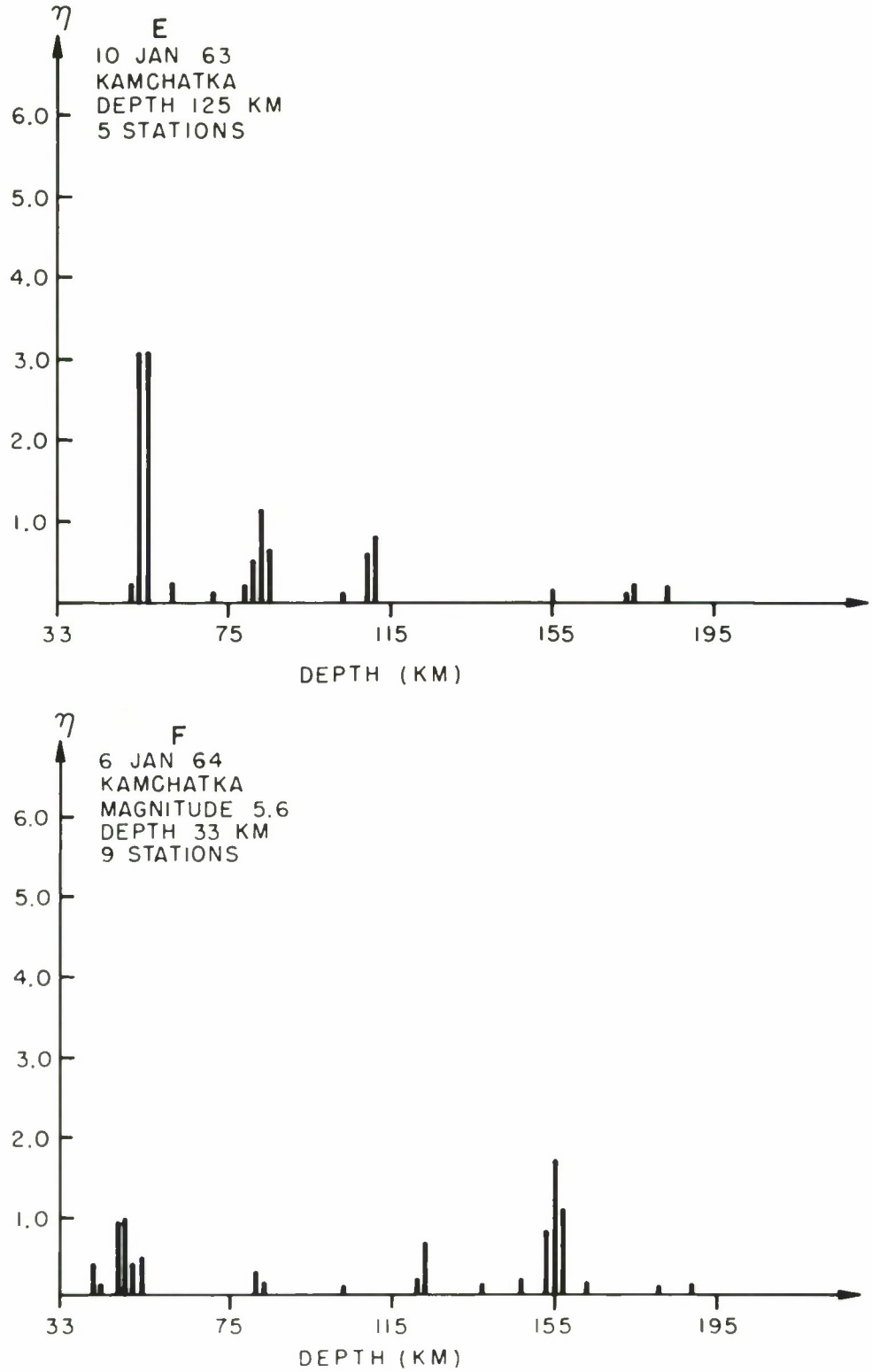

FIGURE 6.2 (E-F)
EXTENDED AUTOMATIC $_p$P TEST

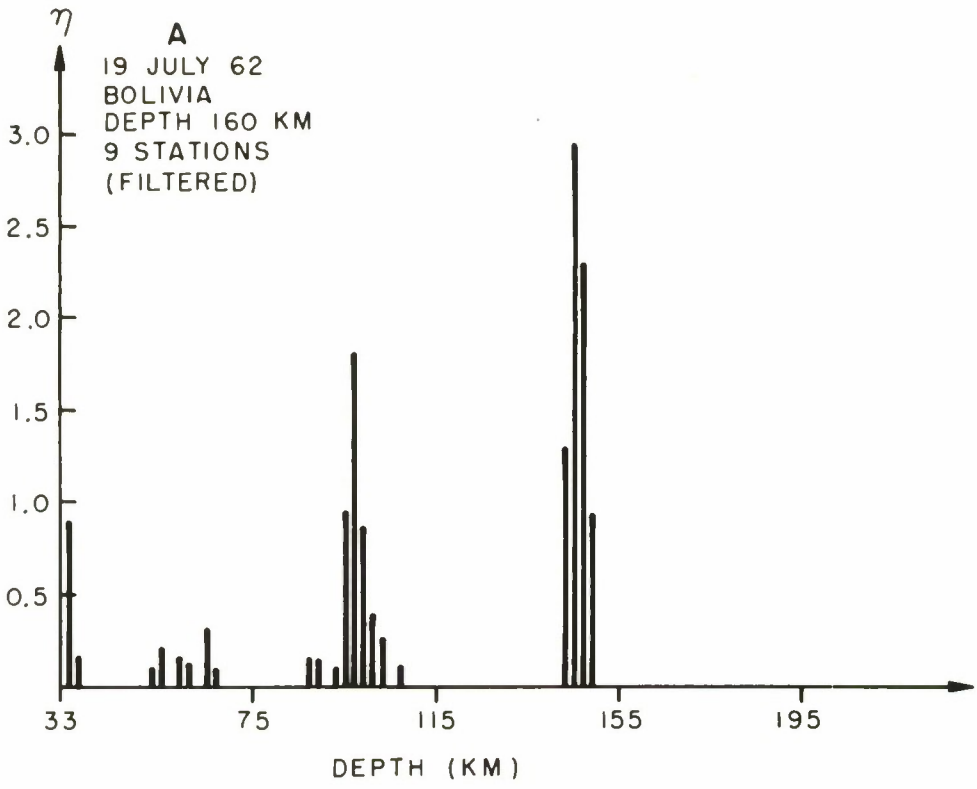

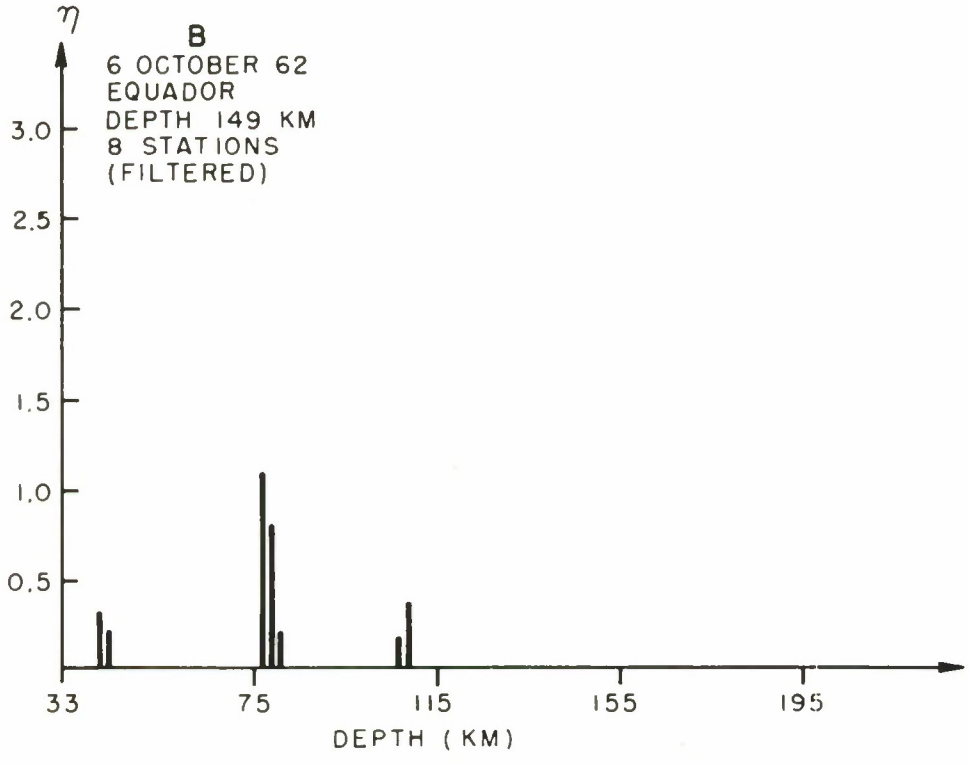

FIGURE 6.3 (A-B)
EXTENDED AUTOMATIC $_p$P TEST

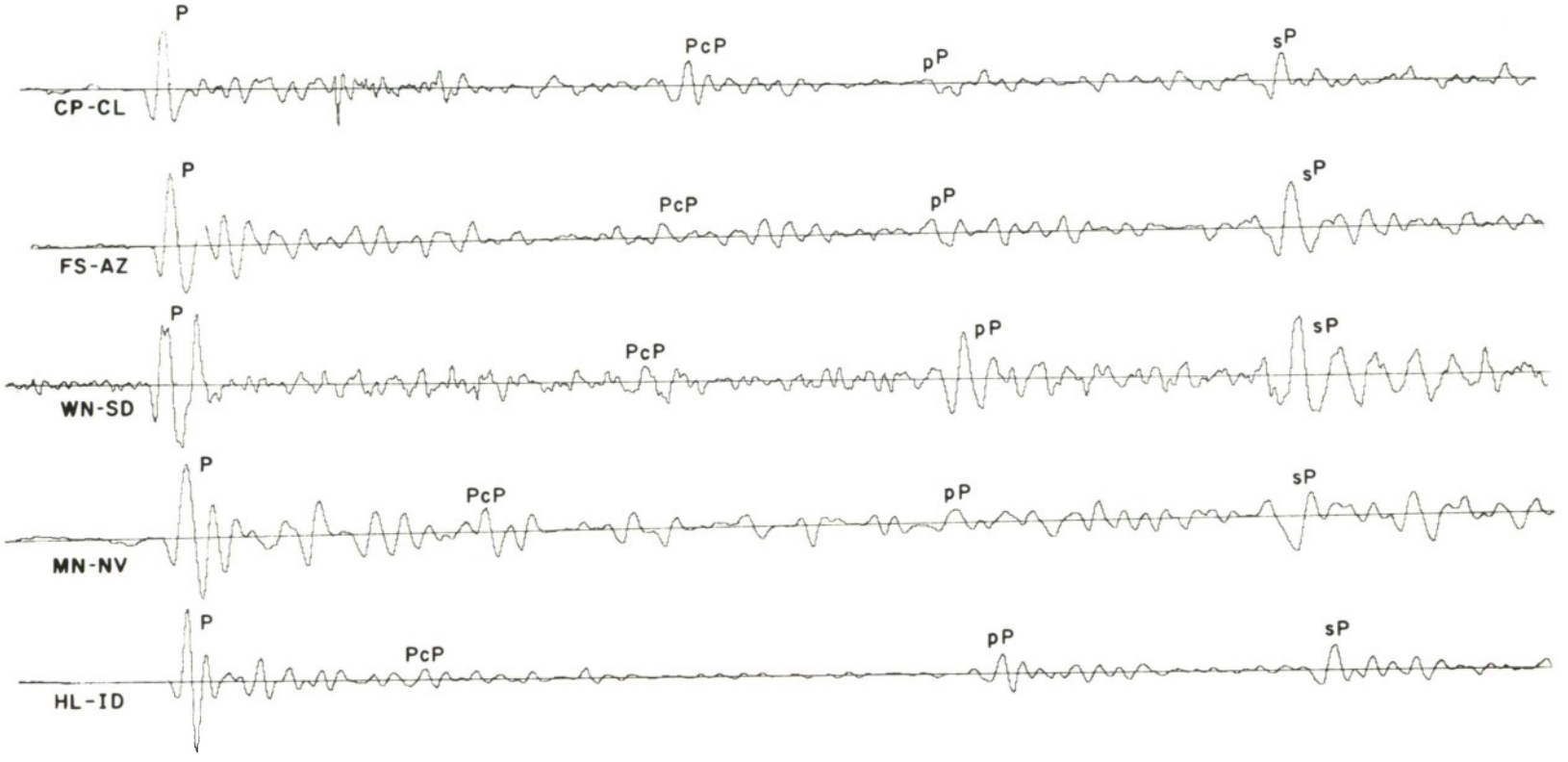

FIGURE 6.4
SEISMOGRAMS FOR 12 SEPTEMBER 1962 EVENT

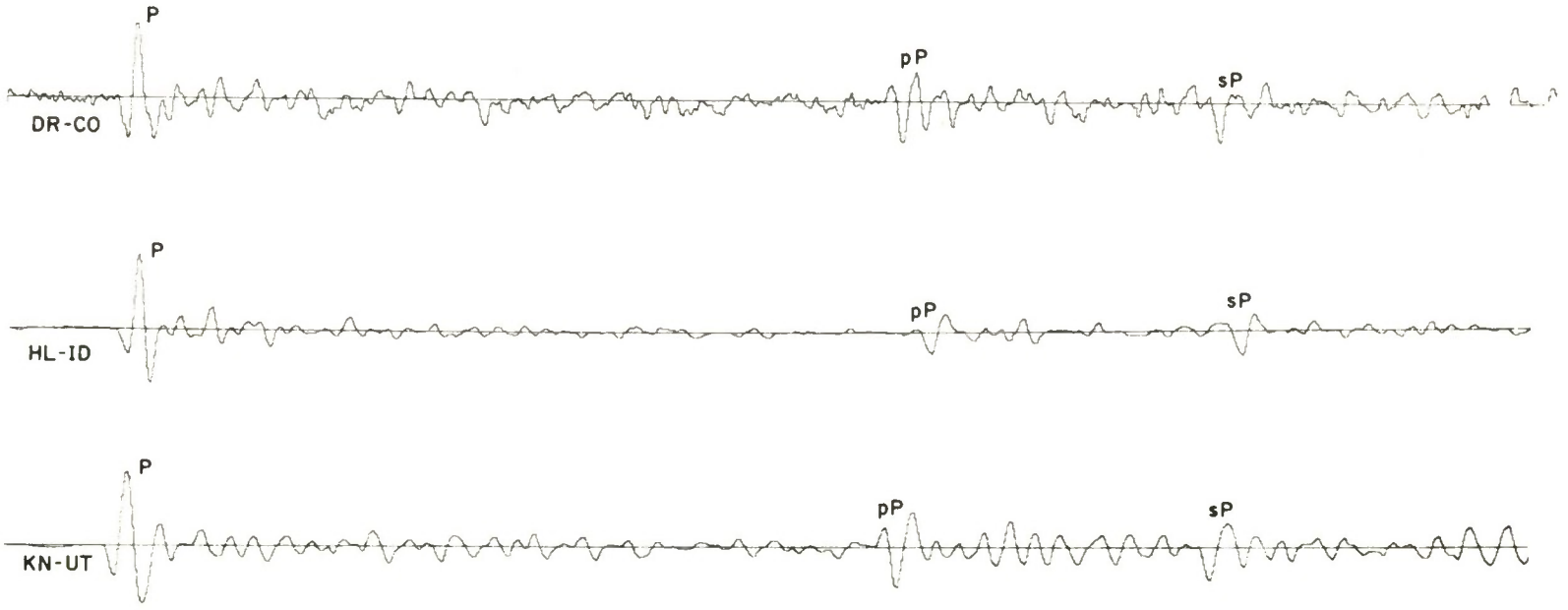

FIGURE 6.5
SEISMOGRAMS FOR 19 JULY 1962 EVENT

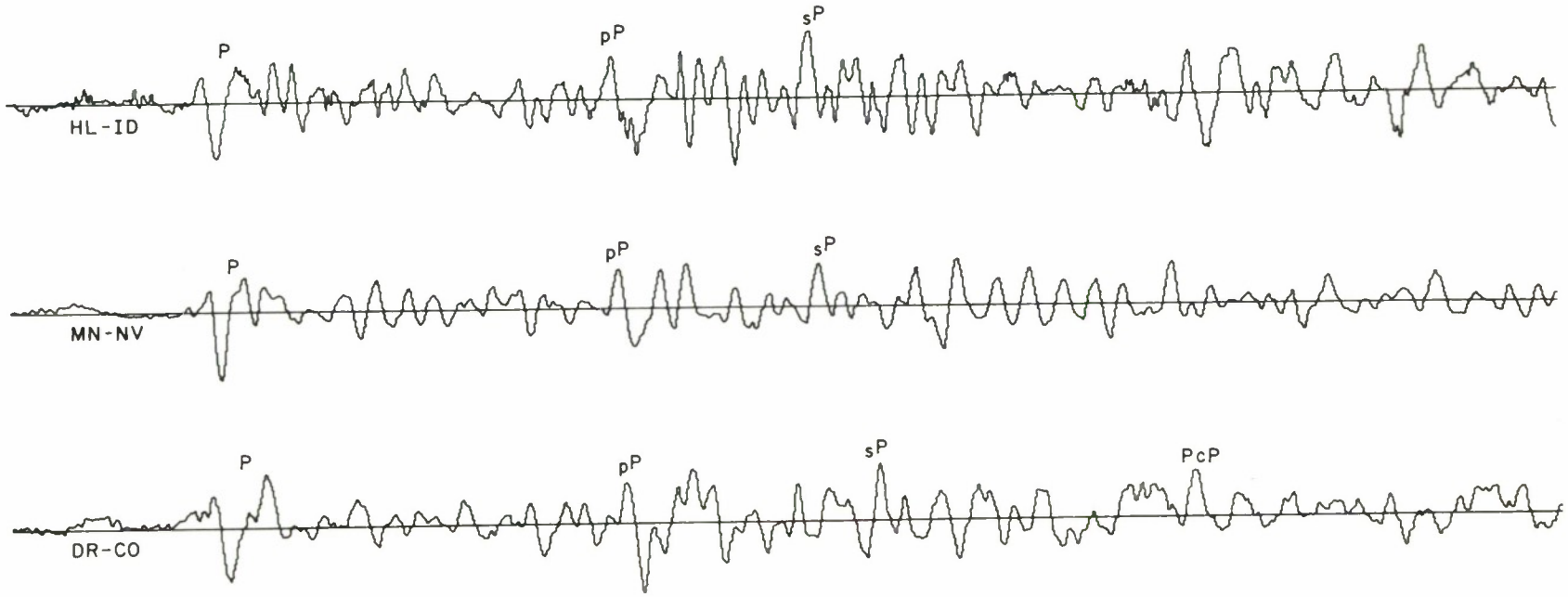

FIGURE 6.6
SEISMOGRAMS FOR 10 JANUARY 1963 EVENT

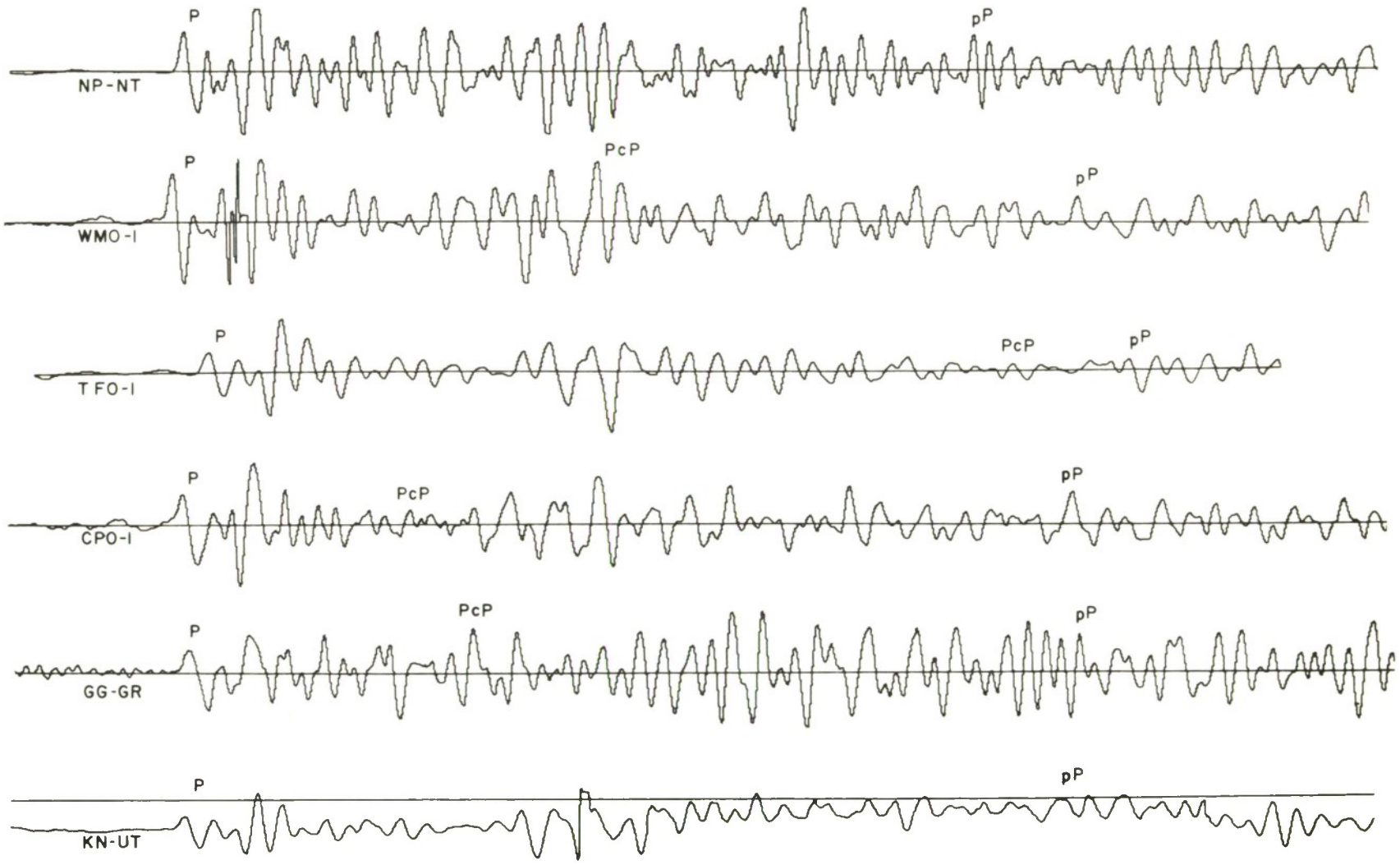

FIGURE 6.7
SEISMOGRAMS FOR 6 JANUARY 1964 EVENT

APPENDIX A

VARIANCE OF INDIVIDUAL ARRIVAL TIME ESTIMATES

As indicated in Section III, one important technique for epicenter estimation begins with individual arrival time estimates for each record. The variance of these estimates is derived in this appendix for each of three different procedures. In each case the derived results apply only to the case of large signal-to-noise ratios (and hence small errors).

For the purposes of this derivation the assumptions of Section III may be summarized as follows. The available record, $x(t)$, is given by

$$x(t) = s(t-\tau) + n(t) \qquad \text{(A-1)}$$

where $n(t)$ is stationary and has power density spectrum $S_n(f)$, and $s(t)$, the signal, is given by

$$s(t) = \sin 2\pi f_0 t \qquad -T/2 < t < T/2 \qquad \text{(A-2)}$$

$$= 0 \qquad |t| > T/2$$

and

$$2\pi f_0 = \frac{2\pi}{T} = \omega_0 \qquad \text{(A-3)}$$

It is desired to estimate τ from $x(t)$. The assumption of large signal-to-noise ratio implies that τ can be estimated within a fraction of T by a cursory examination of $x(t)$. Therefore, the three techniques to be discussed could be regarded as means of refining the estimate of τ over that which is obvious from the unprocessed record.

A-1 ZERO CROSSING TIME PICK

In this case $\hat{\tau}$ is defined by the zero crossing of $x(t)$ near τ. Expanding $x(t)$ about τ we have

$$x(t) = x(\tau)+(t-\tau)x'(\tau)+\ldots \qquad \text{(A-4)}$$

$$= s(0)+n(\tau)+(t-\tau)s'(0)+(t-\tau)n'(\tau)+\ldots$$

Recognizing that s(0) is zero and defining $\hat{\tau}$ as the point where x(t) is zero yields

$$0 = n(\tau)+(\hat{\tau}-\tau)s'(0)+(\hat{\tau}-\tau)n'(\tau) \qquad \text{(A-5)}$$

or

$$\hat{\tau} = \tau - \frac{n(\tau)}{s'(0)+n'(\tau)} \qquad \text{(A-6)}$$

Assuming that $n'(\tau)$ may be neglected compared to $s'(0)$, this yields

$$\hat{\tau} = \tau - \frac{n(\tau)}{s'(0)} \qquad \text{(A-7)}$$

Therefore, the variance of the estimate is given by

$$\text{var}[\hat{\tau}] = \frac{\text{var}[n(\tau)]}{[s'(0)]^2} = \frac{1}{\omega_0^2}\int_{-\infty}^{\infty} S_n(f)df \qquad \text{(A-8)}$$

A-2 MAXIMUM VALUE TIME PICK

Another approach to estimating the arrival time would be to observe the time near $\tau + T/4$ where a maximum in x(t) occurs. It is easily seen that this problem is equivalent to the zero crossing problem just considered if both signal and noise are replaced by their derivatives. We have therefore

$$\text{var}[\hat{\tau}] = \frac{\text{var}[n'(\tau)]}{[s''(T/4)]^2} = \frac{1}{\omega_0^4}\int_{-\infty}^{\infty} (2\pi f)^2 S_n(f)df$$

$$= \frac{1}{\omega_0^2}\int_{-\infty}^{\infty} \left(\frac{f}{f_0}\right)^2 S_n(f)df \qquad \text{(A-9)}$$

A-3 CROSS-CORRELATION TIME PICK

The third method of estimating arrival times is more sensitive to variations of s(t) from its assumed shape. In the previous two methods, only the behavior of s(t) near zero, or near T/4 mattered, and therefore the analysis might still be valid even if s(t) differed in several respects from its assumed shape.

The correlation method of estimating arrival times is more sensitive to variations in s(t), and might deteriorate badly if the received signal differed appreciably from the assumed s(t).

Basically this method consists of choosing $\hat{\tau}$ as the time at which the cross-correlation function of x(t) and s(t) reaches its maximum. This is equivalent to choosing $\hat{\tau}$ as the time of maximum output for a linear time invariant system with x(t) as input and an impulse response h(t) given by

$$h(t) = s(-t) \tag{A-10}$$

This, in turn, is equivalent to looking for the zero crossing in the output of a filter with impulse response

$$h'(t) = -s'(-t) \tag{A-11}$$

Defining y(t) as the output of the latter system, using $\circledast$ to indicate convolution, using subscripts s and n to indicate the appropriate components in y(t) we have

$$\begin{aligned} y(t) &= x(t) \circledast h'(t) = -x(t) \circledast s'(-t) \\ &= \underbrace{-\, s(t-\tau) \circledast s'(-t)}_{y_s(t-\tau)} \underbrace{-\, n(t) \circledast s'(-t)}_{y_n(t)} \end{aligned} \tag{A-12}$$

The problem is now in the form of the zero crossing problem discussed earlier. That is, from Equation (A-7), the estimate is given by

$$\hat{\tau} = \tau - \frac{y_n(\tau)}{y_s'(0)} \tag{A-13}$$

It only remains to evaluate $y_s'(0)$ and $\mathrm{var}[y_n(\tau)]$ before making the appropriate substitution in Equation (A-8).

$$\begin{aligned} y_s'(t) &= +s(t) \circledast s''(-t) \\ &= \int s(z)s''(-(t-z))dz \\ y_s'(0) &= \int s(z)s''(z)dz \\ &= -\tfrac{1}{2}\omega_0^2 T = -\pi\omega_0 \end{aligned} \tag{A-14}$$

The power density spectrum for $y_n(t)$ is easily obtained as the product of $S_n(f)$ and the magnitude squared of the system function corresponding to h'(t).

$$S_{y_n}(f) = S_n(f)\left|\int h'(t)e^{-j2\pi ft}dt\right|^2$$

$$= S_n(f)\left|\int -s'(-t)e^{-j2\pi ft}dt\right|^2$$

$$= S_n(f)\left[2\sin\frac{\pi f}{f_0} \cdot \frac{ff_0}{f_0^2-f^2}\right]^2 \qquad \text{(A-15)}$$

The detailed calculations required to obtain the last line of Equation (A-15) are straightforward. Finally, we have

$$\text{var}[y_n(\tau)] = \int S_{y_n}(f)df = \int S_n(f)\left[2\sin\frac{\pi f}{f_0} \cdot \frac{ff_0}{f_0^2-f^2}\right]^2 df \qquad \text{(A-16)}$$

Substituting Equations (A-14) and (A-16) into Equation (A-8), we have

$$\text{var}[\hat{\tau}] = \frac{\text{var}[y_n(\tau)]}{[y_s'(0)]^2} = \frac{1}{\omega_0^2}\int\left[\frac{2}{\pi}\sin\frac{\pi f}{f_0} \cdot \frac{ff_0}{f_0^2-f^2}\right]^2 S_n(f)df \qquad \text{(A-17)}$$

APPENDIX B

EQUIVALENCE OF BEAMFORMING AND PLANE WAVE FIT

B-1 CORRELATION TIME PICKS IN PRESENCE OF NOISE

Referring to the definitions in Section III of the text and assuming that the τ_i in Equation (3.1) are zero, we have the following expression for the energy in the output of the array as a function of the estimate $\hat{m}$.

$$f(\hat{m}) = \int \Big(\sum_{i=1}^{N} x_i(t+i\hat{m}) \Big)^2 dt \qquad \text{(B-1)}$$

$$= \int \sum_{i=1}^{N} \sum_{j=1}^{N} [s(t-im+i\hat{m})+n_i(t+i\hat{m})][s(t-jm+j\hat{m}) + n_j(t+j\hat{m})]dt$$

It is assumed that the limits of the integral roughly bound the duration of the signal terms; this will be possible since a large signal-to-noise ratio is assumed. We are interested in choosing $\hat{m}$ to maximize $f(\hat{m})$. In doing so we shall neglect second-order noise contributions. Discarding these terms and changing the variables of integration

$$f(\hat{m}) = \sum_{i=1}^{N} \sum_{j=1}^{N} \int s(t)s(t+(\hat{m}-m)(j-i))dt$$

$$+ \int s(t)n_j(t+\hat{m}(j-i)+im)dt$$

$$+ \int s(t)n_i(t-\hat{m}(j-i)+jm)dt \qquad \text{(B-2)}$$

In order to find the $\hat{m}$ for which $f(\hat{m})$ is a maximum, we solve for $f'(\hat{m}) = 0$.

$$f'(\hat{m}) = \sum_{i,j} (j-i) \int s(t)s'(t+(\hat{m}-m)(j-i))dt \qquad \text{(B-3)}$$

$$+ \int dt s(t) \sum_{i,j} [(j-i)n_j'(t+\hat{m}(j-i)+im) - (j-i)n_i'(t-\hat{m}(j-i)+jm)]$$

Expanding $f'(\hat{m})$ about m,

$$f'(\hat{m}) = f'(m) + (\hat{m}-m)f''(m)+... \tag{B-4}$$

Equating this to zero yields

$$\hat{m} = m + \frac{-f'(m)}{f''(m)} \tag{B-5}$$

Examining Equation (B-3) we have

$$f'(m) = 0+\int dts(t) \sum_{i,j} (j-i)[n_j'(t+jm)-n_i'(t+im)] \tag{B-6}$$

$$f''(m) = \sum_{i,j} (j-i)^2 \int s(t)s''(t)dt + \int dts(t) \sum_{i,j} (j-i)^2 \cdot[n_j''(t+jm)+n_j''(t+im)] \tag{B-7}$$

In Equation (B-7), which gives the denominator for Equation (B-5), we neglect the noise term relative to the signal term. Referring to the derivation of correlation time picks (Equation A-14) we may recognize the signal term

$$f''(m) = [\sum_{i,j} (j-i)^2] \int s(t)s''(t)dt = y_s'(0) \frac{N^2(N^2-1)}{6}$$

$$= -\pi\omega_0 \frac{N^2(N^2-1)}{6} \tag{B-8}$$

In Equation (B-6) it is useful to rewrite the double sum involving the noise terms; we define an equivalent noise $n_e'(t)$ by this summation:

$$n_e'(t) = \sum_{i,j} (j-i)[n_j'(t+jm)-n_i'(t+im)]$$

$$= \sum_{i,j} [jn_j'-jn_i'-in_j'+in_i']$$

$$= 2[N\sum_i in_i' - \frac{N(N+1)}{2} \sum_i n_i']$$

$$= 2N[\sum_{i=1}^{N} (i - \frac{N+1}{2})n_i'] \tag{B-9}$$

We are now ready to relate the beamforming estimate of m to that which would be obtained by individual correlation time picks followed by a least squares slope fit. To do this, recall Equation (A-13) from the correlation time pick discussion which is repeated here with the addition of a subscript.

$$\hat{\tau}_i = \tau_i - \frac{y_{n_i}(\tau_i)}{y_s'(0)} \tag{B-10}$$

where $y_{n_i}(t) = -n_i(t) \otimes s'(-t)$

$$= -\int n_i(t-z)s'(-z)dz$$

$$= -\int n_i(t+z')s'(z')dz'$$

$$= +\int s(z)n_i'(t+z)dz \tag{B-11}$$

and

$$y_s'(0) = \int s(z)s''(z)dz = -\pi\omega_0 \tag{B-12}$$

Assuming the true arrival times, τ_i, are given by

$$\tau_i = mi \tag{B-13}$$

$$y_{n_i}(\tau_i) = +\int s(z)n_i'(z+im)dz \tag{B-14}$$

Substituting Equations (B-6), (B-8) and (B-9) into Equation (B-5) we have

$$\hat{m} = m + \frac{-\int dt s(t)n_e'(t)}{\frac{N^2(N^2-1)}{6} \cdot y_s'(0)} \tag{B-15}$$

$$= m + \frac{-2N\sum(i-\frac{N+1}{2})\int dt s(t)n_i'(t+im)}{\frac{N^2(N^2-1)}{6} y_s'(0)} \tag{B-16}$$

$$= m + \frac{\sum(i-\frac{N+1}{2})\frac{y_{n_i}}{y_s'}}{\frac{N(N^2-1)}{12}} \tag{B-17}$$

Equation (B-17) is identical to Equation (3-10) of Section III if y_{n_i}/y'_s is identified as the random component of the i^{th} arrival-time measurement. And, by Equation (A-13) of Appendix A, y_{n_i}/y'_s is exactly the random component of the i^{th} arrival time measurement when the correlation method of arrival time estimation is used. Therefore, in the case of sufficiently large signal-to-noise ratios, the beamforming method and the correlation time pick followed by a least squares slope fit are identical. That is, they not only perform equally well, they yield the same answer.

B-2 NOISELESS CASE WITH RANDOM TIMING ERRORS

In the noiseless case with random timing errors, we have

$$x_i(t) = s(t-im+\tau_i) \tag{B-18}$$

and by Equation (3-10) the plane wave fit yields

$$\hat{m} = m - \frac{\sum(i - \frac{N+1}{2})\tau_i}{\frac{1}{12}N(N^2-1)} \tag{B-19}$$

If, as in the previous section, we consider

$$f(\hat{m}) = \int(\sum x_i(t+i\hat{m}))^2 dt$$

$$= \int \sum_{i,j} s[t-i(m-\hat{m})+\tau_i]s[t-j(m-\hat{m})+\tau_j]dt \tag{B-20}$$

and choose $\hat{m}$ to maximize the resulting expression, we obtain

$$f'(\hat{m}) = \int \sum_{i,j} 2is'(t-i(m-\hat{m})+\tau_i)s(t-j(m-\hat{m})+\tau_j)dt$$

$$= 2\sum_{i,j} \int is(t)s'(t-(i-j)(m-\hat{m})+(\tau_i-\tau_j))dt \tag{B-21}$$

Assuming that $(i-j)(m-\hat{m})-(\tau_i-\tau_j)$ is small and recognizing that if it were zero the integral would be zero, we have

$$f'(\hat{m}) \approx 2\sum_{i,j} i[(i-j)(m-\hat{m})-(\tau_i-\tau_j)]\int s(t)s''(t)dt = 0 \tag{B-22}$$

and therefore,

$$(m-\hat{m}) \sum_{i,j} (i^2-ij) = \sum_{i,j} i(\tau_i-\tau_j) \tag{B-23}$$

which reduces to

$$\hat{m} = m - \frac{\sum_i (i - \frac{N+1}{2})\tau_i}{\frac{N(N^2-1)}{12}} \tag{B-24}$$

in agreement with Equation (B-19).

REFERENCES

1. General Atronics Corporation, "First Quarterly Technical Report -- Large Aperture Seismic Arrays," September 1967, pp. 17-32.

2. General Atronics Corporation, "Large Aperture Seismic Arrays," June 1967, pp. 95-123.

3. General Atronics Corporation, *op. cit.*, September 1967, pp. 17-32.

4. General Atronics Corporation, *op. cit.*, June 1967, Fig. 10.45, p. 114.

5. *Ibid.*, pp. 50-69.

6. M.G. Kendall and A. Stuart, *The Advanced Theory of Statistics, Vol. 2, Inference and Relationship*, Hafner Publishing Co., New York, 1961, p. 79.

7. General Atronics Corporation, *op. cit.*, June 1967, pp. 124-138.

8. General Atronics Corporation, *op. cit.*, September 1967, pp. 33-59.

9. General Atronics Corporation, *op. cit.*, June 1967, pp. 87-94.

10. General Atronics Corporation, *op. cit.*, September 1967, pp. 33-59.

11. Section IV, this report.

12. General Atronics Corporation, *op. cit.*, June 1967, pp. 70-77.

13. General Atronics Corporation, *op. cit.*, September 1967, pp. 60-68.

14. General Atronics Corporation, *op. cit.*, June 1967, pp. 95-123.

15. Personal communication with Mr. Carl von Hake, C&GS, Rockville, Maryland.

16. Herrin 1966 tables supplied by Seismic Data Laboratory, 300 North Washington Street, Alexandria, Virginia.

UNCLASSIFIED
Security Classification

DOCUMENT CONTROL DATA - R & D

(Security classification of title, body of abstract and indexing annotation must be entered when the overall report is classified)

1. ORIGINATING ACTIVITY (Corporate author) General Atronics Corp. 1200 East Mermaid Lane Philadelphia, Pennsylvania 19118	2a. REPORT SECURITY CLASSIFICATION Unclassified 2b. GROUP N/A

3. REPORT TITLE

SECOND QUARTERLY TECHNICAL REPORT -
LARGE APERTURE SEISMIC ARRAYS (LASA)

4. DESCRIPTIVE NOTES (Type of report and inclusive dates)
None

5. AUTHOR(S) (First name, middle initial, last name)
None

6. REPORT DATE December 1967	7a. TOTAL NO. OF PAGES 102	7b. NO. OF REFS 16
8a. CONTRACT OR GRANT NO. AF19628-67-C-0370 b. PROJECT NO. c. d.	9a. ORIGINATOR'S REPORT NUMBER(S) ESD-TR-67-630 9b. OTHER REPORT NO(S) (Any other numbers that may be assigned this report)	

10. DISTRIBUTION STATEMENT This document has been approved for public release and sale; its distribution is unlimited.

11. SUPPLEMENTARY NOTES	12. SPONSORING MILITARY ACTIVITY Directorate of Planning and Technology, Electronic Systems Division, AFSC, USAF, L G Hanscom Field, Bedford, Mass. 01730

13. ABSTRACT Four topics are discussed in this progress report. The first topic is related to the masking of underground nuclear tests with large earthquakes. Computer simulations, using signals from actual seismic events, suggest that test detonations one magnitude unit smaller than the earthquake can be detected, providing the shot time is some two minutes after the time of occurrence of the earthquake. The second topic deals with the effects of signal-to-noise ratio and local travel time-anomalies on the accuracy of epicenter location using large seismic arrays. Both theoretical analyses and computer simulations indicate standard deviations of angular errors on the order of 0.3° for either a 10 dB signal-to-noise ratio or a peak anomaly on the order of 1/20th of a second. The third topic deals with the application of a previously developed coda-correlation discriminant to DIMUS (hardlimited) seismograms. This discriminant makes use of the average paired correlation coefficient of the 10-second portion of seismic arrivals commencing 3 seconds after P-wave onset for an array of widely separated stations. Results to date indicate a moderate degradation of the discriminant for the DIMUS seismograms compared to the unclipped seismograms. The fourth topic deals with the automatic identification of the pP phase of earthquakes, for events in the 40 to 150 km depth region. Excellent results have been obtained with this automatic scheme, and not only is the pP phase properly identified, but also the sP phase. This combination allows depths to be estimated with considerable confidence.

DD FORM 1 NOV 65 1473

UNCLASSIFIED
Security Classification

14. KEY WORDS	LINK A		LINK B		LINK C	
	ROLE	WT	ROLE	WT	ROLE	WT
Seismology						
Arrays						
Signal Processing						
Seismic Discrimination						
Epicenter Location						
Earthquake Depth Estimation						